

**Crystal structures of the major staphylococcal
Autolysin E:**

**How autolysins recognize and degrade
the Gram-positive cell wall**

Dissertation

der Mathematisch-Naturwissenschaftlichen Fakultät

der Eberhard Karls Universität Tübingen

zur Erlangung des Grades eines

Doktors der Naturwissenschaften

(Dr. rer. nat.)

vorgelegt von

Sebastian Zoll

aus Frankenberg (Eder)

Tübingen

2011

Tag der mündlichen Qualifikation: 05.07.2011

Dekan:

Prof. Dr. Wolfgang Rosenstiel

1. Berichterstatter:

Prof. Dr. Thilo Stehle

2. Berichterstatter:

Prof. Dr. Friedrich Götz

TABLE OF CONTENTS

1. ABBREVIATIONS	II
2. INTRODUCTION	1
2.1. SUPERBUGS – WHY PENICILLIN WAS NOT ENOUGH	1
2.2. STAPHYLOCCI	4
2.2.1. <i>STAPHYLOCOCCUS AUREUS</i> AND <i>STAPHYLOCOCCUS EPIDERMIDIS</i> - PATHOGENESIS AND CLINICAL SIGNIFICANCE	4
2.2.2. COMPONENTS AND COMPOSITION OF THE GRAM-POSITIVE CELL WALL	5
2.2.2.1. Peptidoglycan	6
2.2.2.2. Teichoic acids	8
2.2.3. MUREIN HYDROLYZING ENZYMES AND THEIR ROLE IN CELL WALL TURNOVER	11
2.2.4. THE ATLE AMIDASE	13
2.3. X-RAY CRYSTALLOGRAPHY	15
2.3.1. THE PRINCIPLES OF DIFFRACTION	16
2.3.2. METHODS OF PHASE DETERMINATION	18
3. AIMS	22
4. RESULTS AND DISCUSSION	24
4.1. DEVELOPMENT OF A NOVEL FLUORESCENT SUBSTRATE FOR AUTOLYSIN E, A BACTERIAL TYPE II AMIDASE	24
4.2. ROLE OF STAPHYLOCOCCAL WALL TEICHOIC ACID IN TARGETING THE MAJOR AUTOLYSIN ATL	26
4.3. STRUCTURAL BASIS OF CELL WALL CLEAVAGE BY A STAPHYLOCOCCAL AUTOLYSIN	28
4.4. THE STRUCTURAL BASIS OF STAPHYLOCOCCAL CELL WALL RECOGNITION BY SH3B DOMAINS	32
5. SUMMARY	34
6. ZUSAMMENFASSUNG	36
7. REFERENCES	38
8. APPENDIX	43
8.1. PUBLICATIONS	43
8.2. ACKNOWLEDGMENTS	44

1. ABBREVIATIONS

BSA	Bovine serum albumin
CBR	Cell wall binding region
cMRSA	Community-acquired methicillin-resistant <i>S. aureus</i>
CNS	Coagulase-negative staphylococci
ConA-FITC	Concanavalin A fluorescein isothiocyanate conjugate
CPS	Coagulase-positive staphylococci
CW	Cell Wall
Cy5	Cyanine-5
DAG	Diacylglycerol
Dde	N-1-(4,4-Dimethyl-2,6-dioxocyclohex-1-ylidene)ethyl
DMSO	Dimethyl sulfoxide
DNA	Deoxyribonucleic acid
Dnp	2,4-dinitrophenyl
EDTA	Ethylenediaminetetraacetic acid
ELISA	Enzyme-linked immunosorbent assay
ESI	Electrospray ionization
ESRF	European Synchrotron Radiation Facility
Fmoc	Fluoren-9-ylmethoxycarbonyl
GFP	Green fluorescent protein
Glc	Glucose
GlcNAc	N-acetylglucosamine
GMDP	Glucosaminyl-muramyl dipeptide
Gro	Glycerol
GST	Glutathione S-transferase
HObt	1-hydroxybenzotriazole
HPLC	High-performance liquid chromatography
IPTG	Isopropyl- β -D-1-thiogalactopyranoside
LCMS	Liquid chromatography mass spectrometry
LTA	Lipoteichoic acid
MALDI	Matrix-assisted laser desorption/ionization
ManNAc	N-acetylmannosamine
Mca	(7-Methoxycoumarin-4-yl)-acetyl
MDP	Muramyl dipeptide
MRSA	Methicillin-resistant <i>S. aureus</i>
MRSE	Methicillin-resistant <i>S. epidermidis</i>
MTP	Muramyl tripeptide

MurNAc	N-acetylmuramic acid
OD	Optical density
PAGE	Polyacrylamide gel electrophoresis
PBP	Penicillin Binding Protein
PBS	Phosphate buffered saline
PCR	Polymerase chain reaction
PDB	Protein Data Bank
PGN	Peptidoglycan
PGRP	Peptidoglycan recognition protein
PIA	Polysaccharide intercellular adhesin
PMSF	Phenylmethylsulfonyl fluoride
r.m.s.	Root mean square
RP	Reversed phase
RT	Room temperature
Rto	Ribitol
SDS	Sodium dodecyl sulfate
SEM	Scanning electron microscope
SH3	Src-homology 3
TBTU	2-(1H-benzotriazole-1-yl)-1,1,3,3-tetramethyluronium-tetrafluoroborate
TCA	Trichloroacetic acid
TEM	Transmission electron microscope
TFA	Trifluoroacetic acid
UV	Ultra-violet
VISA	Vancomycin-intermediate <i>S. aureus</i>
VRSA	Vancomycin-resistant <i>S. aureus</i>
WGA-FITC	Wheat Germ Agglutinin fluorescein isothiocyanate conjugate
WTA	Wall teichoic acid

2. INTRODUCTION

2.1. SUPERBUGS – WHY PENICILLIN WAS NOT ENOUGH

Only twelve years after the discovery of penicillin and years before its mass production Abraham and Chain were the first to provide evidence for “An Enzyme from Bacteria able to Destroy Penicillin”:

“FLEMING¹ noted that the growth of *B. coli* and a number of other bacteria belonging to the coli-typhoid group was not inhibited. This observation has been confirmed. [. . .]. This extract [*B. coli*] was found to contain a substance destroying the growth-inhibiting property of penicillin. [. . .]. The conclusion that the active substance is an enzyme is drawn from the fact that it is destroyed by heating at 90° for 5 minutes and by incubation with papain [. . .].” [1]

The enzyme described in the publication of Abraham and Chain was referred to later as penicillinase or β -lactamase. Further investigations in following years revealed that, indeed, some bacteria are naturally resistant against Penicillin while others such as staphylococci, although widely considered to be susceptible, are able to acquire resistance easily [2]. In 1944, Kirby provided the first evidence of a penicillinase-producing *Staphylococcus aureus* strain [3]. However, these findings did only apply to a relatively limited number of isolates and laboratory strains, while community strains were still considered to be susceptible to Penicillin. In World War II, Penicillin was first used in large amounts to prevent post-surgical wound infections in soldiers. The good tolerability in conjunction with few side effects made it an increasingly popular drug and let Penicillin become a standard treatment in hospitals worldwide in the late 1940s and early 1950s. Staphylococci, e.g. *S. aureus* and *Staphylococcus epidermidis*, are natural inhabitants of the human skin and the mucous membranes and as such are in particular subject to the increased selection pressure in hospitals. Resistances spread and made the development of a new class of antibiotics necessary.

In 1959, Methicillin was introduced, a Penicillin derivative with a sterically protected β -lactam ring that is insensitive to β -lactamase. However, as early as 1961 M. P. Jevons reported the first case of hospital acquired methicillin-resistant staphylococci:

“Between the beginning of October and the end of November, 1960, 5,440 strains have been tested. [. . .]. Of the 5,440 strains only three showed significant [methicillin] resistance by the paper-disk method. All three were received from the same hospital, [. . .].” [4]

M.P. Jevons was well aware that hospitals environments in particular favor the propagation of multi-resistant bacteria:

“It is well known that patients with infected skin can be dangerous sources of infection in hospitals, and the finding of just such a patient infected with celbenin- [methicillin] resistant strain in this instance adds an additional warning.” [4]

The upcoming rise of methicillin-resistant staphylococci (MRSA), starting in the late 1960s, had strong similarities with the epidemiology of penicillin-resistant strains. Although derivatives of Methicillin were developed to keep up with the pace of resistance formation, the entire class of β -lactam antibiotics became almost useless against certain strains. In 2009, the European Centre for Disease Prevention and Control reported that, among participating countries, in average approx. one fifth of all clinical staphylococcal isolates are resistant to antibiotics of the Methicillin class (Figure 2.1).

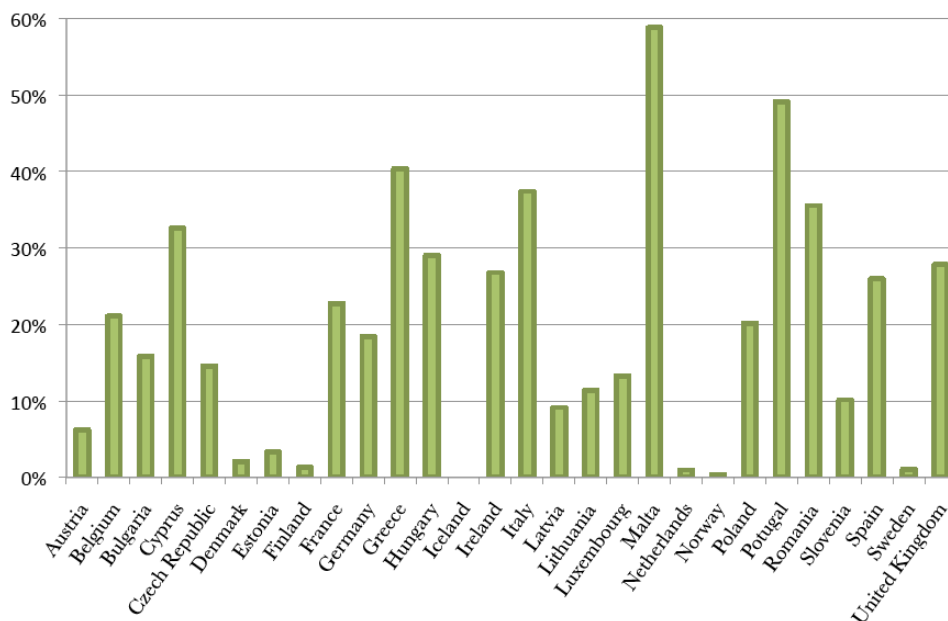


Figure 2.1: Proportion of methicillin-resistant *S. aureus* (MRSA) isolates in European countries in 2009. (European Centre for Disease Prevention and Control, <http://ecdc.europa.eu/en/Pages/home.aspx>)

There are four main mechanisms of antibiotic resistance [5]:

- Altered target sites, e.g. Penicillin Binding Protein (PBP) (β -lactam resistance)
- Decreased uptake of the drug, e.g. Multidrug efflux systems, reduced permeability
- “Bypass” systems, e.g. overproduction of dihydrofolate reductase (Trimethoprim resistance)
- Enzymatic inactivation or modification, e.g. β -lactamase (β -lactam resistance)

Resistances can be natural/intrinsic. However, mutation and dissemination of resistance genes by transposons, plasmids and phages are the main cause for the emergence of multidrug resistance. They are referred to as acquired resistances.

Today Vancomycin is the only effective compound left to successfully treat MRSA infections, and still this compound is only used after all other treatments have failed. Its structure and mode of action are considerably different from β -lactam antibiotics, although both antibiotics prevent crosslinking of peptidoglycan (PGN). PGN is the major compound of the bacterial cell that serves to protect bacteria from environmental stress. It is a macromolecule in which several layers of glycan strands are crosslinked by short peptides. Crosslinkage is crucial in that it accounts for the high rigidity of the cell wall. While β -lactam antibiotics inactivate PBP, a key enzyme in PGN biosynthesis, to prevent crosslinking of PGN, Vancomycin has the same effect by forming a complex with a PGN precursor molecule.

Despite sensible use of Vancomycin, the first *S. aureus* strain with a reduced susceptibility appeared in Japan in 1996 [6]. Six years later the first entirely resistant clinical isolate was reported in the United States [7]. Vancomycin-intermediate *S. aureus* (VISA) and vancomycin-resistant *S. aureus* (VRSA) strains do not show the same epidemiology as β -lactam resistant strains did earlier, but their appearance clearly demonstrates that there is not just one superdrug against multiresistance. New strains with unique combinations of virulence factors such as community-acquired methicillin-resistant *S. aureus* (cMRSA) pose another emerging threat [8] and emphasize the strong need for a continuous development of new drugs.

2.2. STAPHYLOCOCCI

Staphylococci are Gram-positive, catalase and oxidase producing bacteria that are typically arranged in clusters of cocci and can thereby be distinguished from chain-forming streptococci. The genus *Staphylococcus* comprises more than 40 species and subspecies. Biochemical identification is provided by the coagulase test. Coagulase is a staphylococcal pathogenesis factor, which causes clotting of the blood. Coagulase-positive staphylococci (CPS) are *S. aureus*, *S. intermedius*, *S. pseudintermedius*, *S. delphini*, *S. lutrae* and *S. schleiferi* subsp. *coagulans*. Coagulase-negative staphylococci (CNS) are generally regarded to be less pathogenic. *S. epidermidis*, *S. saprophyticus*, *S. haemolyticus* and *S. xylosus* are the most important species belonging to this category.

2.2.1. STAPHYLOCOCCUS AUREUS AND STAPHYLOCOCCUS EPIDERMIDIS - PATHOGENESIS AND CLINICAL SIGNIFICANCE

S. aureus and *S. epidermidis* are the most common species of the genus occurring in humans where they mainly colonize the skin and the mucous membranes. They are also among the main causes of nosocomial infections. While most of these infections are averted by a working immune system, they can be life threatening especially in immunocompromised hosts.

S. aureus, in particular, expresses a large spectrum of virulence factors that account for its pathogenicity. The bacterium is the cause of various acute diseases such as endocarditis, meningitis, pneumonia, septicaemia and toxic shock syndrome [9]. Adherence is a prerequisite for successful colonization of host structures. Proteins such as Protein A, fibrinogen-, fibronectin-, and collagen-binding proteins play an important role in this step where they are responsible for host cell interactions and adherence to artificial surfaces. Another source of virulence are secreted enzymes and toxins. Haemolysins, leukocidin, hyaluronidase and other lipases, proteases and nucleases can cause necrotic lesions and persistent wound infections [10]. They degrade tissue and participate in the invasion of skin and mucous membranes. Secreted toxins (Toxic shock syndrome toxin 1, Exfoliative toxins, Enterotoxins A-E etc.) are mostly associated with specific systemic diseases such as the toxic shock syndrome, the staphylococcal scaled skin syndrome or food poisoning [10].

While *S. aureus* is the most important and best-studied staphylococcal pathogen, the significance of CNS in hospital-acquired infections has long been neglected. Among CNS, *S. epidermidis* has been reported to be the most common cause of infections (70-80%) [11]. Its emergence as a pathogen is closely connected to the now widespread use of implants such as intravascular catheters, prostheses, pacemakers or artificial heart valves [12]. Upon primary attachment to a polymer surface, *S. epidermidis* produces a multilayered polysaccharide matrix that shields the pathogen from host immune defense mechanisms. Biofilm formation is also seen in *S. aureus* and certain other species, but is best studied and mostly associated with *S. epidermidis* derived infections. Mack *et al.* proposed a two-step model [13,14] in which the first step, the primary adherence, is mainly mediated by surface associated proteins such as the major autolysin E (AtlE) [15]. Surface charges and hydrophobic interactions are also being discussed in this process [16,17]. The second step, the accumulation phase, is characterized by production of PIA, a polysaccharide intercellular adhesin that links bacteria in the biofilm. PIA consists of β -1,6-linked glucoseaminoglycan subunits and is encoded by the *ica*-operon [18], which is also present in *S. aureus*. *Ica* mutants showed primary adhesion but were lacking the accumulation phase [19,20].

Multiresistance of *S. aureus* as described earlier (Section 2.1) is a widespread problem known for almost 50 years. However, this does not seem to be an exclusive feature of *S. aureus* anymore. Over the last two decades an increasing number of infections caused by *S. epidermidis* strains with Methicillin resistance (MRSE) [21,22] or even elevated Vancomycin tolerance were reported [23,24,25]. In conjunction with its ability to evade host defense mechanisms by biofilm formation, this clearly emphasizes the urge to develop new therapeutic strategies to treat *S. epidermidis* infections.

2.2.2. COMPONENTS AND COMPOSITION OF THE GRAM-POSITIVE CELL WALL

The cell wall of Gram-positive bacteria (Figure 2.2) stains dark violet in the Gram reaction. In comparison to the cell wall of Gram-negative bacteria, the Gram-positive wall retains the stain since it is approx. ten times thicker. The bacterial cell wall primarily functions as an exoskeleton protecting the cell from osmotic stress, but is also allowing communication with the environment. Its main component, surrounding the

entire cell is PGN, a reticular macromolecule supplemented with accessory molecules such as teichoic acids, teichuronic acids and other glycopolymers [26,27].

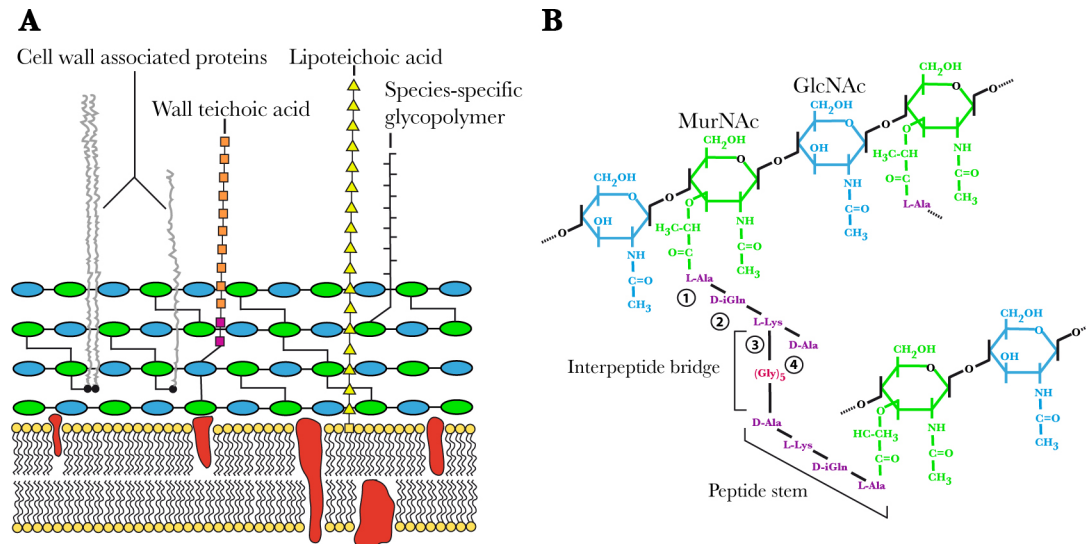


Figure 2.2: The cell wall of Gram-positive bacteria. (A) Schematic drawing. (B) Structure of *S. aureus* PGN in detail. Modified from [11,28].

2.2.2.1. Peptidoglycan

PGN is a highly crosslinked polymer consisting of glycan strands and short peptides. The glycan strands form the backbone of the PGN layer. Depending on the species, they comprise 5 to 30 repeating subunits of N-acetylmuramic acid- (β 1,4)-N-acetylglucosamine (MurNAc-GlcNAc) disaccharides [29,30]. The D-lactyl moiety of MurNAc is linked via an amide bond to a four amino acids long peptide stem, which is mostly further crosslinked by an interpeptide bridge to the stem of a neighbouring strand. In contrast to the uniform structure of the repeating disaccharide that is part of every bacterial PGN structure, composition of the peptide part can vary significantly among species [31]. The peptides stem is unusual in that it consists of L- and D-amino acids. In Staphylococci and most other Gram-positive bacteria the sequence L-Ala, D-isoGln, L-Lys, D-Ala can be found, with the terminal alanine being removed by the action of the coxypeptidase PBP during incorporation of the pentapeptide precursor molecule into the PGN matrix. Nevertheless, other combinations are possible (Table 1).

Position	Residue encountered	Examples
1	L-Ala	Most bacteria
	Gly	<i>Mycobacterium leprae</i> , <i>Brevibacterium imperiale</i>
	L-Ser	<i>Butyribacterium rettgeri</i>
2	D-Isoglutamine	Most Gram-positive species, Mycobacteria
	<i>threo</i> -3-Hydroxyglutamate	<i>Microbacterium lacticum</i>
3	<i>meso</i> -A ₂ pm	Most Gram-negative species, Bacilli, Mycobacteria
	L-Lys	Most Gram-positive species
	L-Lys/L-Orn	<i>Bifidobacterium globosum</i>
	LL-A ₂ pm	<i>Streptomyces albus</i> , <i>Propionibacterium petersonii</i>
	L-2,4-Diaminobutyrate	<i>Corynebacterium aquaticum</i>
	L-Homoserine	<i>Corynebacterium poinsettiae</i>
	L-Ala	<i>Erysipelothrix rhusiopathiae</i>
	L-Glu	Arthrobacter J. 39
	Amidated <i>meso</i> -A ₂ pm	<i>Bacillus subtilis</i>
	L-5-Hydroxylysine	<i>Streptococcus pyogenes</i>
	N ^ε -Acetyl-L-2,4-diaminobutyrate	<i>Corynebacterium insidiosum</i>
4	D-Ala	All bacteria
5	D-Ala	Most bacteria
	D-Ser	<i>Enterococcus gallinarum</i>
	D-Lac	<i>Lactobacillus casei</i> , Enterococci with acquired resistance to Vancomycin

Table 1: Amino acid variations in the peptide stem of Gram-positive bacteria. Modified from [32].

Notably, Gram-positive bacteria show a much broader spectrum of variations than Gram-negative ones [33]. The largest variability can be found at amino acid position three. For example, in most Mycobacteria and Bacillus species lysine is changed to *meso*-diaminopimelic acid, an amino acid that is otherwise common in Gram-negative bacteria. Although less common, modifications may also occur at the second position, where the α -carboxyl group of D-glutamic acid may either be free or amidated (D-iGln) [31,32]. The interpeptide bridge accounts for the great rigidity of the murein structure. It links the ϵ -amino group of L-Lys (or any other amino acid in the third position) to the D-Ala carbonyl of another glycan strand. Much more than the peptide stem, this bridge is prone to modifications in length and composition. In *S. aureus* it is composed of five glycines. However, serine and alanine substitutions can be found in

S. epidermidis, but may vary depending on environmental conditions [33]. The interpeptide bridge can also be shortened (L-Ala-L-Ala in *S. pyogenes*) or absent (*L. monocytogenes*) [31].

Although variations in the PGN structure mainly affect the peptide fraction, modifications of the glycan-strand, such as acetylation of the MurNAc C6 hydroxyl group, have also been reported [34]. To date, this modification has been found in *S. aureus* and only few other human pathogens [35]. The additional acetyl-group renders these bacteria resistant against lysozyme cleavage. This modification is important in that it does not only prevent cell lysis, but also results in a reduced host response due to a decreased release of immune-stimulatory PGN fragments [35].

2.2.2.2. Teichoic acids

Gram-positive bacteria incorporate various classes of glycopolymers into their cell envelope and these differ significantly in structure and composition depending on species or strain. Although showing variations in their sugar moiety, net charge and decoration of the repeating units, teichoic acids represent the most defined class of glycopolymers and can be found in most species [27]. According to their attachment point in the cell envelope, one distinguishes PGN-anchored wall teichoic acids (WTA) and membrane-anchored lipoteichoic acids (LTA) (Figure 2.3). Teichoic acids are involved in most different processes. They are crucial for protection of the cell envelope, regulation of autolysin activity, participate in colonization processes and interact with host immune defense mechanisms.

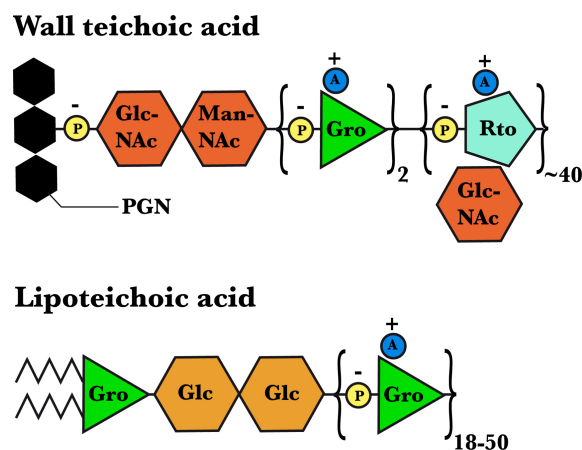


Figure 2.3: Schematic drawing of *S. aureus* wall teichoic and lipoteichoic acid structures. A, D-alanine; **Glc**, glucose; **GlcNAc**, N-acetylglucosamine; **Gro**, glycerol; **ManNAc**, N-acetylmannosamine; **P**, phosphate; **Rto**, ribitol. Modified from [27].

a) Wall teichoic acids

Wall teichoic acids are bound to the glycan backbone of the PGN layer via an anchoring structure, made up of the disaccharide N-acetylglucosamine- (GlcNAc) (β 1,4)-N-acetylmannosamine (ManNAc) and two or three glycerolphosphate units. In this structure, GlcNAc is covalently linked to the hydroxyl-group of the MurNAc C6 carbon via a phosphodiester bond, while the glycerolphosphate units connect to a long polyolphosphate backbone. In *S. aureus*, WTAs are best studied. They contain approx. 40 ribitolphosphate subunits, further supplemented with GlcNAc and D-alanine at the 2' and 4' hydroxyl group [36,37,38,39]. The positively charged amino group of the latter modification confers a zwitterionic character onto the otherwise polyanionic WTAs. In contrast to *S. aureus*, the WTAs of most CNS such as *S. epidermidis*, contain glycerol instead of ribitol [36]. Supplementation with glucose and GlcNAc [36] as well as alanine [40] have also been reported for *S. epidermidis*. However, these investigations are based on different strains. Modifications may generally also vary with the availability of these components in the surrounding medium.

Due to their tremendous structural diversity and the lacking availability of appropriate mutants in the past, it has been difficult to assign specific functions to teichoic acids. Yet, recent constructions of such mutants and subsequent investigations have shed light upon such functions.

The characterization of an *S. aureus* WTA/LTA mutant that is devoid of positively charged alanine substituents ($\Delta dltA$) revealed an increased susceptibility to cationic antimicrobial molecules compared to the wildtype [41]. The ability to regulate alanine incorporation does therefore imply an important mechanism to adapt to hostile environments such as the host immune system. Furthermore, alanine modifications play a crucial role in colonization. Weidenmaier *et al.* reported that the $\Delta dltA$ mutant exhibits a significantly reduced ability to adhere to epithelial and endothelial cells and was consequently less infectious [42,43]. Despite such important roles, WTA seems to be dispensable under laboratory conditions [27]. This could be shown with a WTA deficient *S. aureus* mutant ($\Delta tagO$) that is not impaired in viability compared to the wildtype. However, the $\Delta tagO$ mutant behaved similar to the $\Delta dltA$ mutant and showed a reduced affinity to epithelial cells in an animal colonization model [42]. Another important property of the $\Delta tagO$ mutant is its increased autolysis susceptibility. Based on this observation, Schlag *et al.* demonstrated an important role for WTAs in

targeting the major autolysin Atl, a key enzyme in cell division. In *S. aureus* wildtype cells, WTAs prevented binding of the autolysin to the cell wall and directed it to the cross-wall section to perform the separation of daughter cells. In this region, the concentration of WTAs is low. In the $\Delta tagO$ mutant this avoidance strategy could not take place and resulted in an autolysin distribution over the entire cell wall [43]. Furthermore, WTAs display receptors for phage binding [44]. This was confirmed in *S. aureus* $\Delta tagO$, where comparative analysis revealed that the lack of WTAs renders the mutant strain resistant against infections with phages 3A52 and $\phi 11$ [42].

b) Lipoteichoic acids

Lipoteichoic acids and wall teichoic acids possess different structures in all Gram-positive bacteria except *Streptococcus pneumoniae* [31]. However, both are similar in that they are long polyanionic polymers that extend through the cell wall to the surface. In *S. aureus* LTA, the polyolphosphate backbone comprises 18-50 subunits of 1,3-linked glycerolphosphate, which are tethered to a diglycosyl diacylglycerol (Glc₂-DAG) lipid anchor [45]. The LTAs of *S. epidermidis* also belong to the glycerolphosphate type, but have been reported to be longer than in *S. aureus* [46]. Supplementation with alanine at the 2' hydroxyl group is common in *S. aureus* as well as in *S. epidermidis*. Further glycosylations (e.g. glucose) are possible, but less abundant [47,48].

Not much is known about the specific function of LTAs. Yet, recently a conditionally LTA deficient *S. aureus* mutant became available [49]. The phenotype of this mutant is severely impaired, showing distorted cell shapes and multiple division planes. This is in accordance with previous findings, which suggest a pivotal role for LTAs in binding and positioning of autolysins, key enzymes of the cell division machinery. Fischer *et al.* reported that preincubation of LTAs with autolysins inhibits autolysis. However, this effect was highest for alanine-free LTAs. The increasing content of positively charged alanine substituents compensates the negative charges of the phosphate backbone. As a result, saturation of the extracellularly applied autolysins could not be achieved anymore and the inhibitory activity of the LTAs decreased exponentially [50]. Bierbaum and Sahl pursued the idea that an interaction between autolysins and LTAs might be driven by charge. They could show that autolysins being bound to LTAs can be displaced by addition of cationic peptides [51]. Peschel *et al.* provided further

evidence on this topic by demonstrating that autolysins with cationic C-terminal domains exhibit a higher affinity to cell walls of the alanine devoid *S. aureus* $\Delta dltA$ mutant than to cell walls of the wildtype [52]. However, the molecular details of an interaction between LTAs and autolysins are still not known.

2.2.3. MUREIN HYDROLYZING ENZYMES AND THEIR ROLE IN CELL WALL TURNOVER

Cell division is a complex and in detail not fully understood process that requires the spatial and temporal regulation of cytoplasmatic and extracellular proteins. Briefly, a cell division cycle is started by midcell polymerization of FtsZ, which is conserved in all bacteria (except Chlamydia) and eukaryotic organelles [53]. Polymerized FtsZ forms a ring like structure, the Z-ring, which is tethered to the membrane. Gradual constriction of the Z-ring and simultaneous peptidoglycan synthesis lead to invagination of the septum and finally membrane fusion. At this stage the cells still stick together via newly synthesized PGN. The separation into two daughter cells is then completed by the action of murein hydrolases. In staphylococci the new division plane lies perpendicular to the previous one (Figure 2.4) [31].

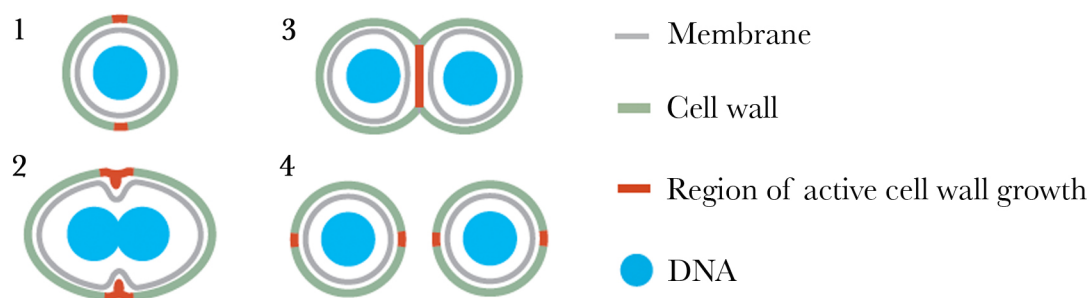


Figure 2.4: Schematic drawing of a cell division cycle in *S. aureus*. **1.** Cell prior to division. **2.** Septum formation due to Z-ring constriction. Simultaneous PGN synthesis. **3.** Membrane fusion. PGN remains contiguous. **4.** Daughter cell separation. Murein hydrolases degrade PGN. Modified from [53].

The structural complexity of PGN, consisting of different glycans, D- and L-amino acids, requires the action of various hydrolases that degrade the cell wall during growth and division. This process, in the course of which PGN is continuously excised

from the cell wall and newly synthesized, is defined as cell wall turnover [54]. In Gram-positive bacteria murein hydrolases can be grouped into four classes according to their enzymatic activities [31]. Figure 2.5 shows the corresponding sites of hydrolysis in the PGN layer.

- Muramidases hydrolyze the glycosidic bond between MurNAc and GlcNAc. Example: Mutanolysin
- Glucosaminidases hydrolyze the glycosidic bond between GlcNAc and MurNAc. Example: AtlE glucosaminidase
- (Endo)Peptidases hydrolyze the amide bonds between amino acids in the peptide stem or the interpeptide bridge. Carboxypeptidases remove the terminal alanine residue from the pentapeptide precursor molecule before its incorporation in the PGN matrix. However, this is not part of the degradation process during cell division. Examples: Lysostaphin, $\phi 11$ hydrolase (LytA-DL)
- (N-Acetylmuramyl-L-alanine) amidases hydrolyze the amide bond between the lactyl moiety of MurNAc and the amino group of the first amino acid in the peptide stem. Examples: AtlE amidase, $\phi 11$ hydrolase (LytA-A)

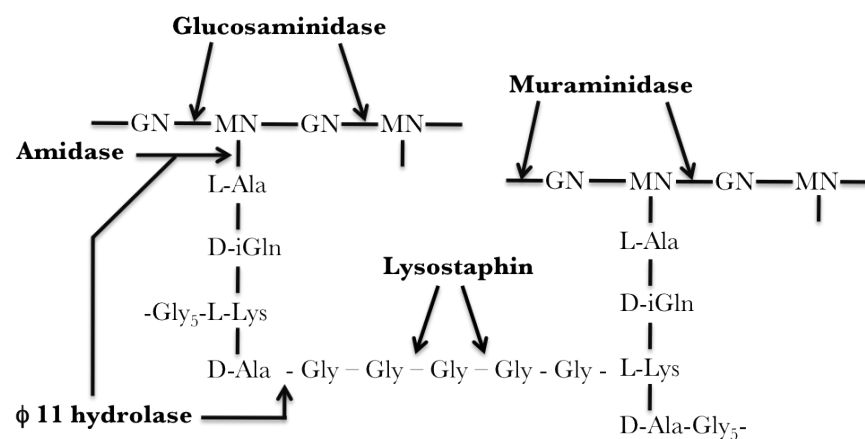


Figure 2.5: Cleavage sites of murein hydrolases in *S. aureus* PGN. Modified from [31].

N-Acetylmuramyl-L-alanine amidases occur widely in bacteria as important enzymes of the cell division machinery. Many species encode several enzymes of the amidase class such as AtlE/Aae (*S. epidermidis*) [15,55] or AmiA-D (*Escherichia coli*) [56,57]. However, the fundamentals for the temporal and spatial coordination of their

activities are not yet fully elucidated. Bacterial amidases are modular enzymes with a catalytic domain being a zinc-dependent metalloenzyme, and a cell wall binding region (CBR) that comprises one or more small, repetitive domains, fused to the N- or C-terminus.

Over the last decade, several structures of the catalytic domains of amidases have been described [58,59,60,61,62]. These revealed that the amidase fold is not only conserved in bacteria, but does also occur in eukaryotes. Peptidoglycan recognition proteins (PGRPs) are pattern recognition molecules that are found both in vertebrates and invertebrates as part of the innate immune system. In insects, PGRPs mainly activate antimicrobial pathways, while mammalian PGRPs are bactericidal by interfering with PGN synthesis. A third group, PGN-hydrolyzing PGRPs, has been found in insects and mammals [63]. Although soluble and membrane-bound variants of PGRPs with different molecular weights exist, all PGRPs possess a domain that closely resembles the bacterial amidase fold. This high degree of conservation depends on the interaction with PGN substrates of high similarity. Although there are species-specific variations of the peptide part, the structure of PGN never shows major deviations from its general schematic.

The amidase repeat domains are biochemically and structurally less well characterized. They likely have a higher structural diversity since possible cell wall associated ligands, such as teichoic acids [50], often have a species- or even strain specific composition [27].

2.2.4. THE ATLE AMIDASE

The major autolysins AtLE (*S. epidermidis*) and AtLA (*S. aureus*) belong to the class of N-Acetylmuramyl-L-alanine amidases (Figure 2.5) that play a pivotal role in the degradation of the bacterial cell wall [64]. They also mediate adhesion to polystyrene surfaces and interact with proteins of the extracellular matrix such as fibronectin and vitronectin [15]. Most recent results also report binding of AtLE to Hsc 70, which may function as a receptor in internalization [65]. During cell division, the major autolysins are responsible for splitting the equatorial septum between two dividing daughter cells [66,67]. Deletion mutants showed a disordered division pattern with large cell clusters and lost their ability to form biofilms [15,64].

AtlE and AtlA exhibit high sequence homology and share the same multidomain structure consisting of the signal peptide (pre-), the pro-peptide, the N-acetylmuramyl-L-alanine amidase, six repeats domains and the C-terminal N-acetylglucosaminidase [15,68] (Figure 2.6). Pre-pro-Atl is secreted and processed extracellularly. Three distinct protein species are generated upon proteolytic cleavage: The mature amidase, the glucosaminidase and the pro-peptide, whose function has not yet been determined. Cleavage between the catalytic domains (AmiE and AmiA, respectively) occurs C-terminal of the fourth repeat. It is worth noting that literature refers to the CBR as three repeats instead of six as mentioned here. However, recent structural data revealed that each of the three repeats can be split into two SH3b (bacterial, SH3 related) domains. Within the CBR, the sequence and structural similarity between every second repeat is higher than between adjacent ones.

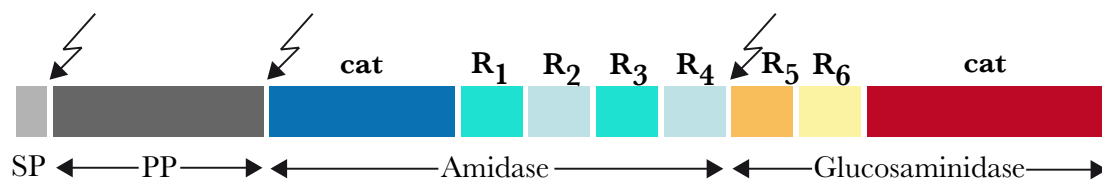


Figure 2.6: Domain arrangement of the bifunctional pre-pro-AtlE. Arrows indicate the post-translational cleavage sites. **SP**, signalpeptide; **PP**, pro-peptide; **cat**, catalytic domain; **R**, repeat domain.

As part of this work, AmiE was structurally characterized [69]. The catalytic domain of the AtlE amidase is a zinc-dependent metalloenzyme that requires a muramylpeptide with at least three amino acids as a PGN minimal motif for hydrolysis. The C-terminal repeats of the amidase domain do not contribute to the lytic activity. However, they are required for anchoring the amidase along the equatorial septum at the future division site [67,68,70]. Lipoteichoic acids have long been discussed as potential ligands on the cell surface [50,51,71]. The work of Yamada *et al.* supported this theory. They demonstrated that the amidase is associated with cellular components protruding from the membrane of *S. aureus* protoplasts (Figure 2.7) [67].

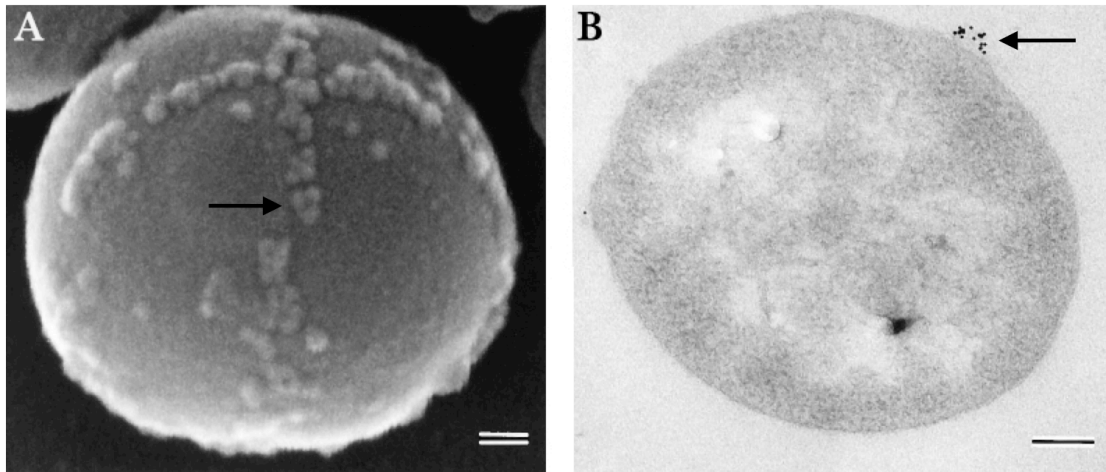


Figure 2.7: Distribution of the AtlA amidase at the surface of an *S. aureus* protoplast determined by gold labeling. Cells were treated with anti-Atl IgG and subsequently with gold-labeled protein A. Arrows indicate the position of the Atl amidase. **(A)** Scanning electron microscopy. **(B)** Transmission electron microscopy; bar=100 nm. Modified from [67].

Recent unpublished results that are part of this work further support the idea that LTAs might serve as anchoring points for the major autolysins AtlE and AtlA. The crystal structure of repeats three and four ($R_{3,4}$) of the CBR reveals distinct and conserved patches of positive charge that would be suitable for accommodating a negatively charged ligand such as LTA. Furthermore, $R_{3,4}$ reveals structural homology to the repeat domains of InlB from *Listeria monocytogenes*, which has been shown to bind to LTAs [72].

2.3. X-RAY CRYSTALLOGRAPHY

The electromagnetic spectrum covers electromagnetic radiation of all wavelengths, including visible light that has a wavelength of 350-750 nm. As light hits an object, diffraction occurs and the object becomes visible to us. However, this applies only to macroscopic and microscopic structures being larger than the wavelength of light. To visualize smaller entities, electromagnetic radiation with a shorter wavelength such as x-rays must be utilized. In x-ray diffraction experiments, macromolecules arranged in a regular array, a crystal lattice, are typically exposed to x-ray radiation in the wavelength of 0.5-2 Å (0.05-0.15 nm), which is well suited to resolve carbon-carbon bonds of 1.5 Å length.

2.3.1. THE PRINCIPLES OF DIFFRACTION

For protein structure determination x-rays are commonly generated with copper anodes, which, upon bombardment with accelerated electrons, emit radiation at specific wavelengths. Since only monochromatic radiation can be used, a filter eliminates the less intense K_{β} -radiation, leaving only K_{α} -radiation with a wavelength of 1.54178 Å. When such an x-ray beam impinges on a molecule, it diffracts by interacting with electrons surrounding the nuclei of the atoms. This gives information about the electron distribution in the molecule, finally resulting in an electron density map. However, a single molecule would be a poor source to obtain useful diffraction data from. It is far too weak a scatterer, letting most x-rays pass through, while the ones being scattered would be barely distinguishable from noise. Furthermore, radiation damage would destroy a single molecule rapidly. A prerequisite for obtaining a protein structure is the growth of crystals of adequate size (50-800 μm), in which a large number of identical molecules are arranged in the same orientation. In this sense, a crystal works as an amplifier by adding up diffraction waves and making them measurable.

The smallest, identical repeating unit in a crystal is the unit cell with three defined axes and three defined angles between them. As a mental construct for understanding the principles of diffraction, one might imagine the unit cell being dissected by sets of evenly spaced planes. These sets of planes are given three numbers according to their intersection points with each cell axis, the *Miller indices* (h,k,l). In the Bragg model of diffraction, diffraction is treated as reflection on such a set of parallel planes. Each set, containing a certain number of atoms i.e. density of electrons, acts hereby as a single diffractor, producing one reflection [73]. X-ray radiation is an electromagnetic wave with an amplitude and a phase. X-rays emerging from different planes can be out of phase and interfere destructively, resulting in a wave with a smaller amplitude or complete extinction. However, some waves add up constructively and produce a reflection. This condition is described in *Bragg's law*, which relates the path difference between two x-rays to a multiple of the utilized wavelength λ [74]. The path difference is hereby dependent on the interplanar lattice spacing d_{hkl} and the angle θ under which the x-rays impinge on successive lattice planes (Figure 2.8, Equation 2.1).

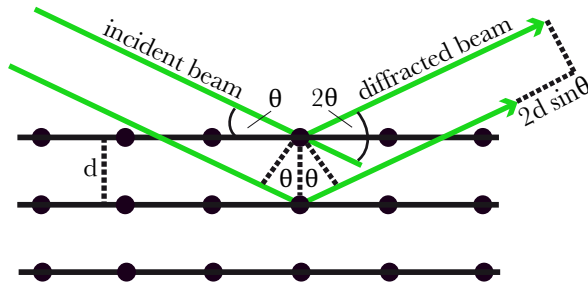


Figure 2.8: Bragg's law. d , distance between lattice planes; θ angle of incidence. Modified from [75].

$$n\lambda = 2d_{hkl}\sin\theta \quad (2.1)$$

The lattice observed upon diffraction is inversely related to the real lattice of the crystal, and therefore called reciprocal lattice. Each lattice point (i.e. reflection) in reciprocal space is linked to a set of parallel, real-space diffraction planes. In reciprocal space Bragg's law can be explained by construction of a reflection sphere with a radius of $1/\lambda$ around the crystal (Figure 2.9 A, B). This sphere is called *Ewald sphere*, after its inventor Paul Peter Ewald [76]. Only reciprocal lattice points that lie on the surface of the Ewald sphere under a given angle θ meet Bragg's law and can be recorded as reflections on a detector. While a crystal is exposed to x-rays, it is constantly rotated on an axis perpendicular to the beam. With the changing angle, more and more reciprocal lattice points fulfil Bragg's law and come in contact with the Ewald sphere. These can then be observed as a typical diffraction image on a detector (Figure 2.9 C).

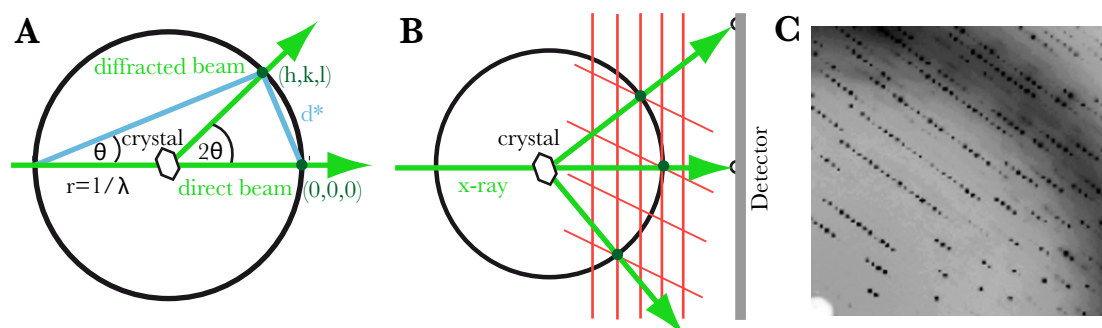


Figure 2.9: The Ewald sphere. (A) Ewald sphere in two-dimensional representation; r , radius of the sphere; λ , x-ray wavelength; (h,k,l) , coordinates of the reflection; $d^*=1/d$. (B) Ewald sphere with intersecting reciprocal lattice (red) and detector. (C) Section of a diffraction image. A, B modified from [75].

From the positions of the recorded reflections, the geometric parameters of the unit cell can be determined. The intensities (I) are directly related to the amplitude of the diffracted wave and contain information about the unit cell content (i.e. the number and structure of the macromolecule). However, a reflection does not contain any phase information. Thus, its structure factor (F), which describes the amplitude and the phase of a diffracted wave, cannot be calculated. This is known as the *phase problem*. The phases have to be obtained in a different process. Only then can an electron density map be calculated by application of a Fourier transformation. A molecular model is then built into this map.

2.3.2. METHODS OF PHASE DETERMINATION

Phases carry the bulk of structural information. They dominate the Fourier synthesis and are therefore a prerequisite for the calculation of an electron density map. However, starting phases obtained from a molecular replacement or derivatized crystals might provide enough information to build a preliminary electron density map that can then be further improved. Initial maps are often difficult to interpret due to errors derived from poorly determined phases.

With more and more protein structures becoming available, molecular replacement is a convenient method to obtain starting phases. It relies on a phase relationship to the diffraction pattern of a similar (>30% sequence identity), already known structure, which can be used as a search probe to fit the position of the target molecule in the unit cell. Generally, molecular replacement is prone to phase bias caused by the phase differences between probe and target.

A second, widely used method to obtain initial phase information is experimental phasing. Experimental phasing is based on intensity differences in the diffraction data of one or more datasets. We distinguish between anomalous/dispersive and isomorphous difference data. The basics of this phasing approach are explained easiest by the latter method, where we deal, in the simplest case, with two datasets derived from two crystals, which have to be isomorphous. This is called *single isomorphous replacement* (SIR). One crystal is native, the other one soaked with a heavy metal compound. The heavy atoms provide an additional source of diffraction and give therefore rise to different reflection intensities in the native (I_p) and derivative

data sets (I_{PH}). The additional heavy atoms can be thought of as a substructure, comprising only a few atoms. The phase of this substructure can therefore be determined separately from intensity differences ($I_{\text{PH}} - I_{\text{P}}$) by using phase independent Patterson functions. The corresponding difference map, then, contains information about the interatomic distances between the substructure atoms, represented as contour peaks. This allows determination of the heavy metal positions in real space and, consequently, calculation of the phase of the structure factor F_{H} . The structure factor of the heavy atom derivative (F_{PH}) is the vector sum of the substructure structure factor (F_{H}) and the structure factor of the native data (F_{P}) (Equation 2.2). Knowing F_{H} , and the reflection intensities I_{PH} and I_{P} makes it then possible to solve the vector equation for F_{P} and to establish the starting phases of the native data.

$$\bar{F}_{\text{PH}} = \bar{F}_{\text{P}} + \bar{F}_{\text{H}} \quad (2.2)$$

The correlation between F_{PH} , F_{P} and F_{H} can be visualized graphically with a *Harker construction* (Figure 2.10). However, the initial phases obtain by SIR are still ambiguous (Figure 2.10 C) and need to be further improved. This can be achieved by narrowing down the phase angle using *density modifications* or *multiple isomorphous replacement* (MIR). The latter method requires the preparation of further derivatives.

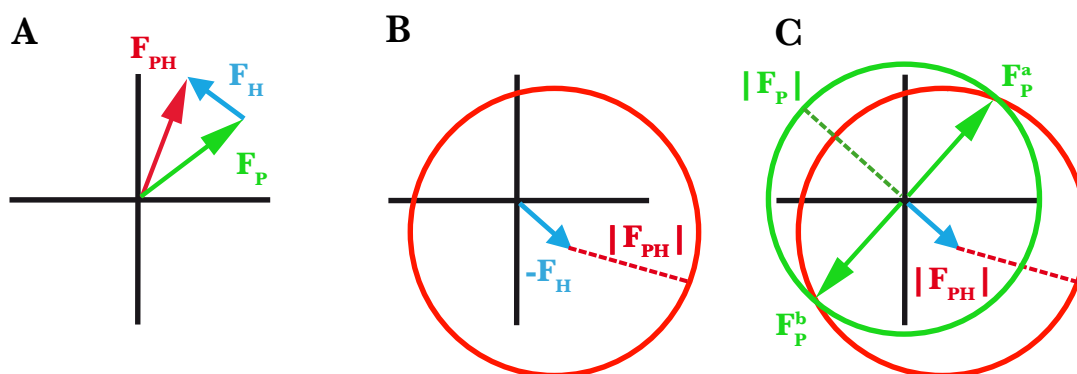


Figure 2.10: Vector diagram (A) and Harker construction (B, C). Vector lengths correspond to reflection intensities, directions to the phase angle. (A) The structure factor F_{PH} for the heavy atom derivative is the sum of contributions from the heavy atom substructure (F_{H}) and the native structure (F_{P}). (B) The phase angle of F_{H} can be determined from the positions of the substructure atoms. All points on the red circle equal the vector sum $|F_{\text{PH}}| - F_{\text{H}}$. (C) Equation (2.2) is fulfilled at points where the green circle, drawn around a possible origin vector $|F_{\text{P}}|$, intersects with the red circle. The solution from a single derivative is ambiguous; the intersections show two possible phase angles of F_{P} . Modified from [73].

The ability of atoms to absorb x-rays displays a second source for intensity differences in diffraction data and can be used in phase determination. Hard x-rays (short wavelength) with a high energy are less likely to be absorbed than low energy, soft x-rays (long wavelength). When an atom absorbs x-rays of a certain wavelength it oscillates, and resonance occurs. Energy transfer is then possible, and an electron can get ejected from one of the atoms shells. This point is called *absorption edge* and specific for every atom. The closer the shell is to the nucleus, the tighter an electron is bound and the higher the energy that is required to eject it. The departing electron leaves a gap in the electron configuration of the respective shell and transfers the atom into an ionized, excited state, which can be relaxed by filling up the gap with an electron from a higher shell. This results in characteristic x-ray emissions.

Especially heavy elements possess several, higher shells and absorption edges in the range of x-ray wavelengths commonly used in diffraction experiments. They are therefore particularly useful in experimental phasing. X-ray emissions at or close to the absorption edge are partially altered in phase. This adds a contribution to the normal, angle-dependent atomic scattering factor: The anomalous, wavelength-dependent scattering factor. As a consequence, *Friedel's law* is violated and *Friedel pairs* are no longer equal in intensity. Friedel pairs are symmetry related (inversion through the origin) Bragg reflections and according to *Friedel's law* equal in intensity and opposite in phase under normal scattering. These anomalous differences are utilized in a *single anomalous diffraction* (SAD) experiment, where diffraction data is collected at the absorption edge of a specific heavy atom present in the crystal. If diffraction data is collected at several wavelengths in a *multiple anomalous diffraction* (MAD) experiment dispersive differences are additionally present. Due to the influence of the wavelength-dependent scattering factor, data collected at, close to and beyond the absorption edge differ in individual reflection intensities.

Anomalous/dispersive difference data can also be used in conjunction with isomorphous difference data to overcome the phase ambiguity. Such combinations are *single isomorphous replacement anomalous signal* (SIRAS) and *multiple isomorphous replacement anomalous signal* (MIRAS).

3. AIMS

Peptidoglycan, the unique component of the bacterial cell wall, is a highly dynamic structure that continuously needs to be degraded and synthesized during bacterial growth and division. Autolysins, such as AtlE from *S. epidermidis* play a pivotal role in this process and therefore display appealing targets for drug design.

At the beginning of this project, functional data on AtlE, which mainly based on characterization of deletion mutants, was already available. It was further known that the AtlE amidase consists of an N-terminal catalytic domain and a CBR, which is necessary for targeting to the septum region. In 2006, the work of Biwas *et al.* revealed crucial insights in the enzymatic function [64]. They determined the exacted PGN cleavage site of AmiE and laid thereby the foundation for further, more detailed investigations of the enzyme-substrate interaction. However, not much was known about an interaction partner of the repeat domains R₁₋₄ that is likely to be present exclusively in the septum region. Lipoteichoic acids were under discussion, but no direct proof had been carried out. Detailed, atomic level information on an enzyme-substrate complex is a prerequisite for the design of specific inhibitors and x-ray crystallography is a suitable tool to gain such insights.

The aim of this work was to define the substrates of the AtlE amidase as well as to determine its crystal structure both alone and in complex with putative interaction partners. The experiments conducted in the course of this thesis, attempted to answer the following questions:

- No structural homologues can be predicted from the primary sequences. What are the tertiary structures of AmiE and R₁₋₄?
- What are the molecular details of AmiE driven PGN hydrolysis? How does the catalytic mechanism work?
- Do teichoic acids bind to R₁₋₄?

- Peptidoglycan and teichoic acids are highly diverse structures. What are key motifs of the ligands, accounting for species-specific recognition?
- The putative interaction partners of the AtlE amidase are polymeric molecules. How can we design ligands suitable for crystallization?
- The AtlE amidase comprises several domains of different function. Do these domains interact? Could this display a mechanism to regulate the enzymatic activity?

Answering these questions will provide the basis for the formulation of a mechanism that contributes to the elucidation of the molecular processes during cell division. Detailed insights into these processes will promote the approach of rational drug design and eventually lead to the development of a new class of antibiotics.

4. RESULTS AND DISCUSSION

4.1. DEVELOPMENT OF A NOVEL FLUORESCENT SUBSTRATE FOR AUTOLYSIN E, A BACTERIAL TYPE II AMIDASE

Lützner N, Pätzold B, Zoll S, Stehle T, Kalbacher H (2009)
Development of a novel fluorescent substrate for Autolysin E, a bacterial type II amidase. *Biochem Biophys Res Commun.* pp. 554-558.

Autolysin activity measurements commonly rely on zymograms, PGN turbidity assays or whole cell lysis assays. These methods are reliable and produce satisfactory results if a qualitative argument regarding presence or absence of activity is required. However, the above methods are time consuming, insensitive and particularly unsuitable for quantification of educt turnover.

Based on the structure of a PGN fragment, a synthetic substrate with the sequence Mca¹-Ala-D-iGln-Lys(Dnp)²-D-Ala-Arg-OH was designed. The fluorophore Mca replaced hereby the disaccharide MurNAc-GlcNAc, which was considered negligible for specific binding based on the previous finding that the GlcNAc moiety is not essential for binding and the MurNAc moiety only engaged in few contacts [77]. Furthermore, disaccharide linked peptides are notoriously difficult to synthesize. The Mca-group is connected to the first amino acid of the peptide stem via an amide bond, thereby mimicking the configuration of the native structure. Internal quenching of the fluorescence is achieved by the Dnp-group, which is located in close vicinity, linked to the ϵ -amino group of lysine. The latter design was chosen for two reasons: Firstly, the proximity to the fluorescence reporter leads to high quenching efficiency and secondly, with the lysine ϵ -amino group also further linked in native PGN, a modification at this position was likely to be tolerated. The arginine present at the C-terminus of the fluorescent substrate is absent in the native form, but had to be added for practical reasons. Initial designs, lacking the terminal arginine, showed good fluorescence, but suffered from low solubility.

¹ (7-Methoxycoumarin-4-yl)-acetyl

² 2,4-dinitrophenyl

This substrate was used in digestion assays together with AmiE, the catalytic domain of the AtlE amidase. Following excitation at 325 nm, enzymatic activity was monitored by fluorescence of the cleaved reporter group at 392 nm. The substrate turnover within a given time frame could then be quantified by the amount of fluorescence emission. An important advantage of the developed fluorescent substrate is its usability in continuous measurements. Such measurements can be conducted in a fast, efficient manner while the turnover of conventional substrates has to be analyzed at distinct time points. This was demonstrated in various assays. A pH profile of AmiE revealed a broad activity range with over 80% residual activity between pH 5.7 and 9. Autolysin E is an extracellular enzyme and has to face changing environmental conditions. A broad tolerance spectrum is therefore mandatory. Further measurements in continuous mode were undertaken with inhibitor substances. EDTA and phenantroline are known zinc-chelating inhibitors of metalloenzymes that completely blocked the activity of AmiE at millimolar concentrations. However, with Benzoyl-Arg-pNO₂-aniline a new type of inhibitor could be identified. A significantly reduced enzymatic activity was already observable at 1 mM, while a ten-fold higher concentration resulted in complete inhibition.

By replacing the sugar moiety and adding a quencher group and a terminal arginine it became clear that AmiE tolerates vast modifications of its natural substrate. To further define the substrate specificity of AmiE, the established fluorescence assay was conducted with several substrate derivatives differing in the composition of their peptide stems. Interestingly, it was found that modifications of the second amino acid have a profound impact on substrate recognition. While changing D-iGln to D-iGlu only resulted in reduced affinity, the presence of a standard glutamine (D-Gln) completely abolished binding. Gram-positive bacteria show many variations in their peptide stem depending on species, strain and environmental conditions. However, (almost) no variations occur at the second position (table 1), rendering the isoform of glutamine one of the most conserved features of PGN. The extended backbone of the isoform is likely to be essential for proper positioning in the active centre of AmiE. Changing it to the standard conformation results in a major structural rearrangement that cannot be tolerated by the enzyme. Surprisingly, substrates with one or two glycine residues, C-terminal of the alanine in the fourth position, were also not recognized by AmiE. Although this arrangement is also present in the native PGN

substrate, it might well be that the enzyme only accepts substrates that were pre-processed in a specific way. Such substrates could have glycine residues attached to the lysine in third position or completely lack the contribution of the interpeptide bridge. Another possible explanation could be that the longer glycine derivatives adopted an unfavorable conformation that prevented recognition by AmiE.

The quenched fluorescent substrate described here is a powerful tool for quantitative, sensitive and fast activity measurements of N-Acetylmuramyl-L-alanine amidases. Its easy modification makes it also particularly useful in screening derivative libraries to test upon enzymatic specificity. However, absolute kinetic parameters obtained with this substrate have to be treated with care due to the named substitutions.

4.2. ROLE OF STAPHYLOCOCCAL WALL TEICHOIC ACID IN TARGETING THE MAJOR AUTOLYSIN ATL

Schlag M, Biswas R, Krismer B, Kohler T, Zoll S, Yu W, Schwarz H, Peschel A, Götz F (2010) Role of staphylococcal wall teichoic acid in targeting the major autolysin Atl. *Molecular Microbiology*. pp. 864-873.

The major autolysins from *S. epidermidis* (AtlE) and *S. aureus* (AtlA) are key enzymes of the cell division machinery and have as such been objects of extensive studies over the last decades. It was shown that autolysins are exclusively present in the septum marking the future division site, and that the C-terminal repeat domains R₁₋₄ are responsible for the targeting [67,70]. However, the mechanisms that underlie these observations have remained unknown.

Teichoic acids have long been discussed as potential interaction partners and regulators of autolysin activity. The WTA deficient *S. aureus* SA113 mutant $\Delta tagO$ therefore displayed a valuable tool for a detailed investigation of autolysin regulation. In comparative cell lysis assays a significantly faster lysis rate was observed for the $\Delta tagO$ mutant after induction of autolysis. Furthermore, the mutant did also reveal significant differences in cell morphology and size compared to the wildtype. In

scanning and transmission electron microscopic images many bobble- and hairy-like protrusions could be observed on the entire surface of the mutant, suggesting a massive degradation of the cell wall. Especially, $\Delta tagO$ cells isolated at later time points after induction of autolysis were showing pronounced phenotypes. The observed phenotypes were consistent with the results from HPLC profiles showing decreased amounts of highly crosslinked PGN in the $\Delta tagO$ mutant. In comparison, the wildtype cell wall appeared to be completely smooth and had a normal degree of crosslinking. These findings lead to the hypothesis that the lack of WTAs in the $\Delta tagO$ mutant might be connected to an increased activity of cell wall degrading enzymes such as autolysins. However, it cannot be ruled out completely that the decreased PGN crosslinking observed in the WTA deficient mutant was a side effect of the knockout.

The question remained whether the increased lysis rate and cell wall degradation observed in the $\Delta tagO$ mutant resulted from a higher susceptibility towards autolysins or a higher binding capacity. To answer this, the binding of externally applied, fluorescence-labeled repeat domains (R₁₋₄) to living cells was investigated. Indeed, a 1.6-fold higher fluorescence emission compared to the wildtype suggested an increased presence of repeats on the cell surface of the WTA deficient mutant. It could be shown that this finding resulted from an altered spatial distribution of the Cy5-labeled repeats. While Cy5-R₁₋₄ clustered in the wildtype, as expected, exclusively in the septum region, the protein was evenly distributed over the entire cell envelope in the WTA deficient mutant. In wildtype *S. aureus* cells, WTAs are ubiquitously present on the surface. This likely prevents autolysins from binding randomly and directs them to the only region that is lacking WTAs, the septum. The same result was obtained with endogenously expressed amidase, which confirmed the hypothesis that targeting of autolysins is based on an avoidance strategy towards WTAs. However, for immunofluorescence detection of the native amidase, protein A deficient mutants (Δspa and $\Delta spa/\Delta tagO$, respectively) had to be used in order to avoid unspecific antibody binding.

Incorporation of WTAs occurs preferentially at sites of high PGN biosynthesis such as the septum at the future division site. This contradicted the hypothesis that septum localization of autolysins is the result of WTA avoidance. To confirm that WTAs are indeed absent in the septum region, localization studies with a fluorescence-labeled

lectin that recognizes teichoic acids were conducted. Unfortunately, the Concanavalin A-fluorescein conjugate (ConA-FITC) binds WTAs as well as LTAs. Therefore, the removal of LTAs by SDS treatment was crucial to obtain conclusive results. ConA-FITC fluorescence visualized the distribution of WTA on the surface of wildtype cells as two crescents with a gap in the septum region. The fluorescence gradually increased then with distance from the septum. These findings clearly confirmed that the septum is either completely devoid of WTAs or exhibits a WTA content that is too low to result in detectable fluorescence. As expected, the ConA-FITC treated $\Delta tagO$ mutant did not show any fluorescence.

The results described here provided for the first time evidence that teichoic acids regulate autolysin activity. However, WTAs do not interact directly with autolysins. They prevent binding of autolysins and thereby direct the enzymes to the WTA-devoid septum. A specific interaction partner is likely to be located here, but still has to be identified.

4.3. STRUCTURAL BASIS OF CELL WALL CLEAVAGE BY A STAPHYLOCOCCAL AUTOLYSIN

Zoll S, Pätzold B, Schlag M, Götz F, Kalbacher H, Stehle, T (2010)
Structural basis of cell wall cleavage by a staphylococcal autolysin. PLoS Pathog. pp. e1000807

Structural information is a prerequisite for a detailed and comprehensive understanding of enzymatic function and the basis for the design of specific inhibitors that can be applied in treatment of infectious diseases. AmiE, the catalytic domain of the major autolysin E was crystallized and its structure determined at 1.7Å resolution. In conjunction with functional studies, the molecular model of AmiE did not only provide crucial insights into the mechanism of PGN recognition and cleavage, but also revealed an unpredicted homology to PGRPs.

AmiE adopts a globular fold with a central, six-stranded β -sheet, surrounded by seven α -helices. The centre of the β -sheet forms the bottom of a large, solvent exposed

groove, which measures about 28 by 10 Å and harbors a zinc ion. The presence of the zinc ion in the centre of this area was visualized by utilizing the anomalous scattering contributions of zinc at a specific wavelength to calculate an anomalous difference Fourier map. A water molecule and the side chains of residues H60, H165 and D179 enclose the zinc ion in a tetrahedral coordination sphere, an arrangement that is common in the active centre of zinc-dependent metalloenzymes. The side chains of H177 and E119 are 4.5 Å and 4.9 Å, respectively, apart from the zinc ion. Both amino acids are not part of the coordination sphere but take over pivotal roles in a probable model of catalysis. Here, the carboxyl-group of the E119 side chain would act as a proton shuttle and facilitate a water-mediated nucleophilic attack on the amide bond between the lactyl moiety of MurNAc and L-Alanine. The protonated side chain of H177 might then serve to stabilize the developing negative charge of the transition state. All amino acids participating in the catalytic cycle cluster in the centre of the solvent exposed groove and are strictly conserved based on a multiple sequence alignment with 28 homologous proteins. Altogether, only 10 out of 213 amino acids in AmiE are strictly conserved. Together with amino acids that possess a lower degree of conservation these residues delineate the entire groove while the remaining surface of AmiE is almost completely devoid of conserved patches. The significantly high conservation of amino acids, the presence of the zinc ion and the overall topology were strong arguments to consider the mentioned groove to be the binding area of a PGN derived substrate. This insight that was later used to define the starting point of a molecular docking approach.

In order to verify the proposed critical roll of the zinc ion in catalysis, inactive mutants of AmiE were generated. The coordinating amino acids H60 and D179 as well as H177 were separately mutated to alanine and the purified proteins subjected to activity tests using PGN lysis assays and zymograms. In comparison to the native enzymes, all three mutations resulted in a loss of activity. This result could be confirmed in *in vivo* studies. The H60A, D179A and H177A mutations were introduced into the pRC20 plasmid that encodes the native amidase and is used to complement the *S. aureus* SA113 Δ atlA mutant. The Δ atlA mutant has a severe growth defect, resulting in large cell clusters that quickly sediment. *S. aureus* cells that carried the H60A and D179A mutation on the complementation plasmid matched the phenotype of the deletion mutant, suggesting that the expressed proteins are not

functional. The H177A mutation had a milder effect *in vivo*. The expressed amidase could partially restore the $\Delta allA$ phenotype to wildtype. The results obtained in *in vitro* and *in vivo* studies clearly confirmed the structure-based postulated roles of amino acids H60, D179 and H177 in the catalytic cycle of AmiE. H60 and D179 are zinc-coordinating residues. Their mutation led to a loss of the zinc-ion and, consequently, to a complete loss of enzymatic activity. H177 is not part of the zinc coordination sphere and its mutation did therefore not result in a loss of the zinc. However, due to its possible role in stabilizing the transition state, the enzymatic function of the H177A mutant was impaired *in vivo*. The *in vitro* assay was most likely not sensitive enough to distinguish between a loss of activity and decelerated reaction kinetics.

The introduction of amino acid mutations may cause conformational changes in a protein. In order to rule out that the lack of activity observed for the mutant enzymes was the result of impaired substrate binding, affinity measurements with biotin-labeled N-acetylmuramyl-L-alanyl-D-iso-glutamyl-L-lysine (Muramyltripeptide, MTP), a PGN-fragment, were conducted. The ELISA assay showed that all catalytically inactive enzymes are still able to recognize a PGN substrate. The H60A and D179A mutants showed a slightly lower affinity to MTP than the native enzyme while binding of the H177A mutant resulted in a higher signal. A possible explanation could be that the absence of the bulky histidine side chain reduced conformational stress on the substrate and thereby allowed for a facilitated binding.

PGN is a large, reticular macromolecule and as such unsuitable for crystallization of an amidase-substrate complex. It was therefore pivotal to define a PGN minimal substrate that is still recognized by AmiE. What are key determinants of binding? It was already known that AmiE does not tolerate a glutamine in a standard conformation at the second position of the peptide stem [78]. The isoform (D-iGln) is essential for binding. However, it could be demonstrated that, besides the specific orientation of the second amino acid, the presence of a third amino acid is crucial for binding. Neither N-acetylmuramyl-L-alanyl-D-iso-glutamine (Muramyl dipeptide, MDP) nor N-acetyl-D-glucosaminyl-(β 1,4)-N-acetylmuramyl-L-alanyl-D-iso-glutamine (Glucosaminyl-muramyl dipeptide, GMDP) were processed as could be judged by HPLC and ESI mass spectrometry. A cleavage product was only detected after incubation with MTP. MTP was not available commercially and had to be synthesized as part of this work.

To further investigate the influence of the side chain of the third amino acid on binding, digestion assays with MTP derivatives were performed. Substrates with one, two or three glycine residues attached to the lysine side chain were prepared as well as a substrate in which the lysine is replaced by an alanine. For each derivative the sugar moiety was replaced by a Mca-group that was known to have little effect on substrate recognition. A Lys-substrate without additional glycines served as a reference. All substrates were cleaved by AmiE. Surprisingly, the Lys-substrate was cleaved significantly faster than the Lys(Gly)_x-substrates, which were all processed equally well. Although the exact number of glycine residues tethered to the amino-group of lysine in a native PGN substrate is not known, the Lys(Gly)_x-substrates matched the native state far better than the charged amino-group present in the Lys-substrate. The additional charge might have led to an artificially enhanced binding that resulted in the increased cleavage rate. The number of glycine residues, however, did not influence the cleavage rate, which pointed to a minor role of the interpeptide bridge in substrate recognition. The Ala-substrate showed the slowest rate of cleavage. In comparison to the Lys(Gly)_x-substrates only half of the educt was cleaved within the same time. The lysine side chain enhanced binding but its absence in the Ala-substrate did not prevent it. This suggested only a minor impact of the lysine side chain on substrate recognition and raised the idea that the main chain atoms of third amino acid could be mainly responsible for key interaction with AmiE.

Molecular docking of MTP supported the findings of the digestion assay and provided further evidence for a crucial role of D-iGln in substrate recognition. In the model, D-iGln forms 6 out of the total 10 hydrogen bonds with the enzyme. Main chain atoms at both ends of the residue as well as side chain atoms are engaged in contacts. Equivalent contacts would not be possible with a standard glutamic acid residue, which stresses the importance of the isoform for substrate recognition. The strictly conserved N112 forms hydrogen bonds to the side chain nitrogen and the two main-chain carbonyl oxygen atoms of D-iGln and L-Lys. N112 is not only structurally conserved in bacterial amidases, but also in all catalytic and non-catalytic PGRPs sharing the amidase fold, which suggests highly similar modes of substrate recognition. In the model, no hydrogen bonds are present between the lysine side chain of the substrate and residues of the AmiE binding groove, supporting the assumption that key interactions are restricted to the main chain atoms of the third amino acid. The

lysine side chain is held in place by van der Waals interactions with the aromatic ring of W105. The model also indicates the possibility for a cation- π bond between the charged ϵ -amino group of the lysine side chain and W105, which would provide an explanation for the enhanced binding of the Lys-substrate observed in the digestion assay.

The structural and functional characterization of AmiE revealed the determinants of enzyme-substrate recognition and established a plausible model of AmiE in complex with a PGN-fragment. However, the data did not explain how species-specific binding of the amidase is ensured. Only a few PGN consensus motifs, present in the cell walls of most bacteria, are required for recognition by AmiE and structurally related proteins. It is therefore likely that a highly selective binding of autolysins is associated with the C-terminal domain R₁₋₄.

4.4. THE STRUCTURAL BASIS OF STAPHYLOCOCCAL CELL WALL RECOGNITION BY SH3B DOMAINS

Zoll S, Schlag M, Götz F, Stehle T. The structural basis of staphylococcal cell wall recognition by SH3b domains. To be published.

Many cell wall associated bacterial enzymes contain small, repetitive domains that target them to specific receptors on the surface [79]. These repeat domains vary in number and orientation relative to the catalytic domains they are attached to [79]. Although being present in a number of well-characterized murein hydrolases, only few structures of repeat domains are available and little is known about their interaction partners [80].

The cell wall binding region of the AtlE amidase comprises four repeat domains that connect C-terminal to the catalytic domain. The sequence and structural similarity between every second repeat is higher than between adjacent ones, which are connected via an extensive network of hydrogen bonds. R_{1,2} and R_{3,4} form tandem-domains and are connected to each other and the catalytic domain via spacers that

are approx. 15 amino acid long. The crystal structure of repeat three and four ($R_{3,4}$) was solved at 2.9 Å. Both domains have a half open beta-barrel conformation and belong to the family of prokaryotic SH3 related domains (SH3b). A superposition of R_3 and R_4 revealed that structural differences are most evident in the loop regions. The structurally conserved β -sheets represent central platforms of the fold and are roofed by the large, projecting RT-loops. Conserved surface patches are present at contact points between the tips of the RT-loops and the central sheets. Interestingly, these areas lie on opposite sites of the protein and show different topologies.

In staphylococci no evidence has been provided for an interaction between amidase repeats and cell wall associated substrates such as LTAs. To address the question whether such interactions occur, binding-impaired mutants of the repeat domains were generated in which putative substrate bindings pockets are inaccessible. These mutants are currently being tested for their ability to attach to staphylococcal cell walls. However, conclusive results from these studies are not yet available.

5. SUMMARY

S. aureus and *S. epidermidis* are among the main causes of nosocomial infections. Treatment of hospital-acquired infections became a challenge since the number of staphylococcus strains with multiple antibiotic resistances increased steadily over the last decades. This emphasized the need for a new class of antibiotics that act on new targets. The major autolysins AtlE and AtlA of *S. epidermidis* and *S. aureus*, respectively, represent such targets. Both enzymes are crucial for cell viability. They take over key roles in cell division where they are responsible for the separation of daughter cells.

The high-resolution structure of AmiE revealed for the first time detailed insights into the enzymatic function of a staphylococcal murein hydrolase and thereby provided the basis for the formulation of a likely mechanism of catalysis. PGN, the substrate of AmiE, is a large, polymeric macromolecule and as such not well suited for crystallization or affinity measurements. Although smaller fragments can be isolated from staphylococcal cell walls, their length and composition is highly dependent on the specific cleavage sites of the different murein hydrolases being used in this process. Furthermore, such purifications may not be completely monodispers. With the synthesis of PGN fluorescent substrates, however, a method was established that offered the possibility to produce substrates of defined length and high purity. Easy modifiability of the synthetic substrates also allowed probing the influence of amino acid substitutions on substrate recognition. In this thesis, a library of synthetic PGN substrates was constructed. The availability of a large range of substrates differing in length and composition of the peptide stem made it possible to define key motifs of PGN. It could be demonstrated that the presence of a third amino acid in the peptide stem as well as the isoform of glutamine in the second position are essential for recognition by AmiE. The carbohydrate moiety and the side chain of the third amino acid play only minor roles. These findings could be confirmed in a docking model. Structural comparisons with other proteins sharing the amidase-fold revealed common features in the substrate grooves, which points to an evolutionary conserved mechanism of PGN recognition.

Contrary to previous assumptions according to which the CBR of the AtlE amidase contained only two repeat domains, the crystal structure of R_{3,4} suggests the presence of four domains that belong to the family of SH3b domains. The sequence and structural similarity between every second repeat in the CBR is higher than between adjacent ones, which are connected via an extensive network of hydrogen bonds. A distinct patch of conserved residues could be located on opposite sides of each repeat in the R_{3,4} molecule. Both patches cover recessed areas with a strong electropositive potential, which might serve as binding pockets for negatively charged ligands such as teichoic acids.

However, WTAs are not interaction partners of the repeat domains. It could be demonstrated that targeting of the AtlE amidase to the septum region is driven by an avoidance strategy towards WTAs, which are absent in this region. In the WTA-deficient *S. aureus* $\Delta tagO$ mutant, binding of autolysins could be observed on the entire cell surface. The spatial distribution of LTAs on staphylococcal cell walls is not known so far. However, based on the position of the LTA synthase LtaS, Schirner *et al.* proposed a septum localization of LTAs for *Bacillus subtilis* [81], a finding that could also apply to Staphylococci. The putative septum localization, the charge complementarities between repeats and LTAs and the fact that binding of LTA was demonstrated for the InlB CBR [72], a structural homologue of the autolysin CBR, are pieces of evidence indicating that LTAs might serve as anchoring points for the major autolysins in the septum. Nevertheless, it has to be clarified if such an interaction would be specific and how autolysins are able to distinguish between molecules that are chemically and structurally as similar as WTAs and LTAs.

6. ZUSAMMENFASSUNG

S. aureus und *S. epidermidis* gehören zu den Haupterregeren nosokomialer Infektionen. Die Behandlung dieser Infektionen wurde in den letzten Jahrzehnten zu einer ernstzunehmenden Herausforderung, da die Zahl multiresistenter Staphylokokkenstämme stetig anstieg. Diese Tatsache betont die Notwendigkeit eine neue Klasse von Antibiotika zu entwickeln welche sich in ihrer Wirkungsweise von bisherigen Präparaten unterscheidet. Die Autolysine AtlE und AtlA von *S. epidermidis* und *S. aureus* übernehmen wichtige Rollen in der Zellteilung und stellen somit mögliche Ansatzpunkte für neue Antibiotika dar.

Die hochauflösende Kristallstruktur von AmiE ermöglichte zum ersten Mal einen detaillierten Einblick in die enzymatische Funktion einer Staphylokokken-Mureinhydrolase. Basierend auf diesen Erkenntnissen konnte ein wahrscheinlicher Katalysemechanismus formuliert werden. Peptidoglykan (PGN), welches von AmiE als Substrat verwendet wird, ist ein polymeres Makromolekül welches sich aufgrund dieser Eigenschaften nicht für die Kristallisation oder Affinitätsmessungen eignet. Obwohl eine Isolierung kleinerer Fragmente aus der Zellwand von Staphylokokken möglich ist, ist die Länge und Zusammensetzung dieser Fragmente von den spezifischen Spaltstellen der Mureinhydrolasen abhängig, die hierfür verwendet werden. Darüber hinaus sind solche Reinigungen nicht vollständig monodispers. Die Synthese von PGN Fluoreszenzsubstraten ermöglichte es hingegen, Substrate definierter Länge und hoher Reinheit herzustellen. Die Modifizierbarkeit dieser Substrate erlaubte es außerdem den Einfluss von Substitutionen im Peptidanteil auf die Substraterkennung zu untersuchen. Im Verlauf dieser Arbeit wurde eine Vielzahl von Substraten synthetisiert welche sich in Länge und Zusammensetzung ihres Peptidanteils unterscheiden. Unter Verwendung dieser Substratderivate konnten schließlich PGN Motive definiert werden die eine Schlüsselposition einnehmen. Es konnte gezeigt werden, dass die Anwesenheit einer dritten Aminosäure im Peptid sowie ein Glutamin-Isomer in der zweiten Position essentiell für die Substraterkennung sind. Der Kohlenhydratanteil und die Seitenkette der dritten Aminosäure sind hingegen von geringerer Bedeutung. Diese Ergebnisse konnten in

einem Docking-Modell bestätigt werden. Strukturelle Vergleiche mit anderen Proteinen welche eine ähnliche Tertiärstruktur aufweisen ließen außerdem gemeinsame Merkmale in der Substrattasche erkennen, was auf einen evolutionär konservierten Mechanismus der PGN Erkennung hindeutet.

Entgegen früheren Annahmen, bezüglich welcher die Zellwandbinderegion (ZBR) der AtlE Amidase nur zwei Repeat Domänen umfasst, lässt die Kristallstruktur von R_{3,4} die Anwesenheit von vier Domänen vermuten, welche zur Familie der SH3b Domänen gehören. Die Aminosäuresequenzen jedes zweiten Repeats in der ZBR sind hierbei ähnlicher zueinander als die Sequenzen benachbarter Repeats, welche miteinander über ein ausgedehntes Wasserstoffbrückennetzwerk verbunden sind. Ein definierter Bereich konservierter Aminosäuren konnte auf einander gegenüberliegenden Seiten jedes Repeat im R_{3,4}-Molekül identifiziert werden. Beide Bereiche liegen in Vertiefungen der Moleküloberfläche und weisen zudem ein hohes, elektropositives Potential auf. Es ist daher denkbar, dass diese Regionen als Bindungstaschen für stark negativ geladene Liganden wie z.B. Teichonsäuren dienen könnten.

Es konnte allerdings gezeigt werden, dass Wandteichonsäuren (WTS) nicht als Interaktionspartner der Repeat-Domänen in Frage kommen. Die zielgerichtete Bindung der AtlE Amidase in der Septumregion ist das Resultat einer Vermeidungsstrategie gegenüber WTS, die in dieser Region fehlen. In der WTS-defizienten *S. aureus* Δ tagO Mutante konnte die Bindung der AtlE Amidase hingegen auf der gesamten Zelloberfläche beobachtet werden. Über die räumliche Verteilung von Lipoteichonsäuren (LTS) auf Staphylokokkenzellwänden ist bisher nichts bekannt. Allerdings schlugen Schirner *et al.*, basierend auf der Position der LTS-Synthase LtaS, eine Septumlokalisation von LTS für *Bacillus subtilis* vor [81]. Eine entsprechende Lokalisierung ist auch in Staphylokokken vorstellbar wo LTS dazu dienen könnten Autolysine in der Teilungsebene zu positionieren. Die Ladungskomplementarität beider Moleküle sowie der Nachweis einer Interaktion zwischen LTS und der Zellwandbinderegion von InlB [72], welche homolog zur ZBR von AtlE ist, unterstützen diese Annahme. Es bleibt jedoch zu klären ob eine Interaktion zwischen Autolysinen und LTS spezifisch ist und wie es Autolysinen gelingt zwischen chemisch und strukturell ähnlichen Molekülen wie WTS und LTS zu differenzieren.

7. REFERENCES

1. Abraham E, Chain E (1940) An enzyme from bacteria able to destroy penicillin. *Nature*. pp. 837.
2. Spink W (1947) Penicillin-resistant staphylococci: mechanisms involved in the development of resistance. *Journal of Clinical Investigation*.
3. Kirby W (1944) EXTRACTION OF A HIGHLY POTENT PENICILLIN INACTIVATOR FROM PENICILLIN RESISTANT STAPHYLOCOCCI. *Science (New York)*.
4. Jevons MP (1961) "Celbenin"-resistant staphylococci. *British Medical Journal*. pp. 124.
5. Hawkey PM (1998) The origins and molecular basis of antibiotic resistance. *BMJ* 317: 657-660.
6. Hiramatsu K, Aritaka N, Hanaki H, Kawasaki S, Hosoda Y, et al. (1997) Dissemination in Japanese hospitals of strains of *Staphylococcus aureus* heterogeneously resistant to vancomycin. *Lancet* 350: 1670-1673.
7. CDC (2002) *Staphylococcus aureus* resistant to vancomycin--United States, 2002. *MMWR Morb Mortal Wkly Rep* 51: 565-567.
8. Zetola N, Francis JS, Nuermberger EL, Bishai WR (2005) Community-acquired methicillin-resistant *Staphylococcus aureus*: an emerging threat. *Lancet Infect Dis* 5: 275-286.
9. Lowy FD (1998) *Staphylococcus aureus* infections. *N Engl J Med* 339: 520-532.
10. Hacker J, Heeseman J (2000) *Molekulare infektionsbiologie: Interaktionen zwischen Mikroorganismen und Zellen: Spektrum Akademischer Verlag*.
11. Kayser FH, Bienz KA, Eckert J, Zinkernagel RM (2001) *Medizinische Mikrobiologie: Georg Thieme Verlag*.
12. O'Gara JP, Humphreys H (2001) *Staphylococcus epidermidis* biofilms: importance and implications. *J Med Microbiol* 50: 582-587.
13. Mack D, Siemssen N, Laufs R (1992) Parallel induction by glucose of adherence and a polysaccharide antigen specific for plastic-adherent *Staphylococcus epidermidis*: evidence for functional relation to intercellular adhesion. *Infect Immun* 60: 2048-2057.
14. Mack D, Nedelmann M, Krokotsch A, Schwarzkopf A, Heesemann J, et al. (1994) Characterization of transposon mutants of biofilm-producing *Staphylococcus epidermidis* impaired in the accumulative phase of biofilm production: genetic identification of a hexosamine-containing polysaccharide intercellular adhesin. *Infect Immun* 62: 3244-3253.
15. Heilmann C, Hussain M, Peters G, Gotz F (1997) Evidence for autolysin-mediated primary attachment of *Staphylococcus epidermidis* to a polystyrene surface. *Mol Microbiol* 24: 1013-1024.
16. Dickinson GM, Bisno AL (1989) Infections associated with indwelling devices: concepts of pathogenesis; infections associated with intravascular devices. *Antimicrob Agents Chemother* 33: 597-601.

17. John SF, Hillier VF, Handley PS, Derrick MR (1995) Adhesion of staphylococci to polyurethane and hydrogel-coated polyurethane catheters assayed by an improved radiolabelling technique. *J Med Microbiol* 43: 133-140.
18. Heilmann C, Schweitzer O, Gerke C, Vanittanakom N, Mack D, et al. (1996) Molecular basis of intercellular adhesion in the biofilm-forming *Staphylococcus epidermidis*. *Mol Microbiol* 20: 1083-1091.
19. Cramton SE, Gerke C, Schnell NF, Nichols WW, Gotz F (1999) The intercellular adhesion (*ica*) locus is present in *Staphylococcus aureus* and is required for biofilm formation. *Infect Immun* 67: 5427-5433.
20. Gerke C, Kraft A, Sussmuth R, Schweitzer O, Gotz F (1998) Characterization of the N-acetylglucosaminyltransferase activity involved in the biosynthesis of the *Staphylococcus epidermidis* polysaccharide intercellular adhesin. *J Biol Chem* 273: 18586-18593.
21. Jarlov JO (1999) Phenotypic characteristics of coagulase-negative staphylococci: typing and antibiotic susceptibility. *APMIS Suppl* 91: 1-42.
22. Tammelin A, Domicel P, Hambræus A, Stahle E (2000) Dispersal of methicillin-resistant *Staphylococcus epidermidis* by staff in an operating suite for thoracic and cardiovascular surgery: relation to skin carriage and clothing. *J Hosp Infect* 44: 119-126.
23. Raad I, Alrahwani A, Rolston K (1998) *Staphylococcus epidermidis*: emerging resistance and need for alternative agents. *Clin Infect Dis* 26: 1182-1187.
24. Villari P, Sarnataro C, Iacuzio L (2000) Molecular epidemiology of *Staphylococcus epidermidis* in a neonatal intensive care unit over a three-year period. *J Clin Microbiol* 38: 1740-1746.
25. Sieradzki K, Roberts RB, Serur D, Hargrave J, Tomasz A (1998) Recurrent peritonitis in a patient on dialysis and prophylactic vancomycin. *Lancet* 351: 880-881.
26. Navarre WW, Schneewind O (1999) Surface proteins of gram-positive bacteria and mechanisms of their targeting to the cell wall envelope. *Microbiol Mol Biol Rev* 63: 174-229.
27. Weidenmaier C, Peschel A (2008) Teichoic acids and related cell-wall glycopolymers in Gram-positive physiology and host interactions. *Nat Rev Microbiol* 6: 276-287.
28. Barnett T (2006) Surface proteins of gram-positive bacteria and how they get there. *Microbiology*.
29. Ghuysen JM, Strominger JL (1963) Structure of the Cell Wall of *Staphylococcus Aureus*, Strain Copenhagen. II. Separation and Structure of Disaccharides. *Biochemistry* 2: 1119-1125.
30. Ghuysen JM, Strominger JL (1963) Structure of the Cell Wall of *Staphylococcus Aureus*, Strain Copenhagen. I. Preparation of Fragments by Enzymatic Hydrolysis. *Biochemistry* 2: 1110-1119.
31. Navarre WW, Schneewind O (1999) Surface proteins of gram-positive bacteria and mechanisms of their targeting to the cell wall envelope. *Microbiol Mol Biol Rev*. pp. 174-229.
32. Vollmer W, Blanot D, de Pedro MA (2008) Peptidoglycan structure and architecture. *FEMS Microbiol Rev* 32: 149-167.
33. Schleifer KH, Kandler O (1972) Peptidoglycan types of bacterial cell walls and their taxonomic implications. *Bacteriol Rev*. pp. 407-477.
34. Tipper DJ, Tomoeda M, Strominger JL (1971) Isolation and characterization of -1,4-N-acetylmuramyl-N-acetylglucosamine and its O-acetyl derivative. *Biochemistry* 10: 4683-4690.

35. Davis KM, Weiser JN Modifications to the peptidoglycan backbone help bacteria to establish infection. *Infect Immun* 79: 562-570.
36. Endl J, Seidl HP, Fiedler F, Schleifer KH (1983) Chemical composition and structure of cell wall teichoic acids of staphylococci. *Arch Microbiol* 135: 215-223.
37. Ward JB (1981) Teichoic and teichuronic acids: biosynthesis, assembly, and location. *Microbiol Rev* 45: 211-243.
38. Neuhaus F, Baddiley J (2003) A Continuum of Anionic Charge: Structures and Functions of D-Alanyl-Teichoic Acids in Gram-Positive Bacteria. *Microbiol Mol Biol Rev.* pp. 686.
39. Sanderson AR, Strominger JL, Nathenson SG (1962) Chemical structure of teichoic acid from *Staphylococcus aureus*, strain Copenhagen. *J Biol Chem* 237: 3603-3613.
40. Sadvovskaya I, Vinogradov E, Li J, Jabbouri S (2004) Structural elucidation of the extracellular and cell-wall teichoic acids of *Staphylococcus epidermidis* RP62A, a reference biofilm-positive strain. *Carbohydr Res* 339: 1467-1473.
41. Peschel A, Otto M, Jack R, Kalbacher... H (1999) Inactivation of the *dlt* Operon in *Staphylococcus aureus* Confers Sensitivity to Defensins, Protegrins, and Other Antimicrobial Peptides. *Journal of biological ...*
42. Weidenmaier C, Kokai-Kun J, Kristian... S (2004) Role of teichoic acids in *Staphylococcus aureus* nasal colonization, a major risk factor in nosocomial infections. *Nature medicine.*
43. Schlag M, Biswas R, Krismer B, Kohler T, Zoll S, et al. (2010) Role of staphylococcal wall teichoic acid in targeting the major autolysin Atl. *Molecular Microbiology.* pp. 864-873.
44. Novick RP (1991) Genetic systems in staphylococci. *Methods Enzymol* 204: 587-636.
45. Duckworth M, Archibald AR, Baddiley J (1975) Lipoteichoic acid and lipoteichoic acid carrier in *Staphylococcus aureus* H. *FEBS Lett* 53: 176-179.
46. Lambert P, Worthington T, Tebbs S, Elliott T (2000) Lipid S, a novel *Staphylococcus epidermidis* exocellular antigen with potential for the serodiagnosis of infections. *FEMS Immunology & Medical Microbiology.* pp. 195-202.
47. Knox KW, Wicken AJ (1973) Immunological properties of teichoic acids. *Bacteriol Rev* 37: 215-257.
48. Wicken AJ, Knox KW (1975) Lipoteichoic acids: a new class of bacterial antigen. *Science* 187: 1161-1167.
49. Gründling A, Schneewind O (2007) Synthesis of glycerol phosphate lipoteichoic acid in *Staphylococcus aureus*. *Proceedings of the National ...*
50. Fischer W, Rosel P, Koch HU (1981) Effect of alanine ester substitution and other structural features of lipoteichoic acids on their inhibitory activity against autolysins of *Staphylococcus aureus*. *J Bacteriol* 146: 467-475.
51. Bierbaum G, Sahl HG (1985) Induction of autolysis of staphylococci by the basic peptide antibiotics Pep 5 and nisin and their influence on the activity of autolytic enzymes. *Arch Microbiol.* pp. 249-254.
52. Peschel A, Vuong C, Otto M, Gotz F (2000) The D-alanine residues of *Staphylococcus aureus* teichoic acids alter the susceptibility to vancomycin and the activity of autolytic enzymes. *Antimicrob Agents Chemother* 44: 2845-2847.

-
53. Goehring NW, Beckwith J (2005) Diverse paths to midcell: assembly of the bacterial cell division machinery. *Curr Biol* 15: R514-526.
54. Doyle RJ, Chaloupka J, Vinter V (1988) Turnover of cell walls in microorganisms. *Microbiol Rev* 52: 554-567.
55. Heilmann C, Thumm G, Chhatwal GS, Hartleib J, Uekotter A, et al. (2003) Identification and characterization of a novel autolysin (Aae) with adhesive properties from *Staphylococcus epidermidis*. *Microbiology* 149: 2769-2778.
56. Heidrich C, Templin MF, Ursinus A, Merdanovic M, Berger J, et al. (2001) Involvement of N-acetylmuramyl-L-alanine amidases in cell separation and antibiotic-induced autolysis of *Escherichia coli*. *Mol Microbiol* 41: 167-178.
57. Uehara T, Park JT (2007) An anhydro-N-acetylmuramyl-L-alanine amidase with broad specificity tethered to the outer membrane of *Escherichia coli*. *J Bacteriol* 189: 5634-5641.
58. Cheng X, Zhang X, Pflugrath JW, Studier FW (1994) The structure of bacteriophage T7 lysozyme, a zinc amidase and an inhibitor of T7 RNA polymerase. *Proc Natl Acad Sci USA*. pp. 4034-4038.
59. Guan R, Wang Q, Sundberg EJ, Mariuzza RA (2005) Crystal structure of human peptidoglycan recognition protein S (PGRP-S) at 1.70 Å resolution. *J Mol Biol* 347: 683-691.
60. Kim M-S, Byun M, Oh B-H (2003) Crystal structure of peptidoglycan recognition protein LB from *Drosophila melanogaster*. *Nat Immunol*. pp. 787-793.
61. Low LY, Yang C, Perego M, Osterman A, Liddington RC (2005) Structure and lytic activity of a *Bacillus anthracis* prophage endolysin. *J Biol Chem* 280: 35433-35439.
62. Kerff F, Petrella S, Mercier F, Sauvage E, Herman R, et al. (2010) Specific Structural Features of the N-Acetylmuramoyl-L-Alanine Amidase AmiD from *Escherichia coli* and Mechanistic Implications for Enzymes of This Family. *Journal of Molecular Biology*. pp. 249-259.
63. Liu C, Xu Z, Gupta D, Dziarski R (2001) Peptidoglycan recognition proteins: a novel family of four human innate immunity pattern recognition molecules. *J Biol Chem*. pp. 34686-34694.
64. Biswas R, Voggu L, Simon UK, Hentschel P, Thumm GN, et al. (2006) Activity of the major staphylococcal autolysin Atl. *FEMS Microbiology Letters*. pp. 260-268.
65. Hirschhausen N, Schlesier T, Schmidt MA, Götz F, Peters G, et al. (2010) A novel staphylococcal internalization mechanism involves the major autolysin Atl and heat shock cognate protein Hsc70 as host cell receptor. *Cellular Microbiology*. pp. 1746-1764.
66. Hobot JA, Rogers HJ (1991) Intracellular location of the autolytic N-acetylmuramyl-L-alanine amidase in *Bacillus subtilis* 168 and in an autolysis-deficient mutant by immunoelectron microscopy. *J Bacteriol* 173: 961-967.
67. Yamada S, Sugai M, Komatsuzawa H, Nakashima S, Oshida T, et al. (1996) An autolysin ring associated with cell separation of *Staphylococcus aureus*. *J Bacteriol* 178: 1565-1571.
68. Oshida T, Sugai M, Komatsuzawa H, Hong YM, Suginaka H, et al. (1995) A *Staphylococcus aureus* autolysin that has an N-acetylmuramoyl-L-alanine amidase domain and an endo-beta-N-acetylglucosaminidase domain: cloning, sequence analysis, and characterization. *Proc Natl Acad Sci U S A* 92: 285-289.
69. Zoll S, Pätzold B, Schlag M, Götz F, Kalbacher H, et al. (2010) Structural basis of cell wall cleavage by a staphylococcal autolysin. *PLoS Pathog*. pp. e1000807.

-
70. Baba T, Schneewind O (1998) Targeting of muralytic enzymes to the cell division site of Gram-positive bacteria: repeat domains direct autolysin to the equatorial surface ring of *Staphylococcus aureus*. *EMBO J*. pp. 4639-4646.
 71. Bierbaum G, Sahl HG (1987) Autolytic system of *Staphylococcus simulans* 22: influence of cationic peptides on activity of N-acetylmuramoyl-L-alanine amidase. *J Bacteriol*. pp. 5452-5458.
 72. Jonquières R, Bierne H, Fiedler F, Gounon P, Cossart P (1999) Interaction between the protein InlB of *Listeria monocytogenes* and lipoteichoic acid: a novel mechanism of protein association at the surface of Gram-positive bacteria. *Molecular Microbiology*. pp. 902-914.
 73. Rhodes G (2006) *Crystallography Made Crystal Clear - A Guide For Users Of Macromolecular Models*: Academic Press.
 74. Bragg W (1912) The Specular Reflection of X-rays. *Nature*.
 75. Kirchner E (2009) Structural and functional studies of the reovirus attachment protein $\sigma 1$ and its interaction with the receptor JAM-A: Eberhard-Karls-Universität Tübingen. 1-111 p.
 76. Ewald P (1969) Introduction to the dynamical theory of X-ray diffraction. *Acta Crystallographica Section A: Crystal Physics, Diffraction, Theoretical and General Crystallography*. pp. 103-108.
 77. Guan R, Roychowdury A, Ember B, Kumar S, Boons G-J, et al. (2005) Crystal structure of a peptidoglycan recognition protein (PGRP) in complex with a muramyl tripeptide from Gram-positive bacteria. *J Endotoxin Res*. pp. 41-46.
 78. Lützner N, Pätzold B, Zoll S, Stehle T, Kalbacher H (2009) Development of a novel fluorescent substrate for Autolysin E, a bacterial type II amidase. *Biochem Biophys Res Commun*. pp. 554-558.
 79. Vollmer W, Joris B, Charlier P, Foster S (2008) Bacterial peptidoglycan (murein) hydrolases. *FEMS Microbiology Reviews*. pp. 259-286.
 80. Xu Q, Sudek S, McMullan D, Miller MD, Geierstanger B, et al. (2009) Structural basis of murein peptide specificity of a gamma-D-glutamyl-L-diamino acid endopeptidase. *Structure*. pp. 303-313.
 81. Schirner K, Marles-Wright J, Lewis RJ, Errington J (2009) Distinct and essential morphogenic functions for wall- and lipo-teichoic acids in *Bacillus subtilis*. *The EMBO Journal*. pp. 830.

8. APPENDIX

8.1. PUBLICATIONS

Discussed publications

Lützner N, Pätzold B, Zoll S, Stehle T, Kalbacher H (2009) Development of a novel fluorescent substrate for Autolysin E, a bacterial type II amidase. *Biochem Biophys Res Commun.* pp. 554-558

Schlag M, Biswas R, Krismer B, Kohler T, Zoll S, Yu W, Schwarz H, Peschel A, Götz F (2010) Role of staphylococcal wall teichoic acid in targeting the major autolysin Atl. *Molecular Microbiology.* pp. 864-873.

Zoll S, Pätzold B, Schlag M, Götz F, Kalbacher H, Stehle, T (2010) Structural basis of cell wall cleavage by a staphylococcal autolysin. *PLoS Pathog.* pp. e1000807

Zoll S, Schlag M, Götz F, Stehle T. The structural basis of staphylococcal cell wall recognition by SH3b domains. To be published.

Other publications

Zoll S, Pätzold B, Schlag M, Götz F, Stehle T (2008) The crystal structure of the staphylococcal amidase AmiE reveals the active site of a metalloenzyme. *Acta crystallographica Section A.* pp. C269

8.2. ACKNOWLEDGMENTS

Thilo Stehle danke ich für die Bereitstellung der notwendigen finanziellen Mittel, die enormen Freiheiten bei der Gestaltung meines Projektes und für stets amüsante und unvergessliche Laborausflüge.

Friedrich Götz danke ich für die Übernahme der Zweitkorrektur meiner Arbeit und für eine stets gute Zusammenarbeit während der vergangenen Jahre.

Martin Schlag möchte ich ebenfalls für die gute Zusammenarbeit während des gesamten „Projekts Autolysin E“ danken.

Berni, alter Spanier, du warst ein Super-Diplomand und der beste Beweis dafür, dass man produktiv zusammenarbeiten und trotzdem unglaublich viel Spaß dabei haben kann. Vamos a tomar una cerveza. Salud!

David, I could have never done it without you!

Dirk, Ich werde niemals unsere nächtlichen Kochveranstaltungen, unseren Griechenlandurlaub und all die unzähligen anderen Dinge vergessen die wir zusammen erlebt haben.

Zaigham, I always enjoyed our conversations about pakistani politics and dinner at your flat. Thanks to you I know now how good mangos can really taste!

Allen anderen ehemaligen und derzeitigen Labormitgliedern, insbesondere Eva, Marco, Niko, JoBa, Volker, Karo, Kerstin, Luisa, Yinglan, Bärbel, Ricky und den Dotd-girls danke ich für viele witzige Stunden auch außerhalb des Labors.

Basti und Magnus, ihr seid tolle Freunde und ich freue mich wirklich dass wir auch nach Marburg in Kontakt geblieben sind. Basti, Dir danke ich besonders dafür das ich mich immer bei Dir in Strasbourg verstecken konnte, wenn Tübingen mal wieder unerträglich wurde.

Hanna, thanks to you everything turned out well in the end. Me koos avastavad maailma!

Meinen Eltern möchte ich für ihre immerwährende Unterstützung in den vergangenen Jahren danken.

Meiner WG danke ich vor allem für allzeit nette Gespräche zwischendurch, die mich sehr oft vom harten Laboralltag ablenken konnten.



Development of a novel fluorescent substrate for Autolysin E, a bacterial type II amidase

Nicolas Lützner^{a,1}, Bernhard Pätzold^{a,1}, Sebastian Zoll^a, Thilo Stehle^{a,b}, Hubert Kalbacher^{a,c,*}

^a Interfaculty Institute for Biochemistry, University of Tübingen, Ob dem Himmelreich 7, 72074 Tübingen, Germany

^b Department of Pediatrics, Vanderbilt University School of Medicine, Nashville, TN, USA

^c Medical and Natural Sciences Research Centre, University of Tübingen, Germany

ARTICLE INFO

Article history:

Received 13 January 2009

Available online 29 January 2009

Keywords:

Staphylococcus epidermidis

Biofilms

Peptidoglycan

Biomaterial-related infection

Antibiotics

Amidase enzyme assay

N-acetylmuramoyl-*L*-alanine amidase

Autolysin E (EC 3.5.1.28)

ABSTRACT

The bifunctional Autolysin E from *Staphylococcus epidermidis*, contains a Zn²⁺-dependent *N*-acetylmuramoyl-*L*-alanine amidase AmiE (EC 3.5.1.28). This enzyme hydrolyzes the amide bond between the carbohydrate chain and the peptide stem of bacterial peptidoglycan. Since peptidoglycan is the major component of bacterial cell walls, type II amidases like Autolysin E play an essential role in the bacterial life cycle. Therefore bacterial amidases are appropriate drug targets in the development of antibiotics. The drug discovery process relies on sensitive enzyme assay systems to test possible lead candidates for enzyme inhibition. However, specific determination of bacterial amidase activity is complicated because a simple and accurate enzyme assay is currently unavailable. In this study we developed a sensitive fluorescent substrate for the type II amidase Autolysin E from *S. epidermidis*, which is suitable for quantifying amidase activity in a high throughput compatible fashion. Using derivatives of the substrate Mca-Ala-D-isoGln-Lys(Dnp)-D-Ala-Arg-OH, we were further able to characterize the amidase substrate specificity of Autolysin E.

© 2009 Elsevier Inc. All rights reserved.

Introduction

Since the discovery of Penicillin in the year 1928, antibiotics became quickly one of the major weapons in the fight against bacterial infections. However, bacteria have become resistant to some of these antibiotics and there are a large number of multi-resistant bacteria strains today. The first *Staphylococci* strains being resistant to antibiotics were discovered in 1968 [1,2] and are now frequently found in hospitals. Especially *Staphylococcus epidermidis* is the cause for complicated infections after implantation of artificial prostheses, central venous catheters, pacemakers and cerebrospinal fluid shunts [3]. One reason for this is its ubiquitous presence on human skin, another is its ability to adhere to biomaterials and form stable biofilms [4–6]. In microbial biofilms adherent bacteria are encased by a polymeric matrix, which protects them from antibiotic action and from the immune system. Therefore, treatment of a bacterial infection is extremely difficult when a biofilm has been formed. Cells lacking type II amidases like Autolysin E

(AtIE), or its homolog Autolysin A from *Staphylococcus aureus*, form large clusters and are hindered in biofilm formation [7]. This supports not only a specific role of AtIE in proliferation and primary adhesion, but also validates AtIE as an appropriate drug target.

AtIE is the major peptidoglycan hydrolase from *S. epidermidis* and comprises a signal peptide, a pro-peptide, an amidase domain (AmiE), which is linked by three consecutive repeat domains to a glucosaminidase domain [9]. AmiE is a Zn²⁺-dependent *N*-acetylmuramoyl-*L*-alanine amidase, an enzyme that is involved in bacterial cell wall metabolism. Polymeric peptidoglycans are the main compounds of the bacterial cell wall, consisting of alternating *N*-acetylglucosamine and *N*-acetylmuramic acid glycan chains, which are cross-linked via short peptide stems. The carboxyl group of *N*-acetylmuramic acid forms an amide bond with the *L*-Ala residue of the peptide stem [8]. This amide bond is hydrolyzed by type II amidases like AtIE.

Although bacterial type II amidase inhibitors have been proposed as antibacterial agents and the drug discovery process relies on sensitive enzyme assay systems, specific determination of bacterial amidase activity is complicated because a simple and accurate enzyme assay is currently not available. Known substrates, like peptidoglycan itself or disaccharide linked peptides, are difficult to synthesize and purify. Moreover, they do not offer the possibility of a continuous measurement, and are therefore not high throughput compatible. This prohibits the screening of large compound libraries. In this study we present for the first time such an

Abbreviations: AmiE, amidase domain of Autolysin E; AtIE, Autolysin E; Dnp, 2,4-dinitrophenyl; Mca, 7-methoxycoumarin-4-yl-acetyl

* Corresponding author. Address: Interfaculty Institute for Biochemistry, University of Tübingen, Ob dem Himmelreich 7, 72074 Tübingen, Germany. Fax: +49 7071 294507.

E-mail address: kalbacher@uni-tuebingen.de (H. Kalbacher).

URL: <http://www.kalbacher.uni-tuebingen.de> (H. Kalbacher).

¹ These two authors contributed equally to this work.

assay system, allowing the quantification of amidase activity and inhibitory effects in a high throughput compatible fashion. The newly designed fluorescent substrate is based on the sequence Mca-Ala-D-isoGln-Lys(Dnp)-D-Ala-Arg-OH, which shows a single cleavage site between Mca and Ala. The fluorescence of the N-terminal Mca is quenched by the Dnp group. Such internally quenched fluorescent substrates are normally used to study protease activity [10], but have never been used to study amidase activity. Using derivatives of the described substrate and determining their kinetic constants, we were further able to characterize the amidase substrate specificity of AtlE. We find that the sugar part of peptidoglycan-like substrates is not essential for the amidase activity of AtlE and could therefore be replaced by the fluorescent Mca group. On the other hand, amino acid substitutions and extension of the substrate length result in complete blockade of the hydrolysis.

Materials and methods

Substrate synthesis: Chemicals were obtained from commercial suppliers and used without further purification. All peptides were synthesized by a solid-phase technique, using the fluoren-9-ylmethoxycarbonyl (Fmoc) strategy on a Syro II synthesizer (MultiSynTech, Witten, Germany). Fmoc-amino acids were purchased from Novabiochem (San Diego, CA, USA), from MultiSynTech or from Iris Biotech (Marktredwitz, Germany). Mca was from Sigma (Deisenhofen, Germany). 2-(1H-benzotriazole-1-yl)-1,1,3,3-tetramethyluronium-tetrafluoroborat (TBTU) and 1-hydroxybenzotriazole (HOBt) were from MultiSynTech. The final deprotected peptides were purified by semi-preparative reversed phase (RP) HPLC, using a Reprisil C-8 column (5 μ m particle size, 150 \times 10 mm) from Dr. Maisch GmbH (Tuebingen, Germany) and a two solvent system: (A) 0.055% (v/v) trifluoroacetic acid (TFA) in water and (B) 0.05% (v/v) TFA in 80% (v/v) ACN in water. Purity and molecular mass of the collected fractions was analysed by matrix-assisted laser-desorption ionization-MS (MALDI-MS), using a MALDI time-of-flight system (Reflex IV, Bruker Daltonics, Bremen, Germany). Substrates were dissolved in DMSO and stored as 2 mM stock solutions at -20°C .

Expression and purification of the Autolysin E amidase domain: The fragment encoding the catalytic amidase domain AmiE residues 302–515 of the AtlE gene was cloned in the pGEX-4T-3 vector (Invitrogen). The *Escherichia coli* strain BL21(DE3) (Invitrogen) was used as expression host. AmiE was expressed under control of the lac promoter as a fusion protein in frame with an N-terminal GST-Tag. After overexpression and lysis, the enzyme was immobilized onto a GST-column (GE Healthcare), cleaved on column using thrombin (GE Healthcare) and further purified using a Superdex 75 gel filtration column (GE Healthcare). Washing and gel filtration was performed with 50 mM Tris/HCl at pH 8.0 with 150 mM NaCl. During lysis of the bacteria 1 mM PMSF was added to the gel filtration buffer.

Continuous fluorescent enzyme assays: The substrate Mca-Ala-D-isoGln-Lys(Dnp)-D-Ala-Arg-OH at a concentration of 20 μ M was processed by 5.2 μ M Autolysin E in digestion buffer (50 mM sodium phosphate buffer, pH 7.2, containing 5 mM zinc acetate) at 37 $^{\circ}\text{C}$. Formation of the fluorescent product was recorded over 4 h, using a fluorimeter (SLT Spectra Fluor, Tecan, Crailsheim, Germany) run in kinetic mode at 37 $^{\circ}\text{C}$ ($\lambda_{\text{ex}} = 340$ nm, $\lambda_{\text{em}} = 405$ nm). The final DMSO concentration in the reaction mixture was 1%. All experiments were performed in triplicates.

Determination of kinetic constants: Substrates at ten different concentrations between 1 and 200 μ M were processed by 5.2 μ M AmiE in digestion buffer at 37 $^{\circ}\text{C}$ as described above. After 1 h, the reaction was stopped by adding TFA to a final concentration of 1%. The reaction mixtures were analysed by analytical RP-HPLC,

using a binary HPLC system (Shimadzu, Tokyo, Japan) with an SPD-10AV UV/vis detector (Shimadzu), an RF-10AxI fluorescence detector (Shimadzu), a Reprisil C-8 column (5 μ m particle size, 150 \times 2 mm) from Dr. Maisch GmbH (Tuebingen, Germany) and a two solvent system: (A) 0.055% (v/v) trifluoroacetic acid (TFA) in water and (B) 0.05% (v/v) TFA in 80% (v/v) ACN in water. The product concentration after 1 h was quantified by fluorescence emission of the N-terminal Mca at 392 nm, following excitation at 325 nm. The molar product concentration was calculated by multiplying the fluorescent peak area of the N-terminal Mca-fragment with a proportional factor, which was calculated based on a Mca standard curve. The kinetic parameters K_m and V_{max} were calculated by nonlinear regression based on the Michaelis–Menten function using the EK13 software version 1.3 (Wiley-VCH, Weinheim, Germany) which uses the regression analysis described in [11]. All experiments were performed in triplicates.

Results and discussion

Design and properties of the fluorescent substrate

While the glycan chains of peptidoglycan are mostly conserved among different bacterial species, they vary in peptide stem composition and crosslinking. Peptidoglycan, the natural substrate of

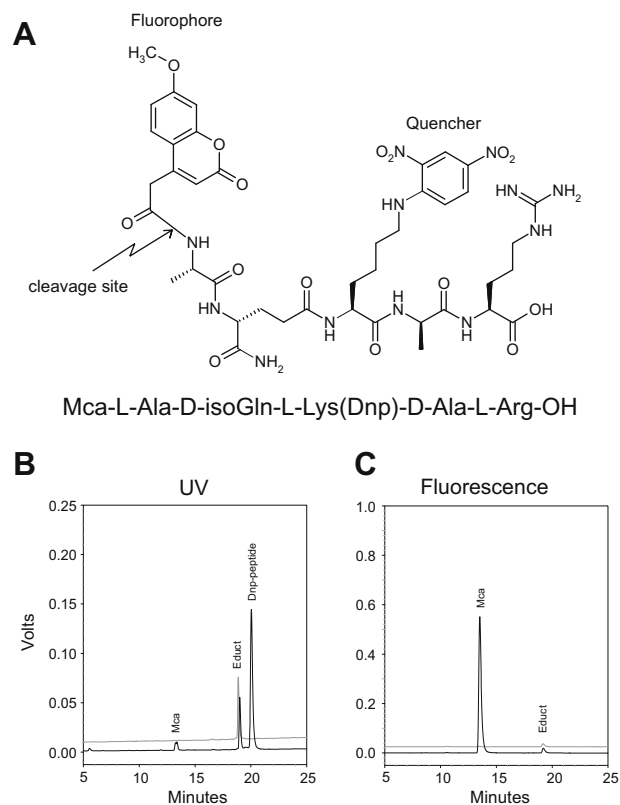


Fig. 1. (A) Structure of the novel Autolysin E amidase substrate Mca-Ala-D-isoGln-Lys(Dnp)-D-Ala-Arg-OH. The fluorescence of the N-terminal Mca group is quenched by the side chain attached Dnp group. Amidase enzyme activity can be detected by hydrolysis induced increase in Mca-fluorescence emission. (B and C) HPLC analysis of the substrate at a concentration of 20 μ M after incubation with 5.2 μ M AmiE for 1 h in digestion buffer at pH 7.2 and 37 $^{\circ}\text{C}$. Digestion products were detected by their UV absorbance at 220 nm (B) and their fluorescence emission at 392 nm following excitation at 325 nm (C). Black lines represent the chromatograms of the digestion mixtures, while grey lines are chromatograms of the undigested negative controls. The fragments Mca (Mca) and Ala-D-isoGln-Lys(Dnp)-D-Ala-Arg-OH (Dnp-Peptide) are generated by the AmiE catalyzed hydrolysis of the substrate Mca-Ala-D-isoGln-Lys(Dnp)-D-Ala-Arg-OH (Educt).

AmiE is divided into two major classes, the meso-diaminopimelic acid type and the Lys-type peptidoglycan, depending on the third residue of the peptide stem. Because cell walls of all known *staphylococci* strains contain Lys-type peptidoglycan, we used the Lys-type peptide stem as a scaffold to design a fluorescent substrate. X-ray structures from homologous proteins like the peptidoglycan recognition proteins [12–16] helped us to identify general peptidoglycan substrate recognition patterns. In naturally occurring peptidoglycan of *S. epidermidis* the ϵ -amino group of the lysine is connected to a pentaglycine bridge. According to the structural data available this glycine bridge is directed to the outside of the protein. Therefore, a modification of this part of the peptide, like the linkage of the Dnp group to the ϵ -amino group of the lysine, should be tolerated. We further replaced the sugar moiety of natural peptidoglycan by Mca, which is used as a fluorescent reporter. Mca has a kink similar to that of muramic acid after the amide bond, connecting it to the peptide stem and therefore was an ideal replacement for the sugar moiety.

Based on these conclusions we synthesized the tetrapeptide Mca-Ala-D-isoGln-Lys(Dnp)-D-Ala. Although this substrate showed a strong fluorescence signal when incubated with AmiE, its solubility and ionization properties in MALDI and ESI-MS were low. To improve these properties we added an additional Arg residue at the C-terminus. This novel substrate Mca-Ala-D-isoGln-Lys(Dnp)-D-Ala-Arg-OH, exhibited excellent solubility and ionization in mass

spectrometry. It has a single cleavage site between Mca and Ala and the fluorescence of the N-terminal Mca group is quenched by the Dnp group (Fig. 1A). The close proximity between Mca and Dnp results in a very high quenching efficiency, providing a very low fluorescent background emission. As shown by HPLC analyses, the fluorescent light emission of the undigested educt is drastically reduced compared to free Mca (Fig. 1C). While the educt is clearly visible in the UV spectra, it yields only a small peak

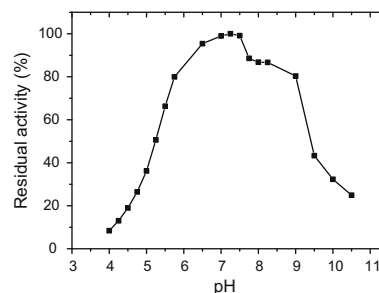


Fig. 3. pH activity profile of AmiE. Initial velocities of AmiE catalyzed Mca-Ala-D-isoGln-Lys(Dnp)-D-Ala-Arg-OH hydrolysis at 37 °C and a concentration of 20 μ M in 50 mM buffer were determined by a continuous fluorescence measurement. Buffers used were sodium acetate (pH 4–5.75), sodium phosphate (pH 6.5–8.25) and glycine (pH 9.0–10.5).

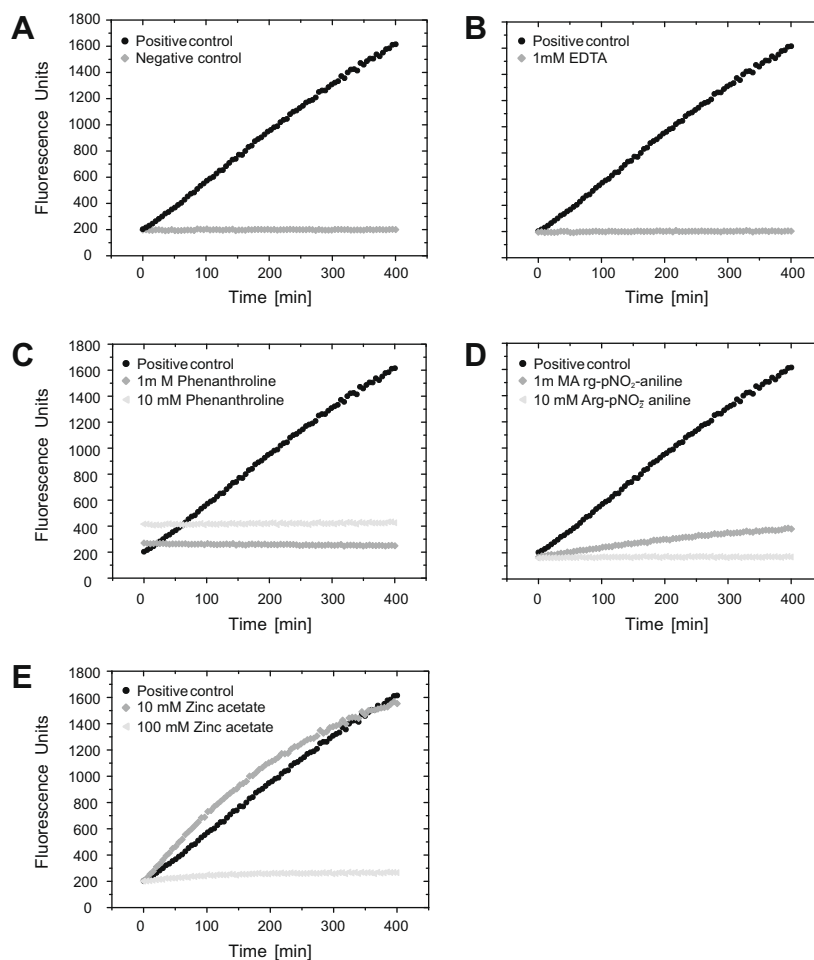


Fig. 2. Time-progress curves of the hydrolysis of the internally quenched fluorescent substrate Mca-Ala-D-isoGln-Lys(Dnp)-D-Ala-Arg-OH at a concentration of 20 μ M catalyzed by AmiE. 5.2 μ M AmiE were pre-incubated for 30 min at 37 °C: (A) Without inhibitor, (●); or with different inhibitors, (◆ and ◀); (B) 1 mM EDTA, (C) 1 and 10 mM Phenanthroline, (D) 1 and 10 mM Benzoyl-Arg-pNO₂-aniline and (E) 10 and 100 mM zinc acetate. Hydrolysis without inhibitor represents the positive control, reaction mixture without enzyme the negative control. Progress of product formation was recorded over 400 min by fluorescence emission of the N-terminal Mca group at 405 nm, following excitation at 340 nm. Figure shows one out of three representative experiments performed at 37 °C in 50 mM sodium phosphate buffer (pH 7.2).

Table 1

Kinetic parameters of substrate derivatives. Amino acid changes compared to the original peptide are highlighted in bold.

Substrate	K_m [μ M]	k_{cat} [1/s]	k_{cat}/K_m [1/(s M)]
Mca-Ala-D-isoGln-Lys(Dnp)-D-Ala-Arg	284.90 \pm 7.36	$1.59 \times 10^{-3} \pm 3.24 \times 10^{-5}$	5.60
Mca-Ala-D-iso Glu -Lys(Dnp)-D-Ala-Arg	360.07 \pm 38.09	$1.63 \times 10^{-3} \pm 1.19 \times 10^{-4}$	4.52
Mca-Ala- Gln -Lys(Dnp)-D-Ala-Arg		No activity	
Mca-Ala-D-isoGln-Lys(Dnp)-D-Ala- Gly -Arg		No activity	
Mca-Ala-D-isoGln-Lys(Dnp)-D-Ala- Gly-Gly -Arg		No activity	
Mca-Ala-D-isoGln- Lys -D-Ala- Gly-Lys(Dnp) -Arg		No activity	

at 392 nm (Fig. 1B). Cleavage of the substrate allows diffusion of the fluorophore from the quencher, resulting in a rapid increase of fluorescence (Fig. 1C). After 1 h substrate hydrolysis, the Mca peak area at 392 nm is approximately 30 times higher than the peak area of the undigested educt, although at this time point only 1.5% of the substrate has been digested. Therefore the substrate allows very sensitive detection of AmiE enzyme activity by hydrolysis induced increase in Mca-fluorescence emission. We found that the replacement of the sugar residue of a peptidoglycan monomer by Mca does not prevent AmiE substrate digestion. Since known AmiE substrates, like peptidoglycan itself or disaccharide linked peptides are difficult to purify or to synthesize, the novel substrate significantly simplifies the synthesis of peptidoglycan-like substrates.

Continuous fluorescent measurement and inhibition

Another advantage of the developed substrate compared to already existing substrates is that it offers the possibility of a continuous activity measurement. While turnover of peptidoglycan-like substrates with carbohydrate residues is normally analysed by mass spectrometry and HPLC after a distinct time point [17], we could show that our assay is suitable for quantifying amidase activity in continuous measurement (Fig. 2A). By testing various known Zn^{2+} -dependent-amidase inhibitors (Fig. 2B–E), we could demonstrate that the substrate can be used to identify and characterize novel inhibitors. Chelating agents like EDTA (Fig. 2B) and phenanthroline (Fig. 2C) at millimolar concentration completely blocked the amidase activity. Zinc acetate at low concentrations (10 mM) activated the enzyme, but inhibited AmiE at high concentrations (100 mM), (Fig. 2E), while a general inhibition of AmiE by high zinc concentrations has been described previously [18], we further identified Benzoyl-Arg-pNO₂-aniline as an unknown inhibitor for AmiE. Benzoyl-Arg-pNO₂-aniline inhibits moderately at 1 mM and completely at 10 mM concentration (Fig. 2D).

Although bacterial type II amidase inhibitors have been proposed as antibacterial agents and are believed to attack bacterial biofilm formation, high throughput compatible tests for drug discovery are unavailable. Our novel microtiter plate assay permits a rapid screening of large compound libraries to identify lead candidates for amidase inhibition.

pH activity profile of AmiE

The novel assay is furthermore suitable to characterize enzyme properties such as the pH activity profile. The pH optimum of AmiE was found to be at pH 7.2, but interestingly the enzyme showed over 80% residual activity at a broad pH range between 5.7 and 9.0 (Fig. 3). This broad pH optimum makes AmiE relatively insensitive to environmental pH changes.

Characterization of amidase substrate specificity

As shown above, AmiE tolerates several modifications of its natural substrate. The most prominent is the exchange of the chair like

muramic acid to the flat ring system of the Mca fluorophore and the addition of the Dnp group to the lysine. Using a series of 5 peptide derivatives, we could further identify key features for substrate recognition and digestion (Table 1). On the one hand we found that the substitution of D-isoGln by D-isoGlu was tolerated, but on the other changing the D-isoGln to an L-Gln result in complete loss of amidase activity. One reason for this could be that the extension of the substrate backbone by D-isoGln compared to normal Gln is essential for substrate recognition. Although both substrates with iso-amino acids were hydrolyzed and showed similar k_{cat} values, the D-isoGlu substrate had a higher K_m and a lower k_{cat}/K_m value, suggesting a lower binding affinity to AmiE. Surprisingly the insertion of one or two glycine residues before the Arg at the C-terminus blocked the amidase activity completely. One reason for this could be an unfavorable interaction that hinders proper substrate recognition and therefore hydrolysis. Another explanation might be that the amidase is only accepting preprocessed peptidoglycan monomers having a linear peptide stem not longer than five residues.

Taken together we have not only established a powerful enzyme assay, but also characterized the substrate specificity of AmiE. Our substrate offers new possibilities to identify antimicrobial drugs and elucidate the complex mechanism of *S. epidermidis* biofilm formation. It needs to be tested in the future how far the substrate is also hydrolyzed by other type II amidases, for example by peptidoglycan recognition proteins.

Acknowledgments

We gratefully acknowledge Andreas Dittmar and Florian Kramer for their technical assistance. We thank Daniel Bächle and Karl-Heinz Wiesmüller for their support and Andreas Maurer for critically reading the manuscript. This work was supported by Deutsche Forschungsgemeinschaft Grants SFB-685 (H.K.) and SFB-TR34 (T.S.).

References

- [1] F.F. Barrett, R.F. McGehee Jr., M. Finland, Methicillin-resistant *Staphylococcus aureus* at Boston City Hospital. Bacteriologic and epidemiologic observations, *N. Engl. J. Med.* 279 (1968) 441–448.
- [2] L.D. Sabath, F.F. Barrett, C. Wilcox, D.A. Gerstein, M. Finland, Methicillin resistance of *Staphylococcus aureus* and *Staphylococcus epidermidis*, *Antimicrob. Agents Chemother.* (Bethesda) 8 (1968) 302–306.
- [3] M.E. Rupp, G.L. Archer, Coagulase-negative *staphylococci*: pathogens associated with medical progress, *Clin. Infect. Dis.* 19 (1994) 231–243 (quiz 244–2445).
- [4] D. Mack, A.P. Davies, L.G. Harris, H. Rohde, M.A. Horstkotte, J.K. Knobloch, Microbial interactions in *Staphylococcus epidermidis* biofilms, *Anal. Bioanal. Chem.* 387 (2007) 399–408.
- [5] J.K. Knobloch, K. Bartscht, A. Sabottke, H. Rohde, H.H. Feucht, D. Mack, Biofilm formation by *Staphylococcus epidermidis* depends on functional RsbU. An activator of the sigB operon: differential activation mechanisms due to ethanol and salt stress, *J. Bacteriol.* 183 (2001) 2624–2633.
- [6] J.P. O'Gara, Ica and beyond: biofilm mechanisms and regulation in *Staphylococcus epidermidis* and *Staphylococcus aureus*, *FEMS Microbiol. Lett.* 270 (2007) 179–188.
- [7] R. Biswas, Characterization of *Staphylococcus aureus* peptidoglycan hydrolases and isolation of defined peptidoglycan structures, Fakultät für Biologie der Eberhard Karls Universität Tübingen, Eberhard Karls Universität Tübingen, Tübingen, 2006.

- [8] W. Vollmer, D. Blanot, M.A. de Pedro, Peptidoglycan structure and architecture, *FEMS Microbiol. Rev.* 32 (2008) 149–167.
- [9] C. Heilmann, M. Hussain, G. Peters, F. Gotz, Evidence for autolysin-mediated primary attachment of *Staphylococcus epidermidis* to a polystyrene surface, *Mol. Microbiol.* 24 (1997) 1013–1024.
- [10] N. Lützner, H. Kalbacher, Quantifying cathepsin s activity in antigen presenting cells using a novel specific substrate, *J. Biol. Chem.* 283 (2008) 36185–36194.
- [11] G.N. Wilkinson, Statistical estimations in enzyme kinetics, *Biochem. J.* 80 (1961) 324–332.
- [12] R. Guan, P.H. Brown, C.P. Swaminathan, A. Roychowdhury, G.J. Boons, R.A. Mariuzza, Crystal structure of human peptidoglycan recognition protein I alpha bound to a muramyl pentapeptide from Gram-positive bacteria, *Protein Sci.* 15 (2006) 1199–11206.
- [13] R. Dziarski, D. Gupta, The peptidoglycan recognition proteins (PGRPs), *Genome Biol.* 7 (2006) 232.
- [14] X. Li, S. Wang, J. Qi, S.F. Echtenkamp, R. Chatterjee, M. Wang, G.J. Boons, R. Dziarski, D. Gupta, Zebrafish peptidoglycan recognition proteins are bactericidal amidases essential for defense against bacterial infections, *Immunity* 27 (2007) 518–529.
- [15] J. Royet, R. Dziarski, Peptidoglycan recognition proteins: pleiotropic sensors and effectors of antimicrobial defences, *Nat. Rev. Microbiol.* 5 (2007) 264–277.
- [16] S. Cho, Q. Wang, C.P. Swaminathan, D. Heseck, M. Lee, G.J. Boons, S. Mobashery, R.A. Mariuzza, Structural insights into the bactericidal mechanism of human peptidoglycan recognition proteins, *Proc. Natl. Acad. Sci. USA* 104 (2007) 8761–8766.
- [17] Z.M. Wang, X. Li, R.R. Cocklin, M. Wang, K. Fukase, S. Inamura, S. Kusumoto, D. Gupta, R. Dziarski, Human peptidoglycan recognition protein-L is an *N*-acetylmuramoyl-*l*-alanine amidase, *J. Biol. Chem.* 278 (2003) 49044–49052.
- [18] S.J. Foster, Molecular characterization and functional analysis of the major autolysin of *Staphylococcus aureus* 8325/4, *J. Bacteriol.* 177 (1995) 5723–5725.

Role of staphylococcal wall teichoic acid in targeting the major autolysin Atl

Martin Schlag,^{1†} Raja Biswas,^{2†} Bernhard Krismer,² Thomas Kohler,² Sebastian Zoll,³ Wenqi Yu,¹ Heinz Schwarz,⁴ Andreas Peschel² and Friedrich Götz^{1*}

¹Microbial Genetics, University of Tübingen, 72076 Tübingen, Germany.

²Cellular and Molecular Microbiology Division, Medical Microbiology and Hygiene Institute, University of Tübingen, 72076 Tübingen, Germany.

³Interfaculty Institute of Biochemistry, Tübingen, Germany.

⁴Max-Planck Institute for Developmental Biology, Tübingen, Germany.

Summary

Staphylococcal cell separation depends largely on the bifunctional autolysin Atl that is processed to amidase-R_{1,2} and R₃-glucosaminidase. These murein hydrolases are targeted via repeat domains (R) to the septal region of the cell surface, thereby allowing localized peptidoglycan hydrolysis and separation of the dividing cells. Here we show that targeting of the amidase repeats is based on an exclusion strategy mediated by wall teichoic acid (WTA). In *Staphylococcus aureus* wild-type, externally applied repeats (R_{1,2}) or endogenously expressed amidase were localized exclusively at the cross-wall region, while in $\Delta tagO$ mutant that lacks WTA binding was evenly distributed on the cell surface, which explains the increased fragility and autolysis susceptibility of the mutant. WTA prevented binding of Atl to the old cell wall but not to the cross-wall region suggesting a lower WTA content. In binding studies with ConcanavalinA-fluorescein (ConA-FITC) conjugate that binds preferentially to teichoic acids, ConA-FITC was bound throughout the cell surface with the exception of the cross wall. ConA binding suggest that either content or polymerization of WTA gradually increases with distance from the cross-wall. By preventing binding of Atl, WTA directs Atl to the cross-wall to perform the

last step of cell division, namely separation of the daughter cells.

Introduction

The major autolysin of *Staphylococcus aureus* (AtlA, 137 kDa) (Oshida *et al.*, 1995) and of *Staphylococcus epidermidis* (AtlE, 148 kDa) (Heilmann *et al.*, 1997) is involved in cell separation of daughter cells after cell division. Atl is a bifunctional protein that consists of a propeptide region, an amidase (AM) and an endo-beta-N-acetylglucosaminidase domain (GL). AM and GL domains are separated by three direct repeated sequences (R₁₋₃), each about 165 aa long. Through proteolytic processing by a so far not characterized process, Atl generates two major extracellular murein hydrolases, Ami-R_{1,2} (62 kDa) and R₃-GL (\pm 52 kDa), which are attached to the cell surface of *S. aureus* or *S. epidermidis*, and can be released by high salt treatment. Ami-R_{1,2} comprises the amidase and two C-terminal located repeats (R_{1,2}); the 50 kDa GL protein has the third repeat (R₃) at its N-terminal region (Heilmann *et al.*, 1997). Atl homologues are very likely present in all staphylococcal species such as the food grade *S. carnosus* where it is named Bph, bifunctional peptidoglycan hydrolase (Rosenstein *et al.*, 2009).

atl deletion mutants form huge cell clusters, which indicates that the cell separation is severely affected (Heilmann *et al.*, 1997). The cell clusters of the mutants can be resolved by adding the purified Ami-R_{1,2} externally. Besides the role in cell separation *atl* mutants are impaired in biofilm formation because adherence to glass and plastic surfaces is severely affected (Bera *et al.*, 2006). Furthermore, it has been demonstrated that Ami-R_{1,2} also binds strongly to vitronectin and fibronectin (Heilmann *et al.*, 1997; Heilmann *et al.*, 2005). Vitronectin is an abundant glycoprotein found in serum and extracellular matrix and promotes cell adhesion and spreading. Fibronectin is a large extracellular matrix protein that triggers invasion of *S. aureus* by binding to integrins (Sinha *et al.*, 1999).

Although the amidase is already known for some time, it was not until recently that the cleavage site of purified Ami-R_{1,2} has been determined and been shown that it cleaves the amide bond between N-acetyl muramic acid

Accepted 1 December, 2009. *For correspondence. E-mail friedrich.goetz@uni-tuebingen.de; Tel. (+49) 7071 2974636; Fax (+49) 7071 295937. †Authors contributed equally to this work.

and L-alanine in peptidoglycan (PGN) (Biswas *et al.*, 2006). It has been also shown that the separately expressed and purified repeat domains ($R_{1,2}$) exhibited high binding affinity to isolated PGN and contributed to the targeting of the amidase to its substrate. Ami and Ami- $R_{1,2}$ revealed a broad substrate preference as they can hydrolyse PGN lacking WTA, O-acetylation, or both (Biswas *et al.*, 2006).

As the autolysins are involved in the separation of daughter cells it has been important to know where the Atl-derived enzymes are localized on the cell surface. This has been investigated by immune electron microscopy using α -62-kDa amidase or α -51-kDa glucosaminidase IgG. Immunogold labelling of ultrathin sections revealed that both amidase and glucosaminidase localize at the equatorial ring on the staphylococcal cell surface that marks the future cell division site (Yamada *et al.*, 1996). It has been assumed that such a preferred localization facilitates partitioning of daughter cells without affecting the entire murein sacculus (Giesbrecht *et al.*, 1998). By fusion of repeat domain (R_2) with enterotoxin B (Seb- R_2), it has been demonstrated that R_2 was sufficient to direct the hybrid protein to the cell wall (CW) envelope and preferentially to the equatorial ring (Baba and Schneewind, 1998), which led to the proposal that there is a specific receptor that is positioned at the equatorial ring on the staphylococcal surface.

Here we addressed the question by which mechanism the Atl-repeats are targeted to the equatorial surface ring in staphylococci. We provide evidence that there is probably not a specific receptor at the septum region for binding the Atl repeats. The targeting is rather based on an avoidance strategy by wall teichoic acid (WTA), which

prevents binding of Atl. As WTA is abundant in the old CW but not at the cross-wall region Atl can only bind to this latter region. This is demonstrated by both endogenously expressed Atl or externally applied $R_{1,2}$. We identified the mechanism behind the long suspected influence of WTA in autolysis.

Results

Wall teichoic acid protects *S. aureus* from autolysis

To investigate the contribution of WTA in autolysis, Triton X-100 induced autolysis assays were performed with wild-type (wt) cells (SA113), the WTA-lacking mutant (SA113 Δ tagO), the complemented mutant [SA113 Δ tagO (pRBtagO)] and the autolysin mutant (SA113 Δ atlA). Lysis was significantly faster in the mutant lacking WTA, while the wt and complemented mutant showed similar autolysis profiles (Fig. 1A). SA113 Δ atlA showed almost no autolysis, which confirms that indeed Atl is the major player in autolysis.

S. aureus strain SA113 Δ tagO has more Atl derivatives bound at the surface

The question is why the WTA-deficient mutant is more susceptible to autolysis than the wt. One possible explanation is that WTA affects the binding of amidase to the CW. To address this question, we detached CW-associated proteins with SDS from SA113 (wt), SA113 Δ tagO, SA113 Δ tagO(pRBtagO) and SA113 Δ atlA, and performed a zymogram containing embedded heat-inactivated SA113 cells with the detached proteins. Bands with lytic activity were observed as clear zones in the

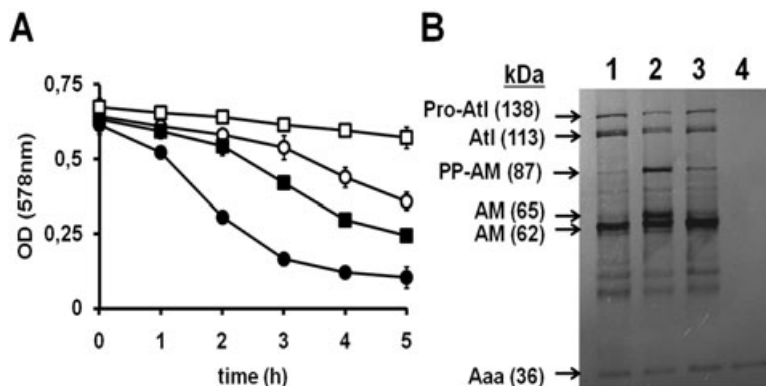


Fig. 1. Autolysis assay and zymogram.

A. Exponentially growing cells of SA113 (○), Δ tagO (●), Δ tagO (pRBtagO) (■) and Δ atlA (□) were harvested by centrifugation and allowed to autolyse in PBS buffer (pH 7.2) containing 0.05% Triton X-100. Decrease of optical density was measured at 578 nm.

B. Bacteriolytic enzyme profiles on a 10% SDS-PAGE gel containing heat inactivated *S. aureus* SA113 cells as substrate. The SDS-PAGE was loaded with proteins released from the cell surface of SA113 (lane 1), Δ tagO (lane 2), Δ tagO(pRBtagO) (lane 3) and Δ atlA (lane 4). Dark bands represent cell lysis zones (the clear zones appear as dark bands with a black background). The sizes of the bacteriolytic surface proteins are indicated. Aaa, 36 kDa *S. aureus* autolysin; AM (62 kDa), amidase with two repeats (Ami $R_{1,2}$); AM (65 kDa) Ami $R_{1,2}$ with very likely portion of the propeptide; PP-AM (87 kDa), Ami $R_{1,2}$ with full-length propeptide; Atl (113 kDa), amidase together with glucosaminidase; Pro-Atl (138 kDa), Atl with full-length propeptide.

opaque gel (Fig. 1B); the clear zones appeared as dark bands after photography against a dark background. Apart from the 36 kDa band of Aaa (autolysin/adhesion protein of *S. aureus*) (Heilmann *et al.*, 2005), all other bands must represent differently processed Atl forms, as in the *atl* mutant the corresponding autolysis bands were missing (Fig. 1B, lane 4), and SA113 and SA113 Δ tagO(pRBtagO) show a similar lysis pattern. However, the lysis pattern of the SA113 Δ tagO released proteins differs in so far as there are two predominant lytic proteins in the range of 66 and 87 kDa. The 87 kDa protein represents the propeptide-amidase portion (PP-AM), the 66 kDa protein very likely comprises a differently processed amidase (AM) form. In conclusion, more processed amidases bound to the CW in the absence of WTA, which explains, to some extent, the increased autolytic activity of the *tagO* mutant.

Binding of amidase repeat domains ($R_{1,2}$) to the cell wall is increased in SA113 Δ tagO

Atl is processed to various lytic protein forms. One processed product comprises the amidase with two repeat domains (Ami- $R_{1,2}$). Recently, we showed that $R_{1,2}$ have a high binding affinity to isolated PGN, thus contributing to the targeting of the amidase to the substrate (Biswas *et al.*, 2006). Here we labelled $R_{1,2}$ with the fluorescence dye Cy5 (Cy5- $R_{1,2}$) and determined its binding to living cells (taken from exponential growth phase) of wt and its Δ tagO mutant as well as the complemented mutant. The extent of Cy5- $R_{1,2}$ binding was determined by fluores-

cence measurement. Indeed, the fluorescence of Δ tagO mutant was 1.6-fold higher than in the wt or the complemented mutant in four independent experiments (Fig. 2A). Cy5-labelled bovine serum albumin (Cy5-BSA) served as a negative control. Amidase without repeats (Cy5-AmiE) showed a similar low binding as Cy5-BSA (data not shown). We also investigated the impact of O-acetylation and alanylation of LTA on Cy5- $R_{1,2}$ binding by performing the same experiment in SA113 Δ oatA and SA113 Δ dltA; these two mutants behaved like the wt (data not shown). These results indicated that Δ tagO mutant binds more autolysins by recruiting more repeat domains, which is in concert with our previous finding that the targeting of amidase to the cell surface was directed by the repeat domains $R_{1,2}$ (Fig. 1A).

Atl loses its selective localization to division sites in the absence of WTA

The observation that Cy5- $R_{1,2}$ binds better to CW of the Δ tagO mutant than to wt prompted us to examine the spatial surface distribution of Cy5- $R_{1,2}$. Previous work showed that Atl is localized preferentially at the septum region of the staphylococcal surface (Yamada *et al.*, 1996). Similar studies with *S. aureus* Δ tagO have not been done so far.

We compared the surface distribution of Cy5- $R_{1,2}$ on wt and the *tagO* mutant cells harbouring pCtufgfp for constitutive GFP expression. In epifluorescence microscopy we saw a clear difference regarding the localization of Cy5- $R_{1,2}$. While Cy5- $R_{1,2}$ is clustered exclusively at the septum

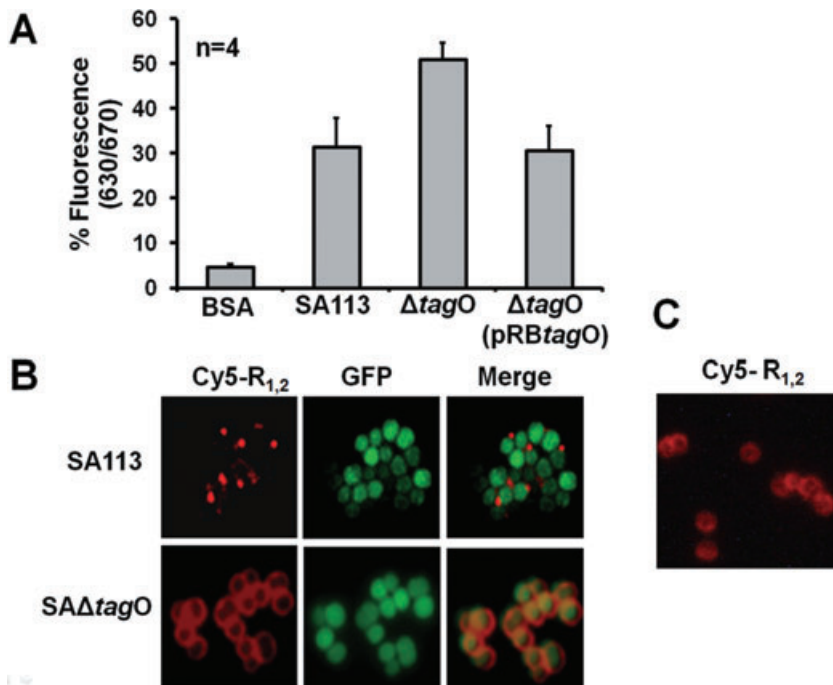


Fig. 2. *In vitro* binding of amidase repeats ($R_{1,2}$) with staphylococcal cells. **A.** SA113 wild-type, wall teichoic acid-deficient Δ tagO mutant and the complemented strain were incubated with Cy5- $R_{1,2}$. Cell wall bound Cy5- $R_{1,2}$ was extracted using 10% SDS and fluorescence was measured in four independent experiments. Cy5-BSA was used as a control. **B.** *In vitro* binding of Cy5- $R_{1,2}$ with SA113 and Δ tagO. Staphylococcal cells expressing green fluorescent proteins from plasmid pCtufgfp were incubated with Cy5- $R_{1,2}$ and visualized using fluorescence microscopy. **C.** Binding of Cy5- $R_{1,2}$ with 10% TCA treated wt.

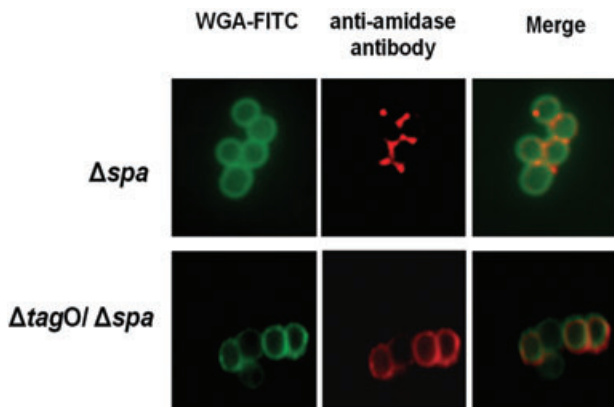


Fig. 3. Visualization of amidase on the cell surface of SA113 and $\Delta tagO$ mutant by immunofluorescence microscopy. Cell envelope of staphylococcal cells was labelled green with Wheat Germ Agglutinin-FITC (WGA-FITC). Cells surface localization of amidase was detected using first rabbit α -amidase antibody and second Alexa Fluor 594 conjugated goat anti-rabbit IgG.

region in the wt, it appears evenly distributed all over the surface in the $\Delta tagO$ mutant (Fig. 2B). GFP fluorescence alone shows that $tagO$ mutant cells are significantly larger than the wt. In the merged green/red fluorescence picture the septum localization of Cy5-R_{1,2} in the wt is more pronounced. When wt cells were treated with 10% TCA for 16 h to remove CW-bound WTA Cy5-R_{1,2} binding was distributed all over the cell surface like in the $tagO$ mutant (Fig. 2C). These results suggest that in wt cells an even distribution of the amidase repeat domains (R_{1,2}) to the cell surface is excluded by WTA; consequently Cy5-R_{1,2} is forced to bind at the septum region, which suggests that the content of matured WTA must be low at this site. Directing the repeat domains to the septum site guarantees that murein hydrolysis preferentially occurs at this part and not at the entire CW, which could weaken the CW integrity and result in increased autolysis as seen in Fig. 1A.

So far we have shown that externally added Cy5-R_{1,2} binds in wt cells preferentially to the septum region. The question is whether natively expressed amidase is located there too. To answer this question by immunofluorescence we created marker-less *spa* (protein A) deletion mutants to avoid antibody interference with Spa. The strains used were SA113 Δspa and the double mutant SA113 $\Delta spa/\Delta tagO$. Cell envelope was labelled with Wheat Germ Agglutinin-FITC (WGA-FITC) that binds to GlcNAc structures to visualize the cell shape. The localization of natively expressed amidase was visualized with rabbit anti-amidase antibody and Alexa Fluor 594 conjugated goat anti-rabbit IgG as secondary antibody. As shown in (Fig. 3) amidase was accumulated at the septum region of SA113 Δspa , and in some cases amidase was already found at the beginning of the

second division plane, while in SA113 $\Delta spa/\Delta tagO$ cells amidase was evenly distributed around the cell surface. In summary, natively expressed amidase is targeted to the same site as the externally applied Cy5-R_{1,2}.

The cross-wall (septum site) of dividing S. aureus cells is devoid of WTA

We proposed that Atl preferentially binds to the cross-wall region because it lacks WTA. To support this hypothesis binding studies with ConcanavalinA-fluorescein conjugate (ConA-FITC) were carried out; ConA is a lectin that binds to teichoic acids (Umeda, 1987). As ConA also recognizes LTA, a crucial step was the removal of LTA by extensive SDS treatment. In the wt strain ConA-FITC was preferentially bound to the old CW, whereas the cross-wall (septum) region was free, giving dividing cells the shape of two facing crescents (Fig. 4). The fluorescence intensity of bound ConA-FITC increased gradually with distance from the cross-wall. In the $tagO$ mutant ConA-FITC did not bind to the cells, indicating that the observed exclusion of Atl binding in the old CW area of the wt was really WTA mediated. As a further control WTA was removed in the wt by hydrofluoric acid treatment; there was no binding observed like in the $tagO$ mutant (data not shown). These results clearly show that in the cross-wall region WTA is not accessible by ConA-FITC, either because WTA is not present or it is not yet fully polymerized.

Size and cell morphology of the SA113 $\Delta tagO$ differs from the wt

The growth behaviour of SA113 and its $\Delta tagO$ mutant in complex medium was very similar. However, a closer look

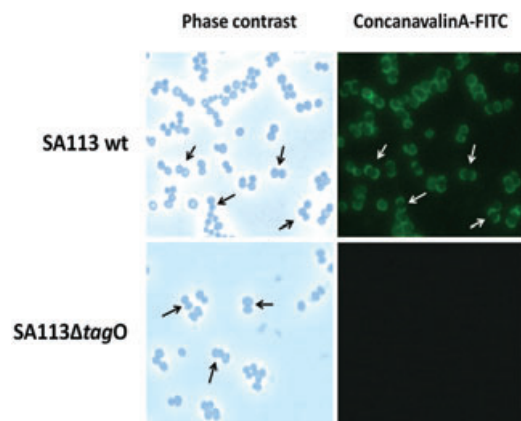


Fig. 4. Visualization of WTA by on the surface of SA113 and $\Delta tagO$ by ConA-FITC. After removal of contaminating compounds, surface bound WTA were stained with concanavalinA-fluorescein (ConA-FITC) conjugate and localization of fluorescent lectin was determined. Arrows indicate sites of cell division.

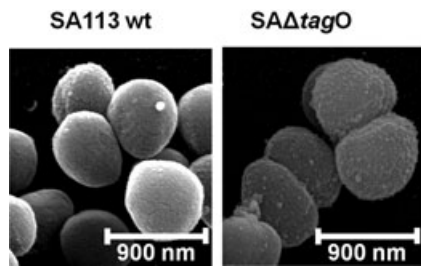


Fig. 5. Comparison of SA113 and its $\Delta tagO$ mutant by scanning electron microscopy (SEM). Mid-log phase cells were fixed and examined SEM.

to cell morphology disclosed some differences. Scanning electron microscopy (SEM) analysis of mid-exponential grown cells revealed that both cell size and cell surface structure is altered in the $\Delta tagO$ mutant (Fig. 5). Cells of the $\Delta tagO$ mutant were significantly larger compared with wt cells. The average cell diameter of wt cells was 635 ± 15 nm ($n = 30$), while for the $\Delta tagO$ mutant it was 751 ± 18 nm ($n = 30$). The surface morphology of the two strains looked also different in SEM microscopy. While the wt was characterized by a smooth surface, the surface of the $\Delta tagO$ strain appeared rough, with bobble- and hairy-like protrusions.

As shown in Fig. 1 autolysis of the $\Delta tagO$ mutant in PBS buffer is much faster than with the wt. We compared the morphological changes during the autolysis process by transmission electron microscopy (TEM) analysis over time (0, 2 and 4 h). As one can see in Fig. 6, the CW of the $\Delta tagO$ mutant is much less electron dense compared with the wt, even immediately after resuspending the cells in PBS (time 0). Furthermore, the surface morphology of the two strains was different. The wt is characterized by a smooth surface and an intact CW, which looked hardly disintegrated after 4 h. In contrast to the wt the CW of the $\Delta tagO$ mutant got frazzled with time and many bobble-like protrusions appeared, suggesting massive degradation and destruction of CW (Fig. 6A).

PGN cross-linking is decreased in WTA-deficient *Staphylococcus aureus*

To analyse differences in the degree of cross-linking in SA113 and SA113 $\Delta tagO$, PGN of these strains was hydrolysed with mutanolysin and soluble PGN fragments were separated by high-performance liquid chromatography (HPLC). The poorly resolved part of the HPLC profile eluting with retention times of greater than > 100 min contains highly cross-linked oligomeric components. The amount of highly cross-linked PGN was 1.4 times lower in the $\Delta tagO$ mutant compared with the wt (Fig. 6B), indicating that the loss of WTA affected cross-linking in *S. aureus*. Similar results have been obtained with selective

staining of unlinked stem peptides with vancomycin FITC-conjugate as an indicator for the degree of cross-linkage (data not shown).

Discussion

Wall teichoic acid plays an important role in staphylococci and other Gram-positive bacteria in various aspects (Weidenmaier and Peschel, 2008). A breakthrough in research of the role of WTA in staphylococci came with the isolation of a $\Delta tagO$ (TagO is the first enzyme in WTA biosynthesis) deletion mutant (Weidenmaier *et al.*, 2004). Comparative analysis with wt revealed that the mutant is resistant to several *S. aureus* phages such as 3A52 and $\Phi 11$ that employ WTA as a receptor for infection of bacterial cells. $\Delta tagO$ mutant was affected in nasal coloniza-

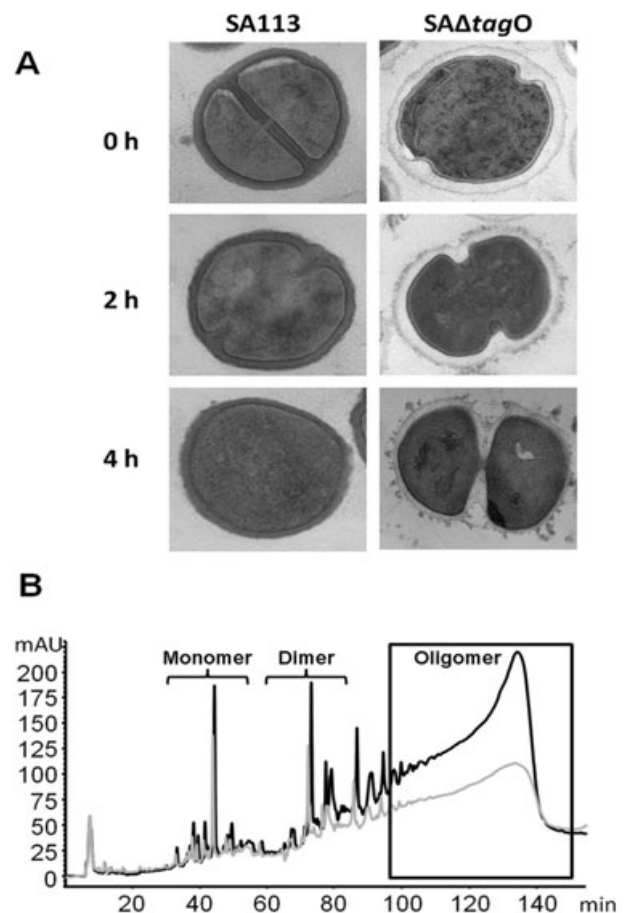


Fig. 6. Transmission electron microscopic (TEM) images of staphylococcal strains during autolysis and changes in PGN cross-linking in staphylococcal strains. A. Changes in CW during gradual autolysis of SA113 and its $\Delta tagO$ mutant cells in PBS (see Fig. 1A) were monitored by TEM. Samples were taken at 0, 2 and 4 h intervals. B. HPLC analysis of mutanolysin digested PGN of SA113 and $\Delta tagO$. Black line: SA113wt, grey line: SA113 $\Delta tagO$. The black frame represents the area of highly cross-linked PGN (oligomer).

tion, a major risk factor in nosocomial infections (Weidenmaier *et al.*, 2004) and it was affected in biofilm formation particularly adherence to polymer structures (Götz, 2002; Vergara-Irigaray *et al.*, 2008). WTA also contributes to lysozyme resistance as a *tagO/oatA* double mutant is highly susceptible to lysozyme (Bera *et al.*, 2007). Recently, it has been shown that WTA protects *S. aureus* against antimicrobial fatty acids from human skin (Kohler *et al.*, 2009).

In the course of studying the role of the major autolysin in staphylococci (Bera *et al.*, 2006), we observed that the $\Delta tagO$ mutant was more susceptible to autolysis than the wt. This observation was the origin of this study as we asked the question, 'why is in $\Delta tagO$ mutants autolysis so much increased?'

To investigate the contribution of WTA in autolysin activity we performed autolysis assays with wt cells (SA113), the WTA-lacking mutant (SA113 $\Delta tagO$), the complemented mutant [SA113 $\Delta tagO$ (pRB*tagO*)] and the autolysin mutant (SA113 $\Delta atlA$). Lysis was significantly faster in the mutant lacking WTA compared with the wt and complemented mutant that showed similar autolysis profiles. We supposed that WTA must play an important role in controlling autolysin activity.

However, we did not know if this phenomenon is due to higher binding capacity of autolysin or increased susceptibility of the $\Delta tagO$ mutant to autolysins. To get an answer to this question we performed zymogram gels with CW released proteins from SA113 wt, $\Delta tagO$, $\Delta tagO$ (pRB*tagO*) and the autolysin mutant $\Delta atlA$. Indeed, the lysis pattern of the various processed forms of AtlA revealed that two lytic Atl-derived amidase proteins in a size of 65 and 87 kDa were predominant in the $\Delta tagO$ cells, indicating that the mutant has bound more amidase. The Atl-derived glucosaminidase that we also isolated showed no activity in the zymogram with heat-inactivated staphylococcal cells. We are therefore pretty sure that all lytic bands seen in the zymogram are due to the amidase activity. The question is why particularly these two forms predominantly adhere to the mutant. A possible answer is that in the mutant Atl processing is retarded and therefore these incompletely processed forms are accumulated. With the exception of the lytic 36 kDa band of Aaa (Heilmann *et al.*, 2005), all other lytic bands must have derived from Atl processing as they were absent in the $\Delta atlA$ mutant (Fig. 1B). The corresponding lytic proteins were previously sequenced N-terminally; they all contained the amidase domain with its repeats (Heilmann *et al.*, 1997). In this zymogram we do not see the lytic 51 kDa glucosaminidase band, as this enzyme hardly lyses *S. aureus* cells but it can lyse *Micrococcus luteus* cells (Heilmann *et al.*, 1997). This result led us to the conclusion that in the absence of WTA more autolysins were bound to the CW. In *Bacillus subtilis* a similar observation was made

with endopeptidase LytF and its CW binding domain LysM. Here too it was found that LytF binding was increased in TagB, TagF or TagO depleted cells (Buist *et al.*, 2008; Yamamoto *et al.*, 2008). For LysM containing proteins there are different CW modifications described that control localized binding (Buist *et al.*, 2008). However, a LysM motif is not present in Atl.

In SEM studies the $\Delta tagO$ mutant showed characteristic differences compared with wt. The cell size was larger and the surface morphology appeared rough, with bobble- and hairy-like protrusions (Fig. 6). Although there is not much difference in growth rate in complex medium we think that the $\Delta tagO$ mutant has all the time to struggle against the increased autolytic vulnerability. In TEM the difference in the CW during the beginning of lysis in buffer is even more pronounced. Already at time 0 the CW of the $\Delta tagO$ mutant has a much lower electron density which could be due to the absence of WTA or to a lower degree of PGN cross-linking as shown by HPLC analysis.

To further analyse the binding of Ami-R_{1,2}, we dissected this protein and expressed and purified only the amidase portion (Ami) and the repeat portion (R_{1,2}). First we carried out binding studies with Cy5-R_{1,2}. The $\Delta tagO$ mutant bound significantly more Cy5-R_{1,2} than wt and the complemented mutant (Fig. 2A). What was even more thrilling was that in wt Cy5-R_{1,2} was accumulated on the cell surface at the site of cell division, while in WTA-less cells such as the $\Delta tagO$ mutant or TCA treated wt it was evenly distributed on the cell surface (Fig. 2B). These results confirm earlier reports (Baba and Schneewind, 1998; Biswas *et al.*, 2006) that the repeat domains essentially mediate the binding of autolysins to CW structures. However, we still do not know which PGN structures are recognized by autolysin. It is shown here that in the absence of WTA significantly more Cy5-R_{1,2} was bound to the cell surface in an untargeted mode, which suggests that WTA hinders binding of the repeat domains. This is most likely the explanation for the higher susceptibility of the $\Delta tagO$ mutant to autolysis. However, we cannot rule out the possibility that increased autolysis susceptibility of $\Delta tagO$ is due to decreased degree of PGN cross-linking. Recently, it has been shown that sublethal concentrations of penicillin, which decreases in PGN cross linking, led to an increased lysozyme susceptibility (Bera *et al.*, 2005).

The next question was whether the endogenously expressed amidase is also differently localized in wt and the $\Delta tagO$ mutant like the external applied Cy5-R_{1,2}.

In order to answer this question by using fluorescence-labelling techniques with anti-amidase antibody we had to construct respective clones in a protein A negative background (Δspa) to avoid unspecific IgG binding. We saw here essentially the same distribution as observed with the externally applied repeat domains. In SA113 Δspa amidase was clustered in the septum region; in

SA113 $\Delta spa\Delta tagO$ mutant amidase could not be specifically targeted to the septum region, it was evenly distributed on the cell surface (Fig. 3). This loss of targeting amidase to the septum region is very likely the explanation for the increased susceptibility of the $\Delta tagO$ mutant to autolysis.

From the results so far it is clear that WTA prevents binding of Atl-derived autolysins. As these autolysins are directed and concentrated at the septum region one must assume that the WTA in this region is very low. This is contradictory to the general assumption that WTA is preferentially incorporated at sites with high PGN biosynthesis, which is the septum region. However, we were able to visualize the distribution of WTA on the bacterial surface with the aid of ConA-FITC that binds to teichoic acids. Indeed, in dividing wt cells ConA was not bound at the cross-wall region only at the old CW. Our hypothesis is therefore that even if WTA is incorporated at the septum site it is not yet fully polymerized to the mature form and does therefore not prevent binding of endogenously expressed amidase or externally applied Cy5-R_{1,2}.

In conclusion, we have shown here that WTA plays a crucial role in targeting the Atl-derived autolysins. The binding specificity of the autolysins lies in the repeat regions. As the repeats hardly bind to WTA containing CW regions the mechanism of targeting the amidase to the septum region is based upon an elimination process. Our results suggest that the outer wall zones of the septum region does either not contain, or contains only premature, WTA thus allowing Atl binding.

Experimental procedures

Bacterial growth conditions

Escherichia coli strains were grown in Luria–Bertani medium at 25°C. Staphylococcal strains were grown in BM broth (1% tryptone, 0.5% yeast extract, 0.5% NaCl, 0.1% K₂HPO₄, 0.1% glucose) with shaking at 37°C supplemented with appropriate antibiotics. Media were supplemented with ampicillin (100 µg ml⁻¹), erythromycin (2.5 µg ml⁻¹), chloramphenicol (10 µg ml⁻¹) where indicated.

Strain and plasmid construction

Construction of *S. aureus* strain lacking WTA (SA113 $\Delta tagO::ermB$) was described earlier (Weidenmaier *et al.*, 2004). The SA113 $\Delta tagO::ermB$ mutant was complemented using plasmid pRB473 $tagO$ containing the $tagO$ gene with its putative promoter (Table 1). For electron microscopic studies a markerless protein-A deletion mutant was constructed using temperature-sensitive plasmid pKOR1. For its construction the upstream and downstream regions of spa were PCR amplified by primer-pairs Spa-del attB2; GGGGACCACTTTGTACAAGAAAGCTGGGATCAG CAAGAAAACACACTTCC / Spa-del rev BgIII; AAAAGATCT AACGAATTATGTATTGCAATAC and Spa-del for BgIII; GTCGAGATCTATAAAAAACAACAATACACAACG / Spa-del attB1; GGGGACAAGTTTGTACAAAAAAGCAGGCCAATAT TCCATGGTCCAGAACT, respectively. The resulting PCR products were subsequently restricted with BgIII and ligated in equimolar amounts. The resulting ligation product was integrated into pKOR1 via *in vitro* recombination (clonase mix from Invitrogen) and the recombination mix was transformed into *E. coli* DH5a. Plasmid from a positive clone was trans-

Table 1. Strains and plasmids.

Strain or plasmid	Description	Source or reference
<i>E. coli</i>		
DH5 α	$\phi 80d lacZ\Delta M15, \Delta(lacZYA-argF)U169, deoR, recA1, endA1, hsdR17(rk^-, mk^+), phoA, supE44, \lambda^-, thi-1, gyrA96, relA1$	Laboratory Strain
Rosetta 2 (DE3)	F ⁻ $ompT hsdS_B(r_B^- m_B^-) gal dcm$ (DE3) pRARE2 (Cam ^R)	Novagen
<i>S. epidermidis</i>		
SE O47	Clinical Isolate	Heilmann <i>et al.</i> (2005)
<i>S. aureus</i>		
SA113	Derivative of NCTC 8325	Iordanescu and Surdeanu (1976)
RN4220	Derivative of NCTC 8325	Kreiswirth <i>et al.</i> (1983)
SA Δatl	SA113 $\Delta atlA::spc$	Biswas <i>et al.</i> (2006)
SA113 $\Delta tagO$	SA113 $\Delta tagO::ermB$	Weidenmaier <i>et al.</i> (2004)
SA113 $\Delta oatA$	SA113 $\Delta oatA::km$	Bera <i>et al.</i> (2005)
SA113 $\Delta dltA$	SA113 $\Delta dltA::spc$	Peschel <i>et al.</i> (1999)
SA113 Δspa	SA113 Δspa markerless deletion	This work
SA113 $\Delta spa/\Delta tagO$	SA113 $\Delta spa/\Delta tagO$ markerless deletion of $spa; tagO::ermB$	This work
Plasmids		
pGEX-Ami	Overexpression plasmid for GST-Ami fusion protein in <i>E. coli</i> ; Amp ^R	Lütznier <i>et al.</i> (2009)
pGEX-R1-2	Overexpression plasmid for GST-R _{1,2} fusion protein in <i>E. coli</i> ; Amp ^R	This work
pKOR1	Knockout plasmid	Bae and Schneewind (2006)
pKOR1-Spa	Knockout plasmid for markerless replacement of $tagO$	This work
pRB473	<i>E. coli/S. aureus</i> shuttle vector; Amp ^R , Cm ^R	Brückner (1997)
pRB473 $tagO$	<i>E. coli/S. aureus</i> shuttle vector carrying the $tagO$ gene; Amp ^R , Cm ^R	This work
pCtuGFP	pCX19 carrying gfp gene under control of the promoter $tufA$; Cm ^R	Biswas <i>et al.</i> (2006)

formed into RN4220 and subsequently to SA113. Spa deletion mutants were constructed using standard methods (Leibig *et al.*, 2008). Δspa mutation was transduced into SA113 $\Delta tagO::ermB$.

Construction of pGEX-Amidase derivatives

For this study we constructed three constructs for the heterologous expression of amidase regions Ami-R_{1,2}, Ami and R_{1,2} in *E. coli*. Restriction sites and stop codons were introduced in the oligonucleotides (italics and underlined respectively). The amidase repeat regions were PCR amplified from *S. epidermidis* O47 chromosomal DNA using the primer pairs Ami 5' (CGGGATCCGTATCTAGTCAAAA)/Ami 3'(GGCTC GAGTCAGCCCCAAGGTGCTAC) for Ami (629 bp) and R₁-BamHI(AAATTAATGGATCCACAACATCTA CAAAAC CGTCAC)/R₂-XhoI (TAAATCTCGAGTCATGCAGTTAAAT AGTATTTACTAATCCAACC) (990 bp) for the CW binding region (R_{1,2}). PCR products were digested with BamHI and XhoI and ligated into the BamHI/XhoI pre-digested vector pGEX 4T-3 (Amersham). The resulting plasmids were designated as pGEX-Ami and pGEX-R_{1,2} and subsequently transformed in *E. coli* Rosetta 2 (Novagen).

Purification of GST fusion proteins

Escherichia coli strains described above were used for induction of expression of proteins. One-litre cultures were grown at 24°C to an optical density of 0.5 at 578 nm. At this point, IPTG was added to 0.3 mM final concentration, and cells were allowed to grow for 5 h at 20°C. Cells were then harvested by centrifugation and resuspended in 20 ml PBS and broken using a French pressure cell. Cell lysates were centrifuged for 30 min at 23 000 *g* to remove cell debris. GST fusion proteins were purified using ÄKTA protein purifier system. Briefly, clear lysates were loaded on pre-equilibrated Glutathione Sepharose column (Novagen) and washed with PBS until the absorbance measured at 280 nm did not change. On-column cleavage of fusion proteins was achieved with 1 U Thrombin/100 µg fusion protein overnight at 22°C. Subsequently, target protein was eluted with PBS. Thrombin was removed in the same step using a Benzamide Sepharose FF column (Amersham) in series with the Glutathione Sepharose column. Fractions containing target protein were pooled and analysed for purity in 12% SDS-PAGE. Purified proteins were stored at -20°C.

Conjugation of dye to protein

The repeat region alone (R_{1,2}) was purified as described above prior to labelling with Cy5 bis-reactive Dye [Cy5-Bis-NHS ester, GE Healthcare (PA15002)]. Proteins to be conjugated were dissolved at 5 mg ml⁻¹ in 50 mM sodium carbonate buffer (pH 9.0). Protein solution was added to 1 mg dry dye, and mix thoroughly without foaming of the protein solution. The reaction mix was incubated for 5 h at RT. Labelled protein was separated from the unconjugated dye by desalting in the Äkta purifier system (Amersham) using 2 × 5 ml columns in series using 50 mM sodium phosphate buffer (pH 6.8) as mobile phase. Coupled protein and

unbound dye eluted as separate turquoise bands. As a control protein bovine serum albumin and AmiE alone was conjugated to Cy5 bis-reactive Dye (Cy5-BSA) with the method described above. The labelled proteins were stored at -20°C without further manipulation.

Autolysis assay

Cells were cultivated to mid-exponential phase, washed twice with phosphate buffer saline (pH 7.2) and once with ice-cold ultrapure water. Cells were resuspended in phosphate buffer (pH 7.2) containing Triton X-100 (0.05%) and autolysis was monitored at 37°C for 5 h as the decrease in OD₅₇₈.

Zymogram

Bacteriolytic enzyme profiles were obtained on a 10% SDS-PAGE with embedded heat inactivated (100°C for 10 min) SA113 cells as substrate. For preparation of CW associated proteins cells were grown to mid-log phase (OD 0.6) and the proteins of 1 ml culture were released by treatment with 100 mM PBS (pH 7.2) containing 2% SDS for 15 min at 37°C. Cells were pelleted and the clear supernatant with the surface released proteins of SA113, SA113 $\Delta tagO$, $\Delta tagO$ (pRBtagO) and $\Delta atlA$ were subjected to electrophoresis. The gel was washed with water for 30 min and then incubated for 16 h in PBS (pH 7.2) at 37°C. The clear zones appeared as dark bands against black background.

Cell wall binding assay

To investigate binding of fluorescent protein to the intact cell surface, cells were grown to mid-exponential phase. Some 200 µl exponential phase cells (OD₅₇₈ 1.0) of SA113 and the corresponding mutants were incubated with 3 µg of Cy-5 labelled R_{1,2} for 1 min at RT. After washing with 1 ml 50 mM sodium phosphate buffer (pH 6.8) the CW bound proteins were released with 200 µl of 10% SDS. Fluorescence of the supernatant was determined in a Tecan fluorescence reader (excitation of 630 and emission of 670 nm) as the ratio of fluorescence of 3 µg Cy5-R_{1,2}.

Localization of amidase

For immunofluorescence microscopy, staphylococcal strains were grown until mid-exponential phase, then harvested by centrifugation, and washed twice with PBS (Sigma). Cells were blocked with 3% BSA in PBS for 30 min, followed by incubation with rabbit α -amidase primary antibody (1:200) for 1 h, washed twice with PBS and incubated with Alexa Fluor 594 conjugated goat anti-rabbit IgG (1:1000) for 1 h. Cells were then washed twice with 1 ml of PBS, and suspended in 200 µl PBS. Cell suspensions (10 µl) were applied to glass slides and viewed with a Leica DMRE fluorescence microscope. For epifluorescence microscopy cells harbouring the plasmid pCtufgfp for cytoplasmatic expression of GFP were grown to exponential phase, washed once with PBS and incubated with 20 µg ml⁻¹ Cy5-R_{1,2} for 5 min at RT. After washing twice with PBS, 15 µl of cell suspension was applied

on 1% agarose-coated glass slides and distribution of fluorescence was examined in a Leica epifluorescence microscope. To prove the effect of WTA, glycopolymers were removed by treatment with 10% TCA for 16 h as negative controls. To remove TCA cells were washed six times with PBS.

Localization of WTA

To examine the localization of WTA on the cell surface, staphylococcal cells were grown to exponential phase, harvested by centrifugation and boiled in 10% SDS in order to remove LTA and other possibly contaminating compounds. After washing with deionized water, cell pellets were resuspended in 50 mM Na-phosphate buffer (pH 6.8). Cells were then incubated with 100 µg ConA-FITC conjugate (Sigma-Aldrich) containing Ca²⁺ as cofactor for 30 min. To remove unbond ConA-FITC, cells were washed twice with PBS and examined as described above.

High-performance liquid chromatography separation of muropeptides

To illustrate the degree of PGN cross-linking in SA113 and SA113ΔtagO, PGN was isolated from exponentially grown SA113, SAΔtagO as described before (Bera *et al.*, 2006). To remove the WTA, purified peptidoglycan was incubated with 10% TCA at room temperature for 24 h. Approximately 2 mg purified peptidoglycan was digested with 100 U mutanolysin in 12.5 mM phosphate buffer (pH 5.5) in a total volume of 500 µl. Digestions were terminated by heating the samples at 90°C for 5 min. Insoluble muropeptides were removed by centrifugation, and soluble fractions were dried in a rotary evaporator. The dried muropeptides were resuspended in water and reduced with sodium borohydride. Excess borohydride was destroyed by adding 20% phosphoric acid. Muropeptides were analysed on an Agilent 1200 HPLC with ProntoSil 120, 3 µm, 250 × 4.6 mm C18 column (Bischoff Chromatography, Leonberg, Germany) using a linear gradient of 10 mM sodium phosphate buffer (pH 2.5) to 30% methanol for 150 min. Muropeptides were detected at 210 nm.

Scanning electron microscopy

For SEM bacterial cells were grown until mid-logarithmic phase in BM medium, harvested by centrifugation, washed twice with PBS (pH 7.2) and fixed using 2.5% glutaraldehyde for 1 h on ice. Cells were post fixed with 1% osmium tetroxide in PBS for 1 h on ice, dehydrated in ethanol and critical-point-dried from CO₂. The samples were sputter-coated with 8 nm gold-palladium and examined at 20 kV accelerating voltage in a Hitachi S-800 field emission scanning electron microscope.

Transmission electron microscopy

To monitor the bacterial lysis, exponentially grown cells were resuspended at 37°C in 6 ml PBS at OD of 0.5 at 578 nm

where cells gradually start to autolyse; 2 ml samples were taken at time points of 0, 2 and 4 h. Samples were processed for TEM as described previously (Biswas *et al.*, 2006). Briefly, cells were fixed using the glutaraldehyde/OsO₄ method. Fixed cells were covered with 2% agarose and blocks were cut out. After washing, agar blocks were dehydrated in an ethanol series beginning with 50% ethanol and finally placed in water-free acetone. Samples were then embedded in Spurr's resin and polymerized at 60°C for 2 days. Ultrathin sections were cut with an ultramicrotome with a diamond knife. Samples were post-stained with 1% uranyl acetate for 5 min and lead citrate for 3 min and examined with a Philips CM10 electron microscope.

Acknowledgements

We appreciate the expert technical help of Mulugeta Nega, Regine Stemmler and Cordula Gekeler. The work was supported by DFG: SFB766, TR-SFB34 and the Graduate College 'Infection biology' (GKI 685).

References

- Baba, T., and Schneewind, O. (1998) Targeting of muralytic enzymes to the cell division site of Gram-positive bacteria: repeat domains direct autolysin to the equatorial surface ring of *Staphylococcus aureus*. *EMBO J* **17**: 4639–4646.
- Bae, T., and Schneewind, O. (2006) Allelic replacement in *Staphylococcus aureus* with inducible counter-selection. *Plasmid* **55**: 58–63.
- Bera, A., Herbert, S., Jakob, A., Vollmer, W., and Götz, F. (2005) Why are pathogenic staphylococci so lysozyme resistant? The peptidoglycan O-acetyltransferase OatA is the major determinant for lysozyme resistance of *Staphylococcus aureus*. *Mol Microbiol* **55**: 778–787.
- Bera, A., Biswas, R., Herbert, S., and Götz, F. (2006) The presence of peptidoglycan O-acetyltransferase in various staphylococcal species correlates with lysozyme resistance and pathogenicity. *Infect Immun* **74**: 4598–4604.
- Bera, A., Biswas, R., Herbert, S., Kulauzovic, E., Weidenmaier, C., Peschel, A., and Götz, F. (2007) Influence of wall teichoic acid on lysozyme resistance in *Staphylococcus aureus*. *J Bacteriol* **189**: 280–283.
- Biswas, R., Voggu, L., Simon, U.K., Hentschel, P., Thumm, G., and Götz, F. (2006) Activity of the major staphylococcal autolysin Atl. *FEMS Microbiol Lett* **259**: 260–268.
- Brückner, R. (1997) Gene replacement in *Staphylococcus carnosus* and *Staphylococcus xylosus*. *FEMS Microbiol Lett* **151**: 1–8.
- Buist, G., Steen, A., Kok, J., and Kuipers, O.P. (2008) LysM, a widely distributed protein motif for binding to (peptido)glycans. *Mol Microbiol* **68**: 838–847.
- Giesbrecht, P., Kersten, T., Maidhof, H., and Wecke, J. (1998) Staphylococcal cell wall: morphogenesis and fatal variations in the presence of penicillin. *Microbiol Mol Biol Rev* **62**: 1371–1414.
- Götz, F. (2002) *Staphylococcus* and biofilms. *Mol Microbiol* **43**: 1367–1378.
- Heilmann, C., Hussain, M., Peters, G., and Götz, F. (1997) Evidence for autolysin-mediated primary attachment of

- Staphylococcus epidermidis* to a polystyrene surface. *Mol Microbiol* **24**: 1013–1024.
- Heilmann, C., Hartleib, J., Hussain, M.S., and Peters, G. (2005) The multifunctional *Staphylococcus aureus* autolysin aaa mediates adherence to immobilized fibrinogen and fibronectin. *Infect Immun* **73**: 4793–4802.
- Iordanescu, S., and Surdeanu, M. (1976) Two restriction and modification systems in *Staphylococcus aureus* NCTC8325. *J Gen Microbiol* **96**: 277–281.
- Kohler, T., Weidenmaier, C., and Peschel, A. (2009) Wall teichoic acid protects *Staphylococcus aureus* against antimicrobial fatty acids from human skin. *J Bacteriol* **191**: 4482–4484.
- Kreiswirth, B.N., Lofdahl, S., Betley, M.J., O'Reilly, M., Schlievert, P.M., Bergdoll, M.S., and Novick, R.P. (1983) The toxic shock syndrome exotoxin structural gene is not detectably transmitted by a prophage. *Nature* **305**: 709–712.
- Leibig, M., Krismer, B., Kolb, M., Friede, A., Götz, F., and Bertram, R. (2008) Marker removal in staphylococci via Cre recombinase and different lox sites. *Appl Environ Microbiol* **74**: 1316–1323.
- Lützner, N., Pätzold, B., Zoll, S., Stehle, T., and Kalbacher, H. (2009) Development of a novel fluorescent substrate for Autolysin E, a bacterial type II amidase. *Biochem Biophys Res Commun* **380**: 554–558.
- Oshida, T., Sugai, M., Komatsuzawa, H., Hong, Y.M., Suginata, H., and Tomasz, A. (1995) A *Staphylococcus aureus* autolysin that has an *N*-acetylmuramoyl-L-alanine amidase domain and an endo-beta-*N*-acetylglucosaminidase domain: cloning, sequence analysis, and characterization. *Proc Natl Acad Sci USA* **92**: 285–289.
- Peschel, A., Otto, M., Jack, R.W., Kalbacher, H., Jung, G., and Götz, F. (1999) Inactivation of the *dlt* operon in *Staphylococcus aureus* confers sensitivity to defensins, protegrins, and other antimicrobial peptides. *J Biol Chem* **274**: 8405–8410.
- Rosenstein, R., Nerz, C., Biswas, L., Resch, A., Raddatz, G., Schuster, S.C., and Götz, F. (2009) Genome analysis of the meat starter culture bacterium *Staphylococcus carnosus* TM300. *Appl Environ Microbiol* **75**: 811–822.
- Sinha, B., Francois, P.P., Nusse, O., Foti, M., Hartford, O.M., Vaudaux, P., *et al.* (1999) Fibronectin-binding protein acts as *Staphylococcus aureus* invasin via fibronectin bridging to integrin alpha5beta1. *Cell Microbiol* **1**: 101–117.
- Umeda, A., Ueki, Y., and Amako, K. (1987) Structure of the *Staphylococcus aureus* cell wall determined by the freeze-substitution method. *J Bacteriol* **169**: 2482–2487.
- Vergara-Irigaray, M., Maira-Litran, T., Merino, N., Pier, G.B., Penades, J.R., and Lasa, I. (2008) Wall teichoic acids are dispensable for anchoring the PNAG exopolysaccharide to the *Staphylococcus aureus* cell surface. *Microbiology* **154**: 865–877.
- Weidenmaier, C., and Peschel, A. (2008) Teichoic acids and related cell-wall glycopolymers in Gram-positive physiology and host interactions. *Nat Rev Microbiol* **6**: 276–287.
- Weidenmaier, C., Kokai-Kun, J.F., Kristian, S.A., Chanturiya, T., Kalbacher, H., Gross, M., *et al.* (2004) Role of teichoic acids in *Staphylococcus aureus* nasal colonization, a major risk factor in nosocomial infections. *Nat Med* **10**: 243–245.
- Yamada, S., Sugai, M., Komatsuzawa, H., Nakashima, S., Oshida, T., Matsumoto, A., and Suginata, H. (1996) An autolysin ring associated with cell separation of *Staphylococcus aureus*. *J Bacteriol* **178**: 1565–1571.
- Yamamoto, H., Miyake, Y., Hisaoka, M., Kurosawa, S., and Sekiguchi, J. (2008) The major and minor wall teichoic acids prevent the sidewall localization of vegetative DL-endopeptidase LytF in *Bacillus subtilis*. *Mol Microbiol* **70**: 297–310.

Structural Basis of Cell Wall Cleavage by a Staphylococcal Autolysin

Sebastian Zoll¹, Bernhard Pätzold^{1,9}, Martin Schlag^{2,9}, Friedrich Götz², Hubert Kalbacher^{1,3}, Thilo Stehle^{1,4*}

1 Interfaculty Institute for Biochemistry, University of Tübingen, Tübingen, Germany, **2** Department of Microbial Genetics, Faculty of Biology, University of Tübingen, Tübingen, Germany, **3** Medical and Natural Sciences Research Center, Tübingen, Germany, **4** Department of Pediatrics, Vanderbilt University School of Medicine, Nashville, Tennessee, United States of America

Abstract

The major autolysins (Atl) of *Staphylococcus epidermidis* and *S. aureus* play an important role in cell separation, and their mutants are also attenuated in virulence. Therefore, autolysins represent a promising target for the development of new types of antibiotics. Here, we report the high-resolution structure of the catalytically active amidase domain AmiE (amidase *S. epidermidis*) from the major autolysin of *S. epidermidis*. This is the first protein structure with an amidase-like fold from a bacterium with a gram-positive cell wall architecture. AmiE adopts a globular fold, with several α -helices surrounding a central β -sheet. Sequence comparison reveals a cluster of conserved amino acids that define a putative binding site with a buried zinc ion. Mutations of key residues in the putative active site result in loss of activity, enabling us to propose a catalytic mechanism. We also identified and synthesized muramyltripeptide, the minimal peptidoglycan fragment that can be used as a substrate by the enzyme. Molecular docking and digestion assays with muramyltripeptide derivatives allow us to identify key determinants of ligand binding. This results in a plausible model of interaction of this ligand not only for AmiE, but also for other PGN-hydrolases that share the same fold. As AmiE active-site mutations also show a severe growth defect, our findings provide an excellent platform for the design of specific inhibitors that target staphylococcal cell separation and can thereby prevent growth of this pathogen.

Citation: Zoll S, Pätzold B, Schlag M, Götz F, Kalbacher H, et al. (2010) Structural Basis of Cell Wall Cleavage by a Staphylococcal Autolysin. PLoS Pathog 6(3): e1000807. doi:10.1371/journal.ppat.1000807

Editor: Partho Ghosh, University of California San Diego, United States of America

Received: August 20, 2009; **Accepted:** February 4, 2010; **Published:** March 12, 2010

Copyright: © 2010 Zoll et al. This is an open-access article distributed under the terms of the Creative Commons Attribution License, which permits unrestricted use, distribution, and reproduction in any medium, provided the original author and source are credited.

Funding: This project was funded by German Research Foundation grants SFB-TR34 (to FG and TS) and SFB-685 (to HK). The funders had no role in study design, data collection and analysis, decision to publish, or preparation of the manuscript.

Competing Interests: The authors have declared that no competing interests exist.

* E-mail: thilo.stehle@uni-tuebingen.de

⁹ These authors contributed equally to this work.

Introduction

Effective treatment of staphylococcal infections remains a worldwide challenge. In the United States alone, Staphylococci are responsible for about 19,000 deaths per year, a number that is higher than that associated with HIV [1]. The ubiquity of Staphylococci contributes to the constant emergence of new strains that are resistant to antibiotics. In particular, staphylococcal infections of immunocompromised individuals can lead to endocarditis, meningitis, pneumonia, septicemia and the toxic shock syndrome. Although many such infections are caused by *S. aureus*, the ability of the closely related *S. epidermidis* to form biofilms upon attachment to polystyrene surfaces poses serious problems during transplantation of medical prostheses [2]. The major autolysin AtlE (autolysin *S. epidermidis*) acts as key virulence factor in this process by mediating the initial attachment in catheter-associated infections [3]. It also binds to vitronectin, suggesting a role in colonizing host factor coated materials and host tissue [4].

Together with the autolysin AtlA (autolysin *S. aureus*), AtlE belongs to a group of peptidoglycan (PGN)-hydrolases that play a pivotal role in the degradation of the bacterial cell wall [5,6,7]. During cell division, these autolysins are responsible for splitting the equatorial septum between two dividing daughter cells [8,9].

Deletion mutants show a disordered division pattern with large cell clusters and were biofilm-negative [4,7,10]. The highly similar AtlA and AtlE proteins consist of a signal peptide, a pro-peptide, a catalytic domain with N-acetylmuramyl-L-alanine amidase activity, three repeats (R1-R3), and a C-terminal catalytic domain with N-acetylglucosaminidase activity (Figure 1B). After secretion, the precursor protein is processed extracellularly to yield the mature amidase (containing the catalytic domain and repeats R1R2) and glucosaminidase (containing repeat R3 and the catalytic domain) proteins. The amidase repeats R1R2 are responsible for attaching the enzyme to the cell wall but do not contribute to lytic activity [7,11]. The catalytic domain, referred to as AmiE in *S. epidermidis* and AmiA in *S. aureus*, cleaves the amide bond between the lactyl moiety of N-acetylmuramic acid (MurNAc) and L-alanine in the PGN structure [7].

To provide a structural basis of autolysis function in *S. epidermidis*, we crystallized the catalytically active AmiE domain and solved its structure at 1.7 Å resolution. Using structure-based mutagenesis experiments and PGN digestion assays, we show that AmiE is a zinc-dependent metalloenzyme that requires a muramylpeptide with at least three consecutive amino acids as a substrate, while the side chain of the third amino acid can vary. Molecular docking provides evidence for extended contacts

Author Summary

Although Staphylococci are common inhabitants of the human skin and the respiratory tract, a number of highly pathogenic strains are a major cause of hospital-associated infections and can be life threatening especially in immunocompromised patients. Moreover, an increasing number of strains has acquired resistance against commonly used antibiotics, which makes treatment of infections a challenge. Therefore, antibacterial drugs that act on new targets are needed to counteract the further spread of multiresistant staphylococci. The autolysins, which are cell wall associated enzymes that are essential for cell proliferation, represent one promising such new target. We used x-ray crystallography to solve the structure of a catalytically active region of the autolysin of *Staphylococcus epidermidis*, AmiE, at atomic resolution. Our studies reveal a defined binding groove for a specific cell wall component on the protein surface. Using *in silico* calculations in combination with biochemical studies, we are able to identify key motifs that are required for the recognition of the cell wall by autolysins. Our data further indicate that, besides these core motifs, species-specific alterations of bacterial cell walls are responsible for the unambiguous identification of ligands. Knowledge of the interactions in an enzyme-substrate complex, as well as information about the mechanism of catalysis, are prerequisites for the successful development of antimicrobial drugs. Our results therefore provide a platform from which a new class of inhibitors can be launched.

between the D-isomer of glutamine (D-iGln) residue of the substrate and conserved residues in the putative ligand-binding groove of AmiE. These findings indicate an essential role of the glutamine isoform for substrate recognition. The structure therefore provides a framework for understanding substrate recognition, selectivity and catalytic mechanism of all staphylococcal amidases. It also reveals a striking and unexpected homology to the family of peptidoglycan recognition proteins (PGRPs), some of which also possess amidase activity. The AmiE fold closely resembles the PGRP-fold, including a conserved location of the active site and an asparagine in a conserved position likely to contact the second and third amino acid of the substrates peptide stem.

Results

Overall structure

The AmiE protein adopts a globular, mixed α/β fold, with a six-stranded, central β -sheet surrounded by seven α -helices (Figure 1A,C). The rear of the β -sheet packs against helices $\alpha 4$ and $\alpha 7$ and is shielded from solvent, while its front forms the bottom of a recessed area that is largely exposed and solvent-accessible. The recessed area, measuring about 28 Å by 10 Å, is walled off by helices $\alpha 2$, $\alpha 3$, $\alpha 5$, and several loops. Located at the center of the recessed area is a zinc ion that is held in place with contacts to side chains of residues H60 ($\beta 2$), H165 ($\alpha 5$) and D179 ($\alpha 5$ - $\alpha 6$ loop). The tetrahedral coordination sphere of zinc is completed by a water molecule, an arrangement often seen in the active sites of zinc-dependent metalloenzymes. Our structure revealed six additional bound zinc ions per monomer, which probably originated from the high concentration of zinc acetate present in the crystallization solution (see Materials and Methods). All six ions are located at or near surface loops. In order to verify that the zinc ion coordinated by residues H60, H165 and D179 is physiologic, we determined the structure of AmiE in a second

crystal form grown without the addition of zinc-containing salts. In this crystal form, AmiE contains only the single zinc ion coordinated by H60, H165 and D179. The identity of this ion was confirmed by calculation of an anomalous difference fourier map (data not shown).

Ligand binding site and enzymatic activity

Alignment of the AmiE sequence with 28 homologous bacterial proteins (Figure 2A) shows that only 10 out of 213 residues are strictly conserved in all sequences. Some of these are buried and likely contribute to the stability of the protein fold. However, the remaining residues cluster at the center of the recessed area, near the zinc ion (red residues in Figure 2B), and include the three zinc-coordinating residues H60, H165 and D179 (Figure 3A). Residues conserved to a lesser degree also cluster in this region, while the remaining AmiE surface is almost completely devoid of conserved amino acids. The conserved residues delineate a groove that runs along the recessed area, extending from the zinc ion to both the top and the bottom of the domain. The shape of the groove and its high degree of conservation indicate that it is the site of interaction with the PGN substrate. Moreover, the presence of zinc at the center of the groove suggests that AmiE functions as a zinc-dependent amidase. Residues E119 and H177, which are near the zinc ion but do not contact it, are likely to be involved in catalysis by facilitating a water-mediated nucleophilic attack at the peptide bond and stabilizing the transition state, as shown in Figure 3B.

In order to determine whether amino acids in the vicinity of the zinc ion are required for enzymatic activity, residues H60, H177 and D179 were separately mutated to alanine. All three mutant proteins were expressed and purified to homogeneity. None of them has lytic activity in zymogram gels with heat-inactivated *S. aureus* cells, whereas the wild type (wt) protein is able to lyse cell walls efficiently (Figure 4A). Similar results were obtained with lysis assays using purified *S. aureus* PGN (Figure 4B). Our results therefore provide evidence for a critical role of the zinc ion and its surrounding residues in catalysis. These findings are consistent with previous studies showing that treatment of the wt amidase with chelating agents such as EDTA or phenanthroline, which likely remove the zinc ion, results in loss of activity [12].

In order to assess the roles of amino acids H60, H177 and D179 *in vivo*, we expressed the wt gene coding for AmiE and repeats R1 and R2 (*amiE-R_{1,2}*) as well as three mutated *amiE-R_{1,2}* genes carrying H60A, H177A and D179A substitutions in an *S. aureus* strain that lacks the autolysin (SA113 Δ atLA, [7]) using the shuttle vector pRC20 [4]. The SA113 Δ atLA strain has a severe growth defect, forming large cell clusters that quickly sediment in liquid medium. In contrast, the wt SA113 strain grows homogeneously and does not form such aggregates. As shown in Figure 4C, only the wt *amiE-R_{1,2}* gene is able to fully complement the Δ atLA mutant. The amidase mutants H60A and D179A are unable to complement the Δ atLA mutant, suggesting that these mutants are not functional *in vivo*. In comparison, the H177A mutant shows a milder phenotype *in vivo* and partially complements the Δ atLA mutant to wt phenotype. Residues H60 and D179 both coordinate zinc and play critical roles in catalysis (Figure 3). The H177 side chain is not part of the zinc coordination sphere, but most likely functions to stabilize the transition state during catalysis (Figure 3B). Our results thus indicate that only mutations directly in the active center are sufficient to abolish enzymatic activity, resulting in a phenotype that matches the deletion mutant. The H177A mutation possibly results in decelerated reaction kinetics, thus producing a less severe phenotype compared to those of the H60A and D179A mutants. The *in vivo* assay can be regarded as more sensitive since cells were grown for 10 h. The small time

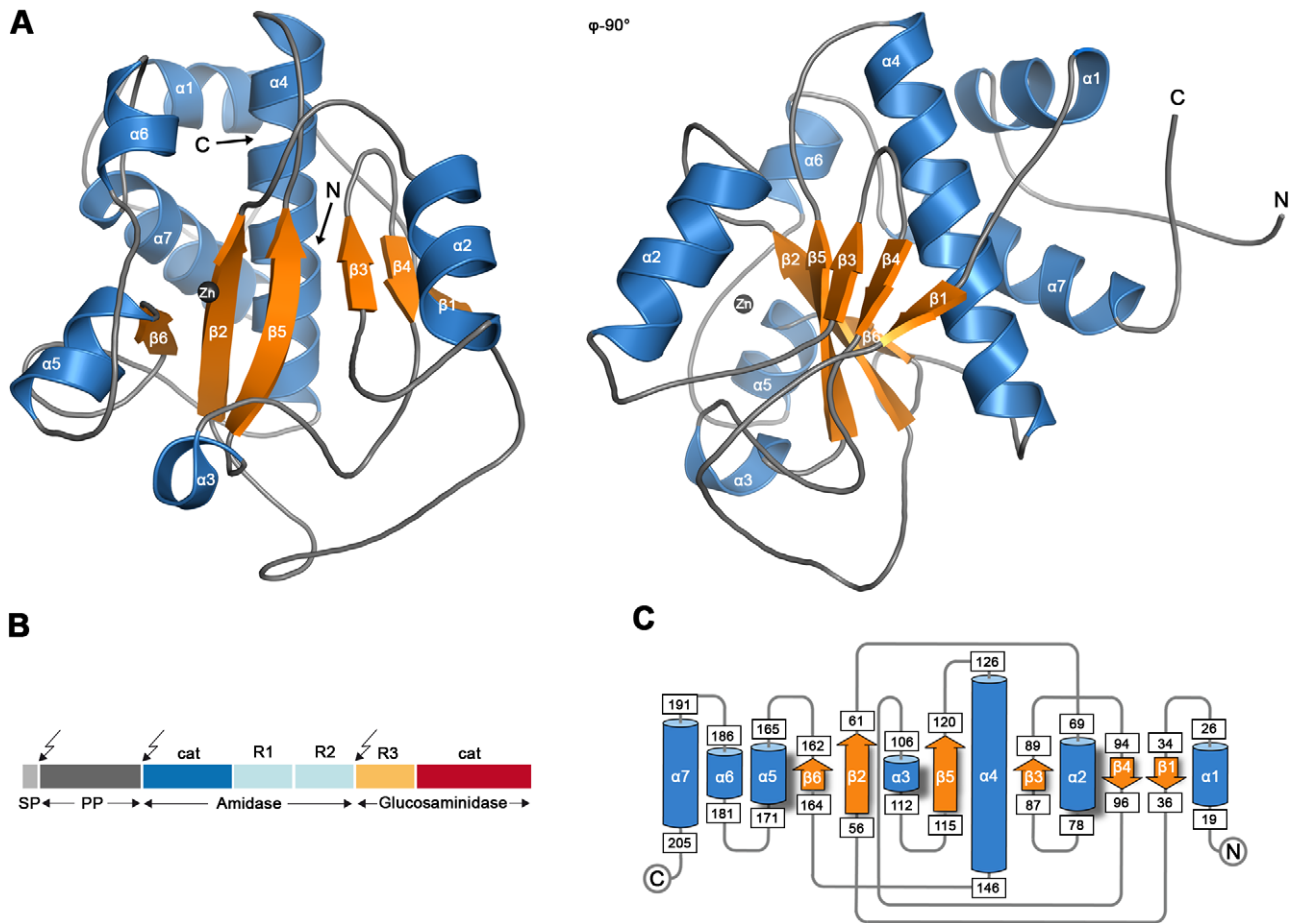


Figure 1. Crystal structure of the catalytic domain of AmiE. (A) Cartoon representation of the AmiE crystal structure. Two views differing by 90° are shown. Helices and strands are colored blue and orange, respectively. The zinc ion bound in the active center is shown as a grey sphere. (B) Domain arrangement of the bifunctional AtIE precursor protein. Arrows indicate the post-translational cleavage sites. **SP** signalpeptide, **PP** propeptide, **cat** catalytic domains, **R1 R2 R3** repeat domains. (C) Topology diagram of the AmiE structure, with helices and strands represented with cylinders and arrows, respectively. Numbers of amino acids are given in rectangles. doi:10.1371/journal.ppat.1000807.g001

frame of the *in vitro* assay is not sufficient to discriminate between an enzyme with a reduced activity and no activity.

The lack of lytic activity in the three mutant proteins could be due to conformational changes that would adversely affect their interaction with ligand. To test this possibility, we generated the PGN-derived N-acetylmuramyl-L-alanyl-D-iso-glutamyl-L-lysine (MTP) ligand as previously described [13] and labeled it by attaching biotin to the ϵ -amino group of L-lysine via a short linker (MTP-Biot) (see Methods). Affinity measurements using an ELISA assay clearly show that all three catalytically inactive mutants are still able to bind MTP-Biot (Figure 4D). Compared with the wt protein, the H177A mutant even shows significantly increased binding. The most likely explanation is that the H177A mutation leads to a smaller structural change in or near the active site that facilitates binding. As with many enzymes, the AmiE active site is probably designed to preferentially bind and stabilize the transition state. Since H177 is likely to participate in this stabilization (Figure 3B), its replacement with alanine may reduce conformational stress on the substrate, allowing for better binding of the native conformation. It is also possible that the wt protein partially cleaves MTP-Biot, which would result in a lower signal. However, as variation of the incubation time does not affect the value for the wt protein (data not shown), we consider this latter possibility unlikely.

Ligand specificity

To determine the minimal PGN sequence that can still be cleaved by AmiE, we performed cleavage assays with three PGN-derived compounds: MTP, N-acetylmuramyl-L-alanyl-D-iso-glutamine (MDP), and N-acetyl-D-glucosaminyl-(1,4)-N-acetylmuramyl-L-alanyl-D-iso-glutamine (GMDP). MDP and GMDP were purchased from Sigma and Calbiochem, respectively, whereas MTP was synthesized as described [13]. All ligands were incubated with the wt protein for 72 h at 37°C , followed by analysis of products with HPLC and ESI mass spectrometry. These experiments demonstrate that neither MDP nor GMDP are cleaved by the wt enzyme (data not shown), whereas MTP is cleaved into two fragments. The H177A mutant, which still binds to MTP, does not cleave MTP and therefore serves as a negative control in this experiment. The m/z profile of the H177A mutant is dominated by peaks at m/z 621 and 649 (Figure 5, right). The latter peak represents the MTP educt plus an unknown additional mass, which probably originates from the synthesis. Both peaks are replaced by peaks at m/z 346 and 374 in the profile for the wt protein (Figure 5, left). The first peak corresponds to the expected mass of the cleaved peptide stem while the second one is the digestion product of the compound with the higher mass. We conclude that cleavage by AmiE requires the presence of a third amino acid in the peptide stem. As the lysine is quite distant from the active site, it is most likely not required for the

A

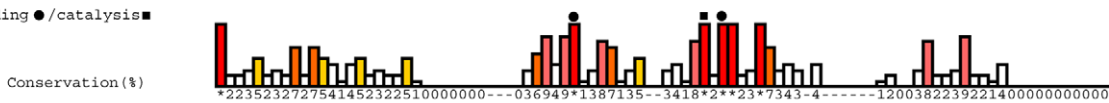
S. e. /AmiE/1-213 39: TSYFFPKYGRNGVGRPEGVIVHEDTAN----DNSTIDGEIAFMKRNYYTN--AFVHAFVD--GNRIETAPTDLYSWAGAPYGNQR-FINNVIVHT--H-DYDS 128
S. ca/1-1395 371: TSYFFPKYGRNGVGRPEGVIVHEDTAN----DNSTIDGEINYMKNYYQS--AFVHAFVD--GNRIETAPTDLYSWAGAPQGNR-FINNVIVHT--H-DYDS 460
S. h./1-1361 355: TSYFFPKYGRNGVGRPEGVIVHEDTAN----DNSTIDGEINYMKNYYNS--AFVHAFVD--GNRIETAPTDLYSWAGAPFNANR-FINNVIVHT--H-DYAS 444
S. a./1-1263 251: TSYFFPKYGRNGVGRPEGVIVHEDTAN----DRSTINGEISYMKNNYQN--AFVHAFVD--GNRIETAPTDLYSWAGAVGNR-FINNVIVHT--H-DYAS 90
S. x./1-1367 341: TSYFFPKYGRNGVGRPEGVIVHEDTAN----ENSTITGEINYMKNYYNS--AFVHAFVD--GNRIETAPTDLYSWAGAPFNANR-FINNVIVHT--H-DYDS 90
S. s./1-1564 632: ASYLLKKNYR--YKPEGVIVHEDTAN----DNSTITGEINFMKNYYN--AFVHAFVD--GNRIETANTDYLAWGGAAANR-FIHVELVHT--H-DYDS 719
S. co/1-1401 484: ASYLPKYYR--YKPEGVIVHEDTAN----DNSTITGEINYMKNYYNS--AFVHAFVD--GNRIETANTDYLAWGGAPFNANR-FIHVELVHT--H-DYDS 568
S. si/1-1266 290: SSYLPKYYR--YKPEGVIVHEDTAN----ENSTINNEVAYMKNWQON--AFVHAFVD--GNRIETANTDYLAWGGAPFNANR-FIHVELVHT--H-DKDS 377
S. sa/1-1463 541: ANYLPQYYR--YKPEGVIVHEDTAN----DNSTITGEINYMKNYYNS--AFVHAFVD--GNRIETANTDYLAWGGAPFNANR-FIHVELVHT--H-DYDS 628
L. d./1-536 67: NKYGRFGRNGVGRPEGVIVHEDTAN----PGATAWDEGRYFNNWMAAYTYVHAFVD--NNOIQIOLMSPDYGVWAGPIANR-YIQVQLCEV--S-TRSQ 158
P. p./1-859 238: THQLSDDEGSDQQTNNVIAHAFV----YAPAEVAIFEKREWDSSESYVQYI--YVTHVVDGGGRVQVAPGQGVYVAGQEGYVANGGEWANENAPVQVLAQT--Y-SDSQ 330
L. b./1-354 53: WNGFPKYYRHGKPKPEGVIVHEDTAN----PSSTIYNEIAYMKNYYQN--AFVHAFVD--GSRINLANTDYLAWGGAPFNANR-FVQFQVHV--H-SKSA 142
O. o./1-231 104: ANYLPQYYR--YKPEGVIVHEDTAN----PRSTITSEITMYMKNWRT--AFVHAFVD--GNSLIGVADTDYQWAGGALANR-FIHVELVHT--H-DYDS 148
L. w./1-604 104: KSQFPKFNRYNGYKPEGVIVHEDTAN----NSSTITGEINYMSTNYNN--AFVHAFVD--KSRILQIHTPTENGWVAGQYANR-FIQHVLVRS--K-TFDE 192
L. i./1-770 104: KSQFPKFNRYNGYKPEGVIVHEDTAN----NSSTITGEISYMSRNYNN--AFVHAFVD--KSRILQIHTPTENGWVAGQYANR-FIQHVLVRS--K-TFDE 193
L. m./1-917 104: KSQFPKFNRYNGYKPEGVIVHEDTAN----NSSTITGEINYMSTNYNN--AFVHAFVD--KSRILQIHTPTENGWVAGQYANR-FIQHVLVRS--K-TFDE 193
L. r./1-307 132: LSIIEFQRGYSSTSSNPRGVVHEDTAN----ENSTITSEVSYMKQNYSSRIVFVHTFID--NQIINLADTKYMAAGAPYANR-FVQFQVHV--Y-TAAS 223
B. c./1-354 33: IPDLPKPIYRNGVAGYEGVVAHSDTAT--PEAPAINIQYBSRTWRN--AFVHAFVD--WNETIQIASANYIAYGAPYANR-FVHVELVHT--H-DYTK 122
E. faecalis/1-365 30: -DPI-NFTYFPGSASNELVTLVHESGNERNL--GPHSLDNEVAYMKNWNSN--KYVSVYVSGGGRVQVAPAGQIQYGAASLANQKAYQIHLART--N-NAAT 124
L. a./1-364 59: YNKFPQYEVK--TGKPEGVIVHEDD--PGATAHDEAIYFNREWPVKYVHAFVD--DDHIQMRSPMGTVAGGALANR-FIHVELVHT--H-TRDA 148
E. faecium/1-341 32: YNLAPNGQ--DSRLAIPNKIILHETGTL--DAPARVAANMKNYYNSGNSYTTDVI--GDGGIYVRVGGQYVSWAGG--NANPYAPVQVLAQT--Y-DKAL 122
L. s./1-694 530: IAGLPHNE----TSQGFIVHESGSGVSGSETDPPALHEAITYMQNNWTS--AYVTHVVDGGGRVQVAPGQGVYVAGQEGYVANGGEWANENAPVQVLAQT--N-NKAK 621
B. sp./1-259 10: MSGLPNQPLT----AIKYVVAHESGNS--TNTGNPALENEIAYMKNRKN--AFVSHVVDGGGRVQVAPVNRVQVCGCFKGNYSYVQVLAQT--S-DKEQ 101
S. p./1-316 9: RTDLPQYGV--OPYRQVHAFSTGN--RNSTVQNEADHYRKPDEL--GFFSHVVG--GRVMQVGPVNDGAWVGGNNAEGYAVQLIES--HESKEE 97
S. mi/1-300 2: RTDLPQYGV--OPYRQVHAFSTGN--RNSTVQNEADHYRKPDEL--GFFSHVVG--GRVMQVGPVNDGAWVGGNNAEGYAVQLIES--HESKEE 97
S. ps/1-316 9: RTDLPQYGV--OPYRQVHAFSTGN--RNSTVQNEADHYRKPDEL--GFFSHVVG--GRVMQVGPVNDGAWVGGNNAEGYAVQLIES--HESKEE 97
S. l./1-259 93: MDTLPKLEYK--NGTYMGVIVHEDVGE--DNRLQVWVDRMYETVTR--AFVHAFVD--NEHLTAPAYEYVWAGGPKANR-FYIQHVLVRS--H-NFDD 180
S. mu/1-327 152: YHQFASYSYFGTSGKPKKIIIDTGN----DSSSIQSEVAYMEKNYKSTGVFVHSHFLD--KNLILQIADDSYMAAGGPKGNR-FYIQHVELVHT--Y-KEDD 243
D. h./1-253 7: VNNRQPEP----LQPGQVIVHEDTAT--PGATAQNEFNPNSQHRA--ASAHYFVD--WLELHAIPENEVAHAGYTAHR--PLSIVMSVDPQGH--DPQK 93

Zn-binding ●/catalysis ■



S. e. /AmiE/1-213 129: FARSNNNYADYAATQLQYYNLEKPDSAEND--GRGTWVTHAISRFL--GGTDAPHPQYFRSH-N----YSYAEYLDLIEYKYLITKQVAPWG 213
S. ca/1-1395 461: FARSNNNYADYAATQLQYYNLEKPDSAEND--GGGTWVTHAISRFL--GGTDAPHPQYFRSH-N----YSYAEYLDLIEYKYLITKQVAPWG 545
S. h./1-1361 445: FAKSMNNYADYAATQLQYYNLEKPDSAEND--GGGTWVTHAISRFL--GGTDAPHPQYFRSH-N----YTNYELYDLIEYKYLITKQVAPWG 529
S. a./1-1263 91: FARSNNNYADYAATQLQYYNLEKPDSAEYD--GNGTWTWTHAISRFL--GGTDAPHPQYFRSH-N----YSYDLIDLENEKYLITKQVAPWG 425
S. w./1-1367 91: FARSNNNYADYAATQLQYYNLEKPDSAEND--GGGTWVTHAISRFL--GGTDAPHPQYFRSH-N----YSYDLIDLENEKYLITKQVAPWG 515
S. x./1-1564 720: FARSNNNYADYAATNLQYYGLVPSDAEYD--GVGTWVTHAISRFL--GGTDAPHPQYFRSH-N----YSYDLIDLENEKYLITKQVAPWG 808
S. co/1-1401 569: FARSNTNYADYAATNLQYYGLVPSDAEYD--GVGTWVTHAISRFL--GGTDAPHPQYFRSH-N----YSYDLIDLENEKYLITKQVAPWG 656
S. si/1-1266 378: FARMNNNYADYAATNLQYYGLVPSDAEYD--GRGTWVTHAISRFL--GGTDAPHPQYFRSH-N----YNYDALDLENEKYLITKQVAPWG 462
S. sa/1-1463 629: FARSNNNYADYAATNLQYYGLVPSDAEYD--GVGTWVTHAISRFL--GGTDAPHPQYFRSH-N----YSYDLIDLENEKYLITKQVAPWG 713
L. d./1-536 159: FVQSVANDYAYTASLHSHNLTSPRASQD--GSGTWVTHAISRFL--GGTDAPHPQYFRSH-N----YSMDQFDLQYYVLDLQKQDTPAKE 203
P. p./1-859 331: FKKYDQYVYVNLRLDRAKKNWLTSLDSNE--YRGIKSEVWITNHV--WG--NVDVYGYLSTH-G----ISQTFADHLDQYVFGSSSDSNTMS 413
L. b./1-354 143: FAHEVANAAYTAYLLEKYNLKPNDAAVD--GKGSVWSDAVTRYL--GGTITVTVGVYENQW-G----YFNFSFVTLNEKYKAIQASKVTVYD 278
O. o./1-231 149: FAREQLNAAKFAADQLNHYHLGAASQ--RKTITWTHDVSRYL--GGTITVTVGVYENQW-G----YFNFSFVTLNEKYKAIQASKVTVYD 278
L. w./1-604 193: FARSNNNYAYYAYLLDQYKLPVDSAHSD--GKGTWVSDAVTRYL--GGTITVTVGVYENQW-G----YFNFSFVTLNEKYKAIQASKVTVYD 275
L. i./1-770 194: FARSNNNYAYYAYLLDQYKLPVDSAHSD--GKGTWVSDAVTRYL--GGTITVTVGVYENQW-G----YFNFSFVTLNEKYKAIQASKVTVYD 278
L. m./1-917 194: FARSNNNYAYYAYLLDQYKLPVDSAHSD--GKGTWVSDAVTRYL--GGTITVTVGVYENQW-G----YFNFSFVTLNEKYKAIQASKVTVYD 275
L. r./1-307 224: FANQGNAAAYTAYILKQNNLPVTKGTDK--GGGTWVTHAISRFL--GGTDAPHPQYFRSH-N----VSEAFRADKRAYHNSVNEVSPVE 200
B. c./1-354 123: FKRSYKRYKLLAKILRNRLSIV--EKGWTHSDVTHYL--GGTDAPHPQYFRSH-N----ISKAQLDQLQVSETGETVITIQP 207
E. faecalis/1-365 125: FKRSYAYYNLARDLQNIQADGFLDSDGT--EGYIVTHDWTIKN--WG--DITVYGYLAWR-G----YSMDQFDLQYYVLDLQKQDTPAKE 203
L. a./1-364 149: FIKSNNNDIYVAKLHRDYKLPNDACDD--GEGTITWTHAISRFL--GGTDAPHPQYFRSH-N----YSMDQFDLQYYVLDLQKQDTPAKE 203
E. faecium/1-341 123: FEKNYRAYEYTRDSAKKYGLPLTLQDQSLFTKGLIISHLWVINYV--WG--NITVYGYLAWR-G----VSKELAYDLAHTPDDTSTENK 238
L. s./1-694 622: FKKDYKAYTWLRLDRAKKNWLTSLDSNE--GNGVKITWISYAY--REVDMVYGYLAWR-G----VSRADFVHDLDQYVFGVQ-- 694
B. sp./1-259 102: FKKDYAYYTWLRLDRAKKNWLTSLDGTG--NGIKSRWITADNL--GGTITVTVGVYENQW-G----VTEAQDKNLEBEELVTSQYNE 184
S. p./1-316 98: FLIDYRLYTELLRNLDDEAGTPKTLDTDD--LAGIKTIEYCTNNPDDNSDIEYFYLAKW-G----ISRECFKQDIEGLTIEAGWQNDT 183
S. mi/1-300 91: FLIDYRLYTELLRNLDDEAGTPKTLDTAD--LAGIKTIEYCTNNPDDNSDIEYFYLAKW-G----ISRECFKQDIEGLTIEAGWQNDT 176
S. ps/1-316 98: FLIDYRLYTELLRNLDDEAGTPKTLDTAD--LAGIKTIEYCTNNPDDNSDIEYFYLAWG-G----ISRECFKQDIEGLTIEAGWQNDT 183
S. l./1-259 181: FAKSNNNQAWLAAYMLKQNGITPTLADDN--AGKGSVISHNAVQKYV--GGTDAPHPQYFRSH-N----YDMHGMFDLQYYVLDLQKQDTPAKE 259
S. mu/1-327 244: FARTQANAYYAAFMKLYKLPVTLRQKN--TSGTWTWTHAISRFL--GGTDAPHPQYFRSH-N----YDMHGMFDLQYYVLDLQKQDTPAKE 327
D. h./1-253 94: FQEVKRTLWLVADAVRYGWT-----THNVFSDISLTY--GETNITVTVGVYENQW-G----DMIMALEGIDGLQKINIGGD 170

Zn-binding ●/catalysis ■



B

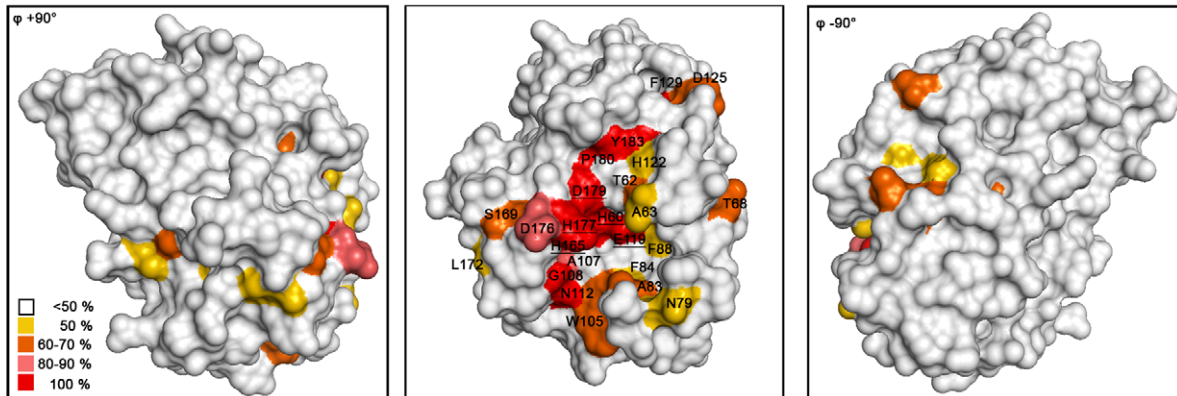


Figure 2. Conserved AmiE residues map to a single ligand-binding groove. (A) Sequence alignment of AmiE and 28 homologous proteins. Alignments were calculated with the programs ClustalW2 [34], MUSCLE [35] and MAFFT [36] and combined into a single output using COMBINE [37,38]. Conserved amino acids are color-coded according to their degree of conservation, ranging from white (not conserved) to red (fully conserved). Residues participating in zinc-binding and catalysis are marked with rectangles and triangles, respectively. Abbreviations are as follows: **S.e** *Staphylococcus epidermidis*, **S.ca** *Staphylococcus caprae*, **S.h** *Staphylococcus haemolyticus* JCSC1435, **S.a** *Staphylococcus aureus* RF122, **S.w** *Staphylococcus warneri*, **S.x** *Staphylococcus xylosum*, **S.co** *Staphylococcus cohnii*, **S.si** *Staphylococcus simulans*, **S.sa** *Staphylococcus saprophyticus*, **L.d** *Lactobacillus delbrueckii* subsp. *bulgaricus* ATCC 11842, **P.p** *Pediococcus pentosaceus* ATCC 25745, **L.b** *Lactobacillus brevis* ATCC 367, **O.o** *Oenococcus oeni* PSU-1, **L.w** *Listeria welshimeri* serovar 6b str. SLCC5334, **L.i** *Listeria innocua* Clip11262, **L.m** *Listeria monocytogenes*, **L.r** *Lactobacillus reuteri* F275, **B.c** *Bacillus cereus* subsp. *cytotoxus* NVH 391–98, **E. faecalis** *Enterococcus faecalis* V583, **L.a** *Lactobacillus acidophilus* NCFM, **E. faecium** *Enterococcus faecium* DO, **L.s** *Lactobacillus sakei* subsp. *sakei* 23K, **B.sp.** *Bacillus* sp. B14905, **S.pn** *Streptococcus pneumoniae*, **S.mi** *Streptococcus mitis*, **S.ps** *Streptococcus pseudopneumoniae*, **S.l** *Staphylococcus lugdunensis*, **S.mu** *Streptococcus mutans* UA159, **D.h** *Desulfitobacterium hafniense* Y51. (B) Conservation pattern of amino acids on the surface of AmiE, shown in three different views. Amino acids are colored according to their degree of conservation using the color scheme of panel A. The majority of conserved residues, including residues with the highest degree of conservation, clusters in a distinct region around the catalytic zinc ion. Underlined letters mark amino acids of the coordination sphere (H60, H165 and D179) as well as H177 and E119, which have roles in catalysis. doi:10.1371/journal.ppat.1000807.g002

catalytic reaction itself but likely serves to anchor the ligand in the binding site. Similar cleavage results have previously been obtained for the catalytically active PGRP-L protein, which also requires MTP for cleavage [14].

Structure-based molecular docking of MTP

Efforts to obtain a crystal structure of AmiE with a bound PGN fragment, either through co-crystallization or soaking, were unsuccessful. We therefore undertook molecular docking studies to establish a plausible mode of interaction for the MTP ligand with AmiE (see Methods). The available biochemical and structural data served as constraints for this approach. The best docking solution, which combines the highest docking score with a sensible orientation in the binding groove, is shown in Figure 6. The solution places the carbohydrate moiety in a relatively open, surface-exposed region at one end of the groove, and the tripeptide stem into the groove. Residues in the active site near the zinc ion, which are likely to play a role in catalysis, are positioned near the bond that is cleaved by AmiE. A nucleophilic attack of this bond by an activated water molecule, as shown schematically in Figure 3B, would therefore easily be possible.

Main chain and side chain atoms of residues in the second and third position of the peptide stem are able to make favorable contacts with residues in the AmiE groove. In particular, the model indicates a significant role for the D-iGln residue in substrate recognition as this residue forms 6 of the total 10 hydrogen bonds with the protein (Figure 6). Main chain atoms at both ends of the residue as well as side chain atoms are engaged in contacts. As equivalent contacts would not be possible with a standard glutamic acid residue, our model presents evidence for the importance of the glutamine isoform for substrate recognition. Asparagine 112 is strictly conserved among proteins that likely share the amidase-like fold (Figure 2) and occupies a position in the short $\alpha 6$ helix that allows the formation of hydrogen bonds between the side chain nitrogen and the two main-chain carbonyl oxygen atoms of D-iGln and L-Lys (see below).

We also note that, in our model, the L-lysine side chain fits into a surface pocket. The hydrophobic portion of its side chain forms extensive van der Waals interactions with the aromatic ring of W105. A prolonged lysine side chain with additional glycines of the interpeptide bridge would most likely run along the mainly hydrophobic chute that starts near W105 (Figure 6B, yellow circles).

The influence of substrate modifications on catalysis

In agreement with the docking model, digestion assays with MTP suggest an important role of the third amino acid in the peptide stem. In order to further investigate the role of the lysine side chain for substrate recognition we performed additional digestion assays

with MTP derivatives. For each of those, the sugar moiety (MurNAc) was replaced with a cleavable fluorescent (7-Methoxycoumarin-4-yl)-acetyl (Mca) reporter group since this group is known to have little effect on substrate recognition [12]. Substrates with one, two or three glycine residues attached to the lysine side chain were prepared (Mca-Ala-D-iGln-Lys(Gly)-D-Ala-Arg-OH, Mca-Ala-D-iGln-Lys(Gly)₂-D-Ala-Arg-OH, Mca-Ala-D-iGln-Lys(Gly)₃-D-Ala-Arg-OH), as well as a compound in which the lysine is replaced with an alanine (Mca-Ala-D-iGln-Ala-D-Ala-Arg-OH). The exact number of glycines tethered to the lysine side chain of the natural PGN substrate recognized by AmiE is still unknown. Nevertheless, the chosen compounds match the *in vivo* conditions better than a terminal lysine side chain with a charged amino group. The Lys-substrate (without glycines) served as a reference.

Our results clearly show that all five substrates can be cleaved by AmiE (Figure 7). However, reaction kinetics are rather slow, which might be due to the fact that the substrates lack the N-acetyl-D-glucosaminyl and N-acetylmuramyl sugar moieties. Approximately 10 percent of the Ala-substrate is cleaved after 6 h. All of the Gly-substrates were processed similarly, with about 20 percent cleaved after 6 h. The Lys-substrate shows the fastest rate of cleavage, with almost half of the educt being digested within the same time. Comparison of the cleavage efficiencies between the Lys(Gly)_x-substrates and the Ala-substrate reveals that the lysine side chain does not appear to have a significant impact for substrate recognition as the mutation of Lys to Ala only slows cleavage but does not prevent it. Furthermore, the negligible differences among the Lys(Gly)_x-substrates show that an increasing number of glycines does not result in enhanced binding to AmiE. As our docking model shows, the charged ϵ -amino group of the Lys-substrate could easily form a cation- π bond with W105 at the end of the PGN-groove (Figure 6A), leading to enhanced binding and perhaps accounting for the increased cleavage rate observed for this compound. Such an interaction would however not occur *in vivo*.

Structural relationships

Although the amino acid sequence of AmiE does not exhibit significant homology to other structurally known proteins, we were surprised to find that its fold is strikingly similar to that observed in other zinc-dependent amidases. A DALI analysis [15] shows that the closest structural homolog of AmiE is the N-terminal domain of PlyL, a prophage endolysin encoded by the *Bacillus anthracis* genome (Z-score = 18.4, rmsd = 2.1) [16]. Like AmiE, PlyL is an N-acetylmuramyl-L-alanine amidase, cleaving PGN at the same site. Interestingly, the domain organization of PlyL, which contains an N-terminal catalytic domain and a C-terminal cell-wall binding domain, mirrors that of AtlE, which also has an N-terminal amidase followed by repeats that are reported to interact with components of the staphylococcal cell wall [7].

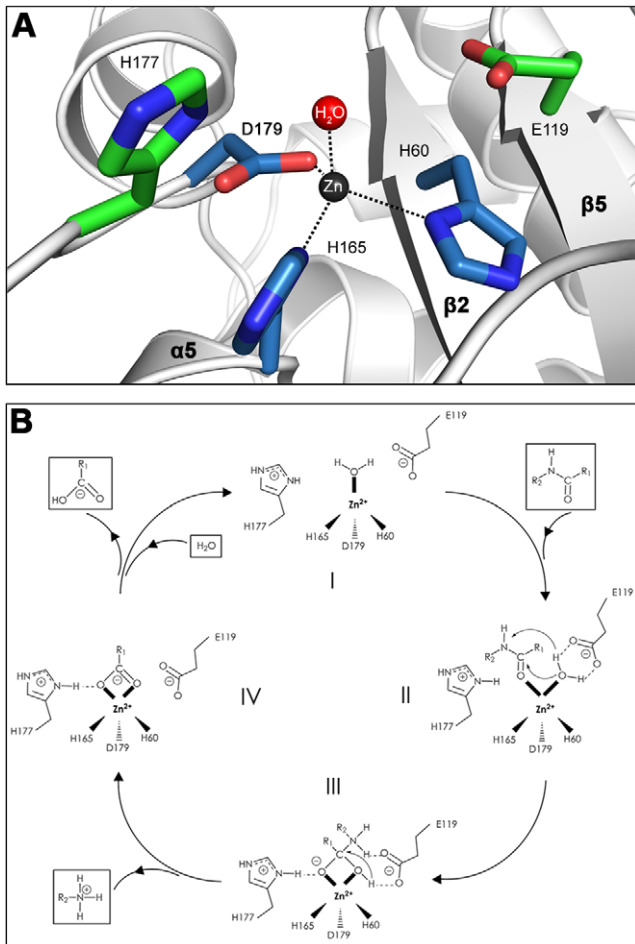


Figure 3. Close-up view of the AmiE active center and mechanism of catalysis. (A) Architecture of the active site. Side chains of H60, H165, D179 (blue) and a water molecule (red) coordinate a central zinc ion. Side chains of H177 and E119 (green) are 4.5 Å and 4.9 Å, respectively, apart from the zinc. E119 likely acts as a proton shuttle while the protonated side chain of H177 probably serves to stabilize a transition state. (B) Proposed mechanism of catalysis. The free enzyme is shown in (I). Upon docking of a PGN-fragment the Michaelis-Menten complex is formed (II). Acting as an electrophilic catalyst, the zinc ion accepts an electron pair from the carbonyl oxygen of the lactyl moiety, which becomes wedged between the water molecule and the side chain of H177. This results in a pentacoordinated zinc ion and a displacement of the water molecule towards the E119 side chain. The strong polarization between the positively charged zinc ion and the negative carboxylate of E119 leads to a nucleophilic attack of the water oxygen on the carbonyl carbon, which is in close vicinity. In this process, E119 serves as a proton shuttle by transferring the accepted proton to the nitrogen of the peptide bond. This results in the formation of a transition state (III), in which the former carbonyl carbon is now tetrahedral. The negative charge on the carbonyl oxygen in this state is stabilized by the protonated side chain of H177. In the next step (IV), E119 acts again as a proton shuttle by transferring the second proton. Thus, it promotes cleavage of the peptide bond and subsequent release of the peptide stem. In this state, MurNAc is still attached to the zinc ion via the lactyl carboxyl-group. Replacement against an incoming water molecule closes the catalytic cycle and reconstitutes the initial state (I). doi:10.1371/journal.ppat.1000807.g003

The AmiE structure is also highly homologous to the PGRP family of proteins (Figure 8). PGRPs are pattern recognition molecules that are conserved both in vertebrates and invertebrates and recognize PGN, the unique cell wall component of bacteria. In insects, PGRPs mainly activate antimicrobial pathways.

Mammalian PGRPs are not involved in signaling pathways, but are bactericidal by interfering with PGN synthesis. A third group, PGN-hydrolyzing PGRPs, has been found in insects and mammals. Although soluble and membrane-bound variants of PGRPs with different molecular weights exist, all PGRPs possess a domain that closely resembles the AmiE fold. To date, structures of this domain from *Drosophila melanogaster* (PGRP-LB and PGRP-SA) and *Homo sapiens* (PGRP-I α C and PGRP-S) are known. All four PGRPs can be superimposed with AmiE with low r.m.s. deviations (Figure 8). Only PGRP-LB functions as a PGN-hydrolyzing amidase, whereas the other structurally known PGRPs can bind PGN but are unable to cleave it. Non-lytic PGRPs lack zinc-coordinating residues in the active site. They likely interfere with bacterial growth by enclosing parts of the PGN layer and thereby preventing further crosslinking [17].

The superposition of AmiE with PlyL and the PGRPs shows that the best agreement is seen around the putative PGN-binding groove and the active site (Figure 8B,C). The coordination of zinc in the amidases PGRP-LB and PlyL closely resembles the zinc-binding site in AmiE. The histidines surrounding the zinc ions are in equivalent positions, while D179 is replaced with cysteines in PGRP-LB and PlyL. Both aspartates and cysteines can ligate zinc. In addition, the carboxylate groups of E119 in AmiE and E90 in PlyL occupy similar positions. E90 has been suggested to act as a proton shuttle in the catalytic cycle of PlyL, similar to the proposed role of E119 in AmiE (Figure 3B). This role is taken over by the deprotonated side chain of Y78 in PGRP-LB, which protrudes from the adjacent α 2- β 3 loop, bringing its phenol oxygen in close proximity to the E119 carboxylate in the superposition (Figure 8B). The side chain of AmiE residue H177 lies near the side chain of K135 in PlyL. Both residues in the same position are predicted to stabilize a transition state during substrate cleavage.

All six structures also have a conserved asparagine at the end of their putative PGN-binding sites (Figure 8C). For the non-catalytic amidases, it has been shown [18] that an asparagine in this position contacts the carbonyl oxygens of D-iGln and L-Lys (PGRP-I α C, PGRP-SA) of MTP via hydrogen bonds. In the docking model of PGRP-S, only L-Lys is contacted by the corresponding asparagine. Our docking model of AmiE and MTP shows that N112 is engaged in hydrogen bonds with the D-iGln and L-Lys carbonyls (Figure 6). Both hydrogen bonds are likely critical for anchoring the substrate as we find that compounds that lack the third amino acid cannot be processed by AmiE.

As expected, regions more distant from the substrate-binding groove are structurally more diverse. AmiE and the N-terminal PlyL domain are modular proteins that are connected to additional domains that mediate interactions with the cell wall. AmiE mainly differs from PlyL by a unique 20 residue N-terminal extension, including helix α 1. As this helix lies close to the C-terminus of AmiE (Figure 1A), it likely interacts with the repeats R1 and R2, probably forming an adapter between the catalytic domain and the cell wall binding domain. The PGRPs differ in number and arrangement of α -helices at their C-terminus from AmiE and PlyL. They also all have an additional 3_{10} helix, which is absent in the bacterial amidases. This helix is located in the so-called PGRP-specific segment, near the N-terminus, which serves to bind different non-PGN substrates such as effector molecules or molecules involved in signaling pathways.

Discussion

We have solved the crystal structure of the AtE amidase AmiE from *Staphylococcus epidermidis* at high resolution. This is not only the first structure of a staphylococcal amidase, but also of an amidase

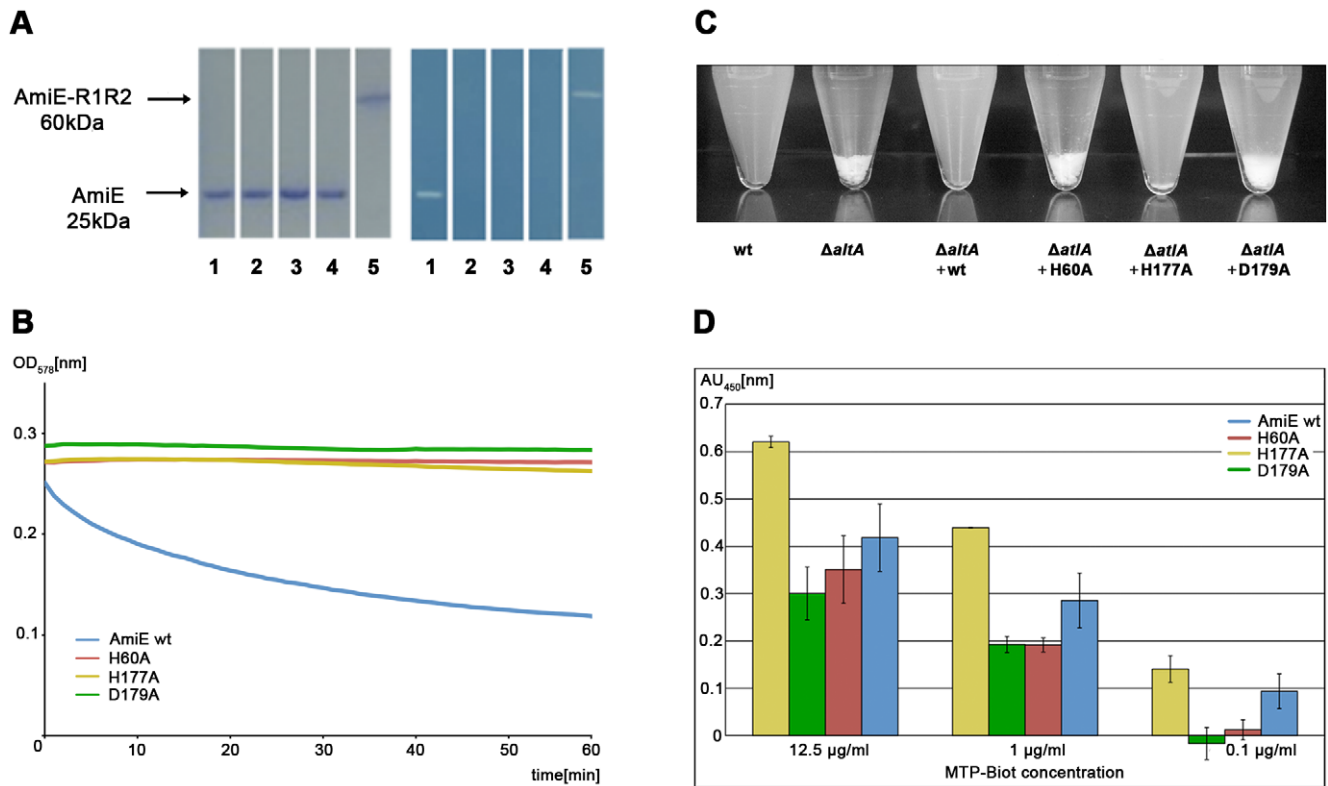


Figure 4. Activity and binding assays of amidase mutants. (A) Coomassie staining of the purified proteins after SDS-PAGE (left) and the corresponding methylene blue stained zymogram (right) with embedded heat-killed *S. aureus* cells. Lanes: **1.** wt AmiE, **2.** AmiE D179A, **3.** AmiE H177A, **4.** AmiE H60A, **5.** AmiE-R1R2 (control). (B) Digestion of *S. aureus* peptidoglycan in sodium phosphate buffer (100 mM, pH 7.0) at 37°C with 20 μ g of the respective enzymes. Lysis of peptidoglycan was measured as the decrease in optical density at 578 nm. (C) Complementation of the *S. aureus* SA113 Δ atI mutant. SA113 wt and SA113 Δ atI mutant strains carrying different point mutations in the complementation plasmid pRC20 were grown for 10 h in B-broth. Sedimentation (aggregation) of cells was observed as a consequence of the inability of the cells to separate SA113 wt, SA113 Δ atI, SA113 Δ atI (pRC20_wt), SA113 Δ atI (pRC20_H60A), SA113 Δ atI (pRC20_H177A), and SA113 Δ atI (pRC20_D179A). (D) Binding affinities of biotin labeled MTP to inactive mutants. ELISA assay after 60 min of incubation with Streptavidin horseradish peroxidase at different MTP-Biot. concentrations. The best signal to noise ratio was obtained at a concentration of 12.5 μ g/ml MTP-Biot. doi:10.1371/journal.ppat.1000807.g004

from any bacterium with a gram-positive cell wall architecture. Comparison with related bacterial enzymes reveals few conserved residues. Almost exclusively, these map to an elongated groove on

one side of the protein. Architecture and size of the groove indicate that it is likely to serve as the binding site for a portion of PGN. A tetrahedrally coordinated zinc ion at the center of the

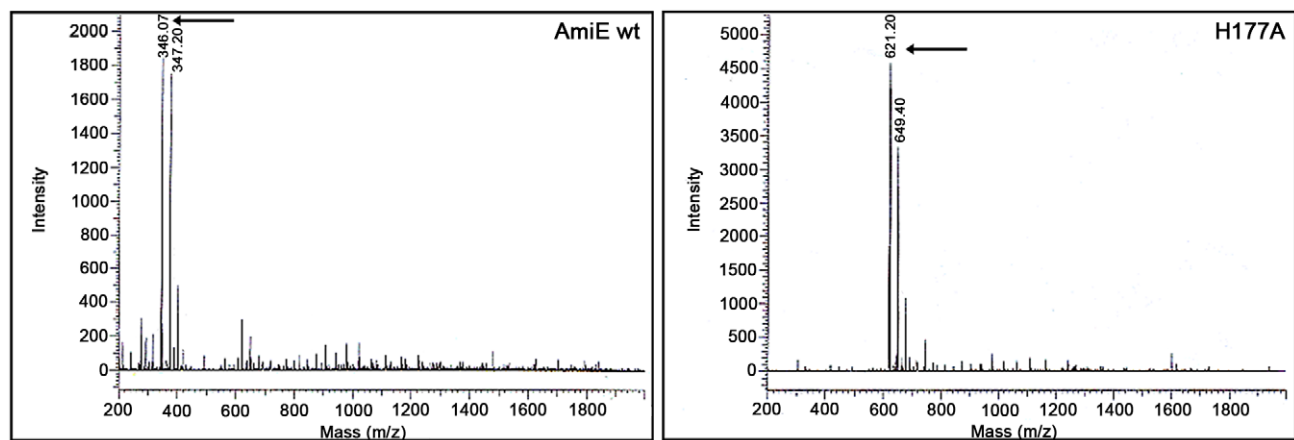


Figure 5. MTP digestion assay. ESI-MS spectra of MTP digest with AmiE wt and H177A. The wildtype enzyme and an inactive mutant (H177A) were incubated for 72h with MTP. ESI-MS spectrum of AmiE wt + MTP (left). Arrows indicate the masses of the digestion products. The main peaks are at m/z 346 and 374, which correspond to the cleaved peptide stem. ESI-MS spectrum of MTP + H177A (right). The m/z peaks at 621 and 649 correspond to MTP as synthesized. doi:10.1371/journal.ppat.1000807.g005

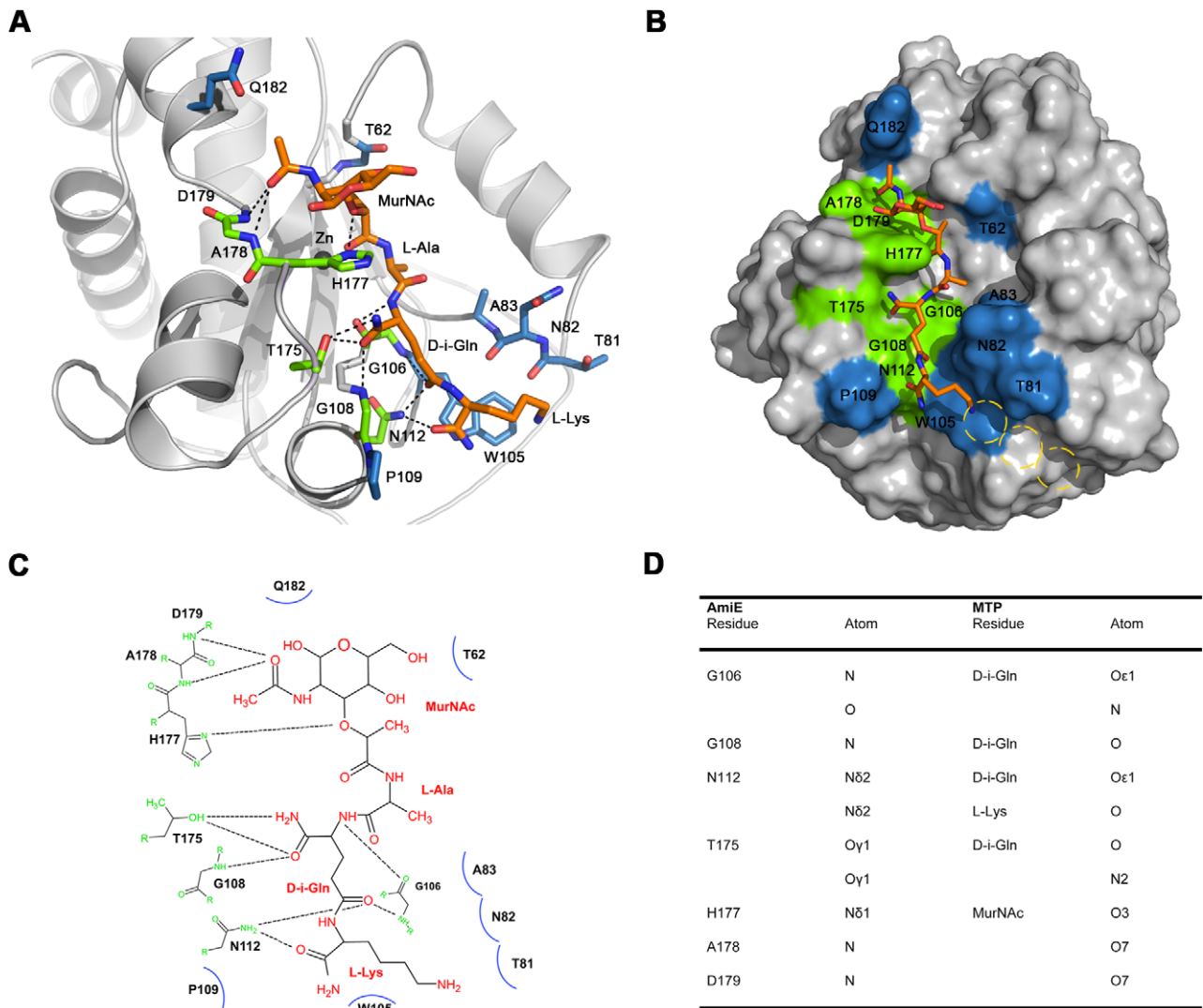


Figure 6. Results of docking of AmiE with the MTP ligand. (A) Putative interactions between AmiE (grey) and MTP (orange) in the docking model. AmiE residues forming hydrogen bond are colored green, residues making three or more van der Waals interactions are colored blue. Hydrogen bonds are indicated with dashed lines. (B) Surface representation of AmiE with MTP docked into the binding groove. Residues forming hydrogen bonds and van der Waals interactions were calculated using the PISA server (http://www.ebi.ac.uk/msd-srv/prot_int/pistart.html) [39]. The putative locations of glycine residues, which would be attached to the lysine side chain in the natural ligand, are indicated with yellow circles. (C) Schematic representation of interactions between AmiE and MTP. Van der Waals interactions are represented with arcs. The same color scheme for contacting residues was used in panels A, B and C. (D) Summary of the observed hydrogen bonds in the model. doi:10.1371/journal.ppat.1000807.g006

groove marks the active site of the enzyme. Mutagenesis experiments at this site provide strong evidence that AmiE functions as a zinc-dependent metalloprotease.

Currently, fourteen protein structures that share the N-acetylmuramyl-L-alanine amidase-like fold observed in AmiE have been deposited in the Protein Data Bank. Five of these structures show catalytic activity, but so far none of the catalytically active enzymes has been crystallized in complex with a ligand. Therefore, the principles that guide the interaction of these enzymes with their substrates remain undefined. In order to provide a basis for understanding their ligand-binding and activity properties, we first defined MTP as the minimal ligand that can still be cleaved by AmiE, and then performed docking studies with this ligand. Our results indicate that the carbohydrate moiety plays a minor role in binding. However, the glutamine isoform in the second position and presence of a third amino acid in the peptide

stem are key determinants of binding, needed to position the ligand in the binding groove. Furthermore, mutation of lysine in the third position to an alanine does not abolish substrate recognition by the enzyme, indicating that contacts with the third amino acid are restricted to the main-chain of the peptide stem. This finding is consistent with our docking results. The digestion assays, using substrate derivatives with one, two and three glycines residues attached to the lysine side chain, show that all three substrates are processed equally well, but show a significantly higher binding affinity than the alanine derivative, which is likely due to additional van der Waals interactions with either the lysine side chain or the first glycine residue.

What are the key requirements for successful PGN binding and cleavage by AmiE? Replacing MurNAc with a fluorophore, changing the amino acid in the third position, and absence of the D-iGln amidation [12] clearly do not prevent binding, and thus

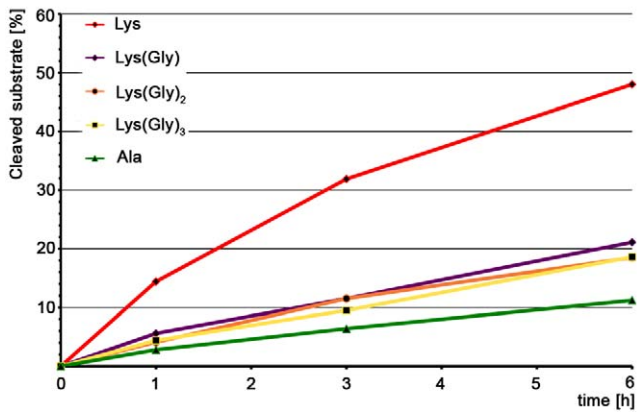


Figure 7. Digestion assay with modified AmiE substrates. Five substrates, differing in the modification of the third amino acid, were digested by AmiE over 6 h at 37°C. The amount of cleaved substrate was measured at the indicated time points. doi:10.1371/journal.ppat.1000807.g007

variations and extensions at these positions can likely be tolerated by the enzyme. However, the presence of the glutamine isoform at position two of the peptide is likely critical for binding. It was previously shown that a three amino-acid substrate with a glutamine in its standard configuration is not recognized by AmiE [12]. Our docking experiments clearly show that the D-iGln residue forms the majority of hydrogen bonds with AmiE, supporting a critical role for this residue. Moreover, a standard glutamic acid at the equivalent position would not be accommodated by AmiE, as its side chain would clash with residues lining the groove. The results from our docking studies are also consistent

with structural information on a complex of PGRP-I α C with PGN and docking models of PGRP-S and PGRP-SA. All of these show extensive contacts with D-iGln [18]. The digestion assay with an alanine substrate clearly showed that the absence of the lysine side chain has only a minor impact on substrate recognition when compared to the Lys(Gly)_x substrates. Our docking model, in which the main chain of the third amino acid is primarily involved in interactions, supports these data. The main chain of the third amino acid can therefore be described as a minimal motif that is essential for recognition of the substrate.

N112, which is located towards the lower end of the groove, is strictly conserved in bacterial amidases (Figure 2A). We were surprised to find an asparagine at an equivalent position in catalytically active as well as inactive PGRPs (Figure 8C). This residue is the only conserved amino acid among bacterial and eukaryotic amidases that participates in PGN binding. Its conservation therefore indicates that it is required for the recognition of a muramylpeptide with a three-peptide stem. In our docking model, the $\delta 2$ nitrogen of N112 forms hydrogen bonds with the main chain carbonyl oxygens of D-iGln and L-Lys. We therefore postulate that a common PGN binding mode is shared by all proteins with an N-acetylmuramyl-L-alanine amidase-like fold.

Our data show that only a small number of PGN consensus motifs are required for recognition by AmiE. Such motifs are present in many different types of cell walls. How does the amidase then ensure species-specific binding to the bacterial cell wall, and how does this compare with other amidases that have similar catalytic activities but act on different cell wall types? It is likely that AmiE uses a dual strategy to ensure species-specific substrate recognition with high affinity. In the first step, the repeating units that follow AmiE in sequence (Figure 1B) likely mediate cell wall

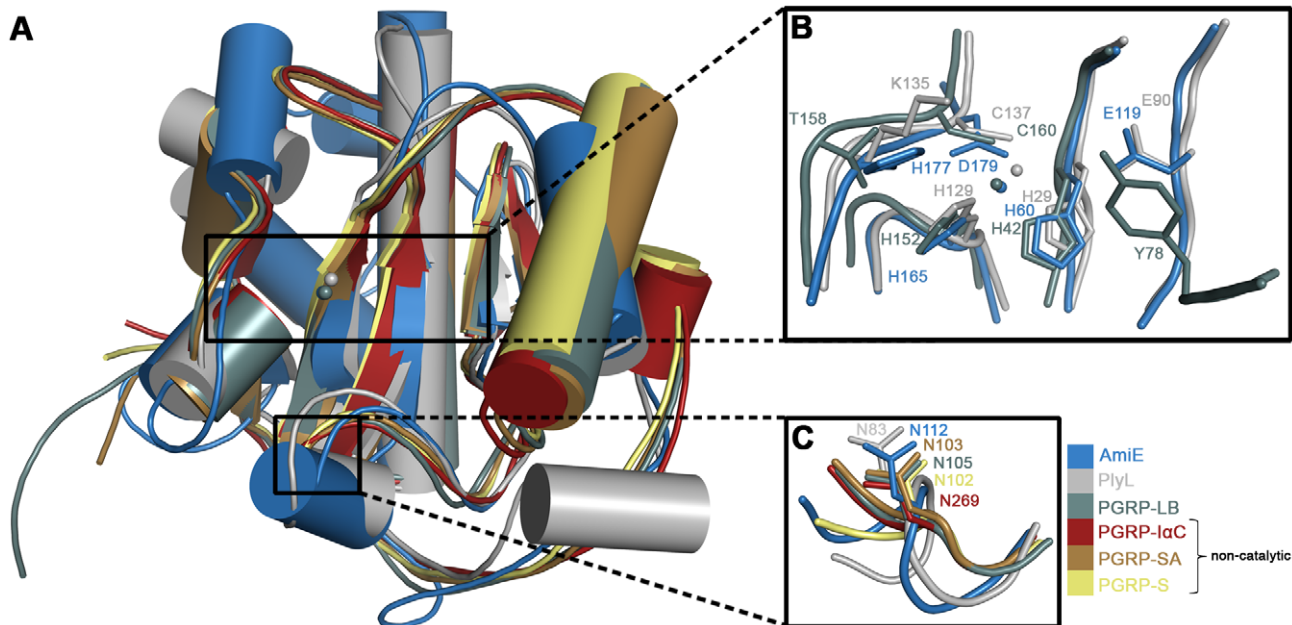


Figure 8. Structural comparison of AmiE with homologous proteins. (A) Representation of the overall fold. Helices are shown as cylinders, strands as arrows. Zinc ions in the active centers are shown as spheres. R.m.s. deviations and Z-scores were calculated by the DALI server [15]. PlyL (*B. anthracis* prophage) has the strongest structural homology to AmiE (Z-score = 18.4, rmsd = 2.1). This is followed by *D. melanogaster* PGRP-LB (Z-score = 12.4, rmsd = 2.3), *H. sapiens* PGRP-S (Z-score = 12.4, rmsd = 2.4), *H. sapiens* PGRP-I α C (Z-score = 12.3, rmsd = 2.3) and *D. melanogaster* PGRP-SA (Z-score = 12.1, rmsd = 2.4). Alignments were calculated with the program lsqkab from the CCP4 suite [23]. (B) Close-up view on the superimposed active sites. Zinc-coordinating residues and residues participating in catalysis are labeled and color-coded. (C) Superimposition of structurally conserved asparagine residues making contacts with the second and third amino acid in the peptide stem of MTP. doi:10.1371/journal.ppat.1000807.g008

binding and help to position the catalytic domain correctly. Such a cell wall anchoring function has been described for the *S. epidermidis* AtlE repeats R1R2 [7] as well as for the repeat domains of PlyL from a *B. anthracis* prophage [16]. The repeat domains are highly positively charged and might interact with the zwitterionic backbone of lipoteichoic acids on the cell surface [19]. Upon initial attachment via the repeat domains, the catalytic domain would then be close enough to the PGN substrate to bind and cleave it at the appropriate location.

All bacterial cell walls share common PGN motifs recognized by amidases, while other motifs are more variable among different species. Among those are the amidation of the D-iGln side chain, the variable third amino acid in the stem, and the number and type of amino acids in the interpeptide bridge. All these variations likely increase amidase affinity to specific cell walls. It has previously been shown that lack of the D-iGln amidation results in a lower binding affinity to AmiE [12]. Nothing is known about either the mode of interaction between repeat domains and lipoteichoic acids or the influence of the interpeptide bridge on binding of the PGN-substrate. This bridge, which consists of five glycines in *S. aureus* and various other staphylococcal species, links the third and fourth amino acids of two neighboring PGN-strands and is responsible for crosslinking. Number and type of amino acid are highly variable among different species and could therefore play a crucial role for species-specific recognition. Further investigations will be necessary to complete the picture concerning the interactions between AmiE, the repeat domains and their substrates.

It has been clearly demonstrated that proper function of autolysins is essential to allow for normal cell division and therefore growth of Staphylococci. We show here that alterations in the active center of AmiE directly affect cell proliferation and therefore are likely to prevent spreading of a Staphylococci infection. The structure-function analysis presented here therefore provides the framework for understanding a key step in the function of all staphylococcal autolysins: the recognition, selectivity, and catalytic mechanism of cleavage of a PGN fragment. This information should therefore guide efforts to design specific inhibitors that can block autolysin function and thus prevent staphylococcal growth.

Materials and Methods

Protein expression and purification

A DNA fragment coding for amino acids 303 to 516 of the *atlE* gene product was amplified via PCR from *S. epidermidis* O-47 [20] genomic DNA and cloned into the pGEX 4T-3 expression plasmid (GE Healthcare) using *Bam*HI and *Xho*I restriction sites. The protein was expressed in *Escherichia coli* BL21 (DE3) (Stratagene) fused to a thrombin cleavable N-terminal GST-tag. Bacteria were grown at 37°C in LB-medium supplemented with 50 µg mL⁻¹ ampicillin until the OD₆₀₀ had reached ~0.4. Expression of the fusion protein was induced with 1 mM isopropyl-β-D-1-thiogalactopyranoside (IPTG). The temperature was then reduced to 25°C, and growth of the culture continued for 6 h. Cells were harvested and resuspended in lysis buffer (50 mM Tris/HCl pH 8.0, 150 mM NaCl, 1 mM Phenylmethylsulfonyl-fluoride (PMSF)). After lysis, the mixture was centrifuged for 30 min at 50000xg to remove insoluble material. The soluble fraction was passed through a 0.45 µm filter and applied to a 5 ml GSTrap FF column (GE Healthcare). After washing, the protein was released from the GST-tag by on-column cleavage with 10 units thrombin/mg fusion protein. The eluate was concentrated and applied to a Superdex 75 16/60 gel filtration column (GE

Healthcare), again using the lysis buffer (without PMSF). The purified enzyme was >95% pure as judged by SDS-PAGE, and was used for crystallization.

Crystallization and structure determination

Purified AmiE (20 mg/ml) was mixed in a 1:1 ratio with crystallization buffer containing 22% (v/v) 1,4-butanediol, 0.1 M imidazole pH 7.0 and 0.15 M zinc acetate. Crystals grew at 4°C using the hanging drop method. Prior to freezing in liquid nitrogen, the crystals were placed in crystallization solution supplemented with 20% glycerol as cryoprotectant. For phase determination, crystals were soaked for 5 min in crystallization solution supplemented with 10 mM samarium chloride before cryoprotection and freezing. Crystals of AmiE belong to space group P4₃2₁2 with two molecules in the asymmetric unit (Table 1). Native data were collected at beamline X06S at the Swiss Light Source (Villigen, Switzerland) using a Mar225 CCD detector. Data collection of derivatized crystals was performed using a Rigaku Micromax 007 HF rotating anode X-ray generator and a Mar345 dtb detector. Data were indexed, integrated and scaled using the XDS package [21] and the HKL software package [22]. Phases were determined by single isomorphous replacement. Native and derivative data were scaled with Scaleit [23]. Heavy atom sites were identified by manual inspection of difference Patterson maps calculated with fit [23] and refined using MLPhaRe [23]. The initially obtained phases were improved by density modification as implemented in DM [23]. At this point, secondary structure elements could clearly be identified in the electron density map. Non-crystallographic averaging (DM & O) [23,24] further improved the density. Model building was performed manually using Coot [25]. The structure was refined to 1.7 Å resolution with CNS [26,27] and Refmac5 [23]. The final model comprises amino acids 7–214. Although present in the purified protein, the six N-terminal residues are not visible in the electron density map and were therefore not built. The structure also contains 14 zinc ions per monomer. Coordinates and structure factors have been deposited with the Protein Data Bank with the accession code 3LAT. A second crystal form, which could be obtained from a zinc free crystallization condition, contains only the zinc ion in the active site. Data for this crystal form were collected at the ESRF (Grenoble, France).

Construction of amidase mutants, and complementation assay

Amino acids H60, H177 and D179 were each mutated to alanine by site directed mutagenesis using the QuikChange II XL Kit (Stratagene) with primer pairs H60A_5' (5'-GAAGGTATCGTT-GTTGCTGATACTGCAAATGATA-3'), H60A_3' (5'-TATCAT-TTGCAGTATCAGCAACAACGATACCTTC-3'), H177A_5' (5'-GGAGGT ACTGATGCTGCTGACCCTCACC-3'), H177A_3' (5'-GGTGAGGGTCAAGCAGCAT CAGTACCTCC-3'), D179A_5' (5'-CTGATCACGCTGCTCCTCACCAA TATTTAAG-3'), and D179A_3' (5'-CTTAAATATTGGTGAGGAGCAGCGTGATC-AG-3'). The pGEX 4T-3 expression plasmid carrying the *amiE* gene fragment was used as the template. The mutated plasmids were then used for protein overexpression in *E. coli*. In addition, the mutated amidase genes were assayed with respect to their ability to complement the *S. aureus* SA113Δ*atlA* mutant *in vivo*. Therefore, the same mutations were introduced into the *E. coli*/*Staphylococcus sp.* shuttle vector pRC20 [4]. Briefly, pRC20 containing the mutated *amiE-R*_{1,2} gene was isolated from *E. coli* DH5α and transformed first into *S. aureus* RN4220 and subsequently into *S. aureus* SA113Δ*atlA* by electroporation. Transformants in *S. aureus* were selected with chloramphenicol. The DNA sequence was verified

Table 1. Data collection and structure refinements statistics.

	Native	SmCl ₃
Data collection		
Space group	P4 ₃ 2 ₁ 2	P4 ₃ 2 ₁ 2
Cell dimensions (Å)	99.45, 99.45, 148.78	99.57, 99.57, 149.15
Wavelength (Å)	0.9999	1.5418
Resolution (Å)	40.0–1.70 (1.76–1.70)	40.0–2.30 (2.38–2.30)
R _{sym} *	0.09 (0.33)	0.08 (0.32)
I/σI	19.6 (2.40)	18.8 (1.92)
Completeness (%)	99.4 (99.4)	80.2 (78.2)
Redundancy	10.0 (6.2)	1.8 (1.9)
Total reflections	824913	50047
Unique reflections	82089	27285
Refinement		
Resolution (Å)	30.8–1.7	
R _{work} /R _{free} #	0.143/0.167	
Number of atoms		
Protein	3408	
Ligand/ion	28/15	
Water	523	
B-factors (Å ²)		
Protein	25.8	
Ligand/ion	33.4/25.7	
Water	46.7	
r.m.s. deviations		
Bond lengths (Å)	0.009	
Bond angles (°)	1.150	
Ramachandran plot (%)		
Most favored region	96.01	
Additionally allowed region	3.99	

r.m.s., root-mean-square. Values in parentheses correspond to highest resolution bin.

*R_{sym} = $\sum |F_{obs}(hkl) - F_{calc}(hkl)| / \sum |F_{obs}(hkl)|$

#R-factor = $\sum |I - \langle I \rangle| / \sum I$

doi:10.1371/journal.ppat.1000807.t001

using amidase-specific primers. For the complementation assay, mutant cells were allowed to grow for 10 h in 50 ml liquid medium at 37°C under shaking. Aliquots were transferred into plastic tubes, allowed to settle for 2 min and photographed against a dark background.

ELISA assay

ELISA assays were carried out with MTP-Biot. Greiner Microcolon plates were incubated for 24 h with 100 µl protein solution at a concentration of 10 µg/ml in PBS (pH 7.3) at 4°C. All following steps were done at 20°C. All washing steps were repeated three times with 250 µl wash buffer (0.05% (v/v) Tween 20 in PBS). Surfaces were blocked for 1 h with 250 µl milk powder (4% (w/v) in PBS), followed by a wash step. The coated plates were then incubated for 30 min with 100 µl of MTP-Biot solution (12.5 µg/ml in PBS). After washing, the wells were incubated for 1 h with Streptavidin linked to horseradish peroxidase solution. Unbound Streptavidin was removed by washing. For detection, 100 µl of 3,3', 5,5'-tetramethylbenzidine solution was added to the wells for 3–5 min until a slight blue color appeared. The reaction

was stopped by adding 100 µl 1 M H₂SO₄. Products were detected at 450 nm using an ELISA-reader (Thermo Multiscan).

Synthesis of MTP compounds

Compounds MTP and MTP-Biot were synthesized as previously described [13] using standard solid phase synthesis protocols. Protection groups that rely on strong acids for cleavage were avoided. All peptides were synthesized by a solid-phase technique, using the fluoren-9-ylmethoxycarbonyl (Fmoc) strategy on a Syro-II-synthesizer (MultiSynTech). Fmoc-amino acids were purchased from Novabiochem, from MultiSynTech or from Iris Biotech. 2-(7-Aza-1H-benzotriazole-1-yl)-1,1,3,3-tetramethyluronium hexafluorophosphate (Applied Biosciences) was used as a coupling agent. The sugar moiety was obtained as Benzyl N-acetyl-4,6-O-benzylidenemuramic acid (Sigma). The benzyl group was removed by incubation with ammonium formate at 40°C for 24 h in the presence of 10% Pd on charcoal (Acros organics). Purity and molecular mass of the product was analyzed by liquid chromatography mass spectrometry (LCMS) using a reversed phase C8 column for separation and ESI-MS for mass determination.

MTP digestion assays

For each assay, 10 µg of wt or mutant protein and 0.1 mg of the appropriate ligand were incubated in 10 µl gel filtration buffer (50 mM Tris/HCl pH 8.0, 150 mM NaCl). The reaction was stopped after 72 h by adding 100 µl acetonitrile with 0.05% (v/v) formic acid. The sample was then frozen at -20°C until used for ESI-MS.

Docking

The Schrodinger Suite [28,29,30] was used to perform docking simulations. In order to obtain a starting point for the docking, the only two available PGRP structures with a bound ligand (PDB codes: 2aph, 1twq) were superimposed onto the AmiE wt structure. The structure 1twq contains MTP as a ligand, while 2aph contains an MTP-based compound that is extended by two D-alanine residues at the C-terminus. Superposition was in each case performed using a least-squares fit algorithm in Chimera [31]. The superimposed structures were used to define a starting position and the boundaries of the docking grid. Since our own studies had shown that MTP is the minimal ligand for AmiE, we generated 64 MTP conformers using the docking algorithm implemented in the program Glide [28,29] in the Schrodinger Suite. The docking was performed in two steps. A constrained initial docking using the XP algorithm was performed first, followed by an unconstrained QM-polarized docking protocol [32]. During the initial docking, the carbonyl atom in the peptide bond linking N-acetylmuramic acid to alanine was constrained to stay near the zinc ion in the active site. All solutions from this initial docking were then redocked using the unconstrained QM-Polarized Ligand Docking protocol. All results from the second docking protocol were similar with regard to their energy values. Therefore, each solution was inspected visually. Eight out of the ten reported solutions showed twisted conformations or unreasonable orientations in the binding cleft, and they were therefore not considered further. The remaining two solutions differ primarily in the orientation of the carbohydrate. The solution presented here has more hydrogen bonds and was therefore considered to be more likely.

Synthesis of substrate derivatives

All peptides (Mca-Ala-D-iGln-Lys-D-Ala-Arg-OH, Mca-Ala-D-iGln-Lys(Gly)-D-Ala-Arg-OH, Mca-Ala-D-iGln-Lys(Gly)2-D-Ala-

Arg-OH, Mca-Ala-D-iGln-Lys(Gly)3-D-Ala-Arg-OH, Mca-Ala-D-iGln-Ala-D-Ala-Arg-OH) were synthesized by a solid-phase technique, using the fluoren-9-ylmethoxycarbonyl (Fmoc) strategy on a Syro II synthesizer (MultiSynTech, Witten, Germany). Peptide synthesis was performed according to Lützner et al. [12]. In contrast to the original protocol, the fluorescence of the N-terminal Mca-group is not quenched. Since the side chain of the alanine substrate is not long enough to bring an attached quencher-group in close proximity to the fluorophore it was left also left out for the other peptides. The C-terminal arginine was attached for reasons of solubility.

For the incorporation of the glycine at the side chain of lysine, a Fmoc-Lys(Dde)-OH protected derivative was used. After the final deprotection of the Fmoc group, the free amino group was reacted with di-*tert*-butyl-dicarbonate. The Dde group was cleaved with 3% of hydrazine and then manually coupled with glycine. Fmoc-amino acids were purchased from Novabiochem (San Diego, CA, USA), from MultiSynTech or from Iris Biotech (Marktredwitz, Germany). Mca was obtained from Sigma (Deisenhofen, Germany). 2-(1H-benzotriazole-1-yl)-1,1,3,3-tetramethyluronium-tetrafluoroborate (TBTU) and 1-hydroxybenzotriazole (HOBt) were from MultiSynTech. The final deprotected peptides were purified by semi-preparative reversed phase (RP) HPLC, using a Reprosil C-8 column (5 µm particle size, 150×10 mm) from Dr. Maisch GmbH (Tuebingen, Germany) and a two solvent system: (A) 0.055% (v/v) trifluoroacetic acid (TFA) in water and (B) 0.05% (v/v) TFA in 80% (v/v) ACN in water. Purity and molecular mass of the collected fractions was analyzed by matrix-assisted laser-desorption ionization-MS (MALDI-MS), using a MALDI time-of-flight system (Reflex IV, Bruker Daltonics, Bremen, Germany). Substrates were dissolved in DMSO and stored as 2 mM stock solutions at -20°C.

Digestion assays with substrates derivatives

The five substrates, each at a concentration of 70 µM, were processed by 7.2 µM AmiE at 37°C in digestion buffer (50 mM sodium phosphate buffer, pH 7.2). After 1, 3 and 6 h, the reaction was stopped by adding trifluoroacetic acid to a final concentration of 1%. Decrease of the initial substrate and formation of the Mca product were analyzed by analytical RP-HPLC using a binary HPLC system (Shimadzu, Tokyo, Japan) with a UV detector, a Nucleosil C-18 column (5 µm particle size, 150×2 mm) from Dr

Maisch GmbH (Tuebingen, Germany) and a two solvent system: (A) 0.055% (v/v) TFA in water and (B) 0.05% TFA in 80% acetonitrile in water. The substrate was well separated from the generated cleavage product Mca, and was quantified at 214 nm.

Zymogram analysis, lysis assay and peptidoglycan purification

Bacteriolytic enzyme profiles were obtained with zymograms and lysis assays. The cell wall lytic activity of recombinant proteins purified from *E. coli* was analyzed in 12% (v/v) polyacrylamide gels with heat-killed cells of *S. aureus* SA113 embedded at a concentration of 0.2% (w/v) [4]. Protein concentration was measured using the Sigma protein detection kit with bovine serum albumin as standard. To gain a higher contrast, the gels were stained with 0.1% (w/v) methylene blue for 5 min and washed until clear bands became visible. Peptidoglycan was isolated from stationary phase cultures of *S. aureus* SA113 [33]. Briefly, cells were harvested by centrifugation and boiled for 60 min in 4% (w/v) SDS. After washing with H₂O_{dest}, the cell wall fragments were incubated with 0.5 mg ml⁻¹ trypsin for 16 h at 37°C to degrade cell-bound proteins. After centrifugation and washing with water, the cell walls were incubated for 5 h with 10% TCA to remove teichoic acids. For a quantitative analysis of lysis, purified peptidoglycan of *S. aureus* SA113 was dissolved in 1 ml 100 mM sodium phosphate buffer and adjusted to OD₅₇₈ = 0.3. The insoluble PGN was mixed with 20 µg of purified enzyme. Cell lysis was measured as the decrease in OD₅₇₈ in a spectrophotometer.

Acknowledgments

We thank Felix Büttner for AmiE purification, Andreas Dittmar for synthesis of Mca substrate derivatives, ALMO for general assistance, and the staff at Swiss Light Source beamline X06SA and at ESRF beamline ID14 for assistance with data collection.

Author Contributions

Conceived and designed the experiments: SZ BP FG HK TS. Performed the experiments: SZ BP MS TS. Analyzed the data: SZ BP TS. Contributed reagents/materials/analysis tools: MS HK. Wrote the paper: SZ BP FG HK TS.

References

- Zeller JL, Burke AE, Glass RM (2007) JAMA patient page. MRSA infections. JAMA 298: 1826.
- Franson TR, Sheth NK, Rose HD, Sohler PG (1984) Scanning electron microscopy of bacteria adherent to intravascular catheters. J Clin Microbiol 20: 500–505.
- Rupp ME, Fey PD, Heilmann C, Gotz F (2001) Characterization of the importance of Staphylococcus epidermidis autolysin and polysaccharide intercellular adhesin in the pathogenesis of intravascular catheter-associated infection in a rat model. J Infect Dis 183: 1038–1042.
- Heilmann C, Hussain M, Peters G, Gotz F (1997) Evidence for autolysin-mediated primary attachment of Staphylococcus epidermidis to a polystyrene surface. Mol Microbiol 24: 1013–1024.
- García P, Mendez E, García E, Ronda C, Lopez R (1984) Biochemical characterization of a murein hydrolase induced by bacteriophage Dp-1 in Streptococcus pneumoniae: comparative study between bacteriophage-associated lysin and the host amidase. J Bacteriol 159: 793–796.
- Croux C, Ronda C, Lopez R, García JL (1993) Interchange of functional domains switches enzyme specificity: construction of a chimeric pneumococcal-clostridial cell wall lytic enzyme. Mol Microbiol 9: 1019–1025.
- Biswas R, Voggu L, Simon UK, Hentschel P, Thumm G, et al. (2006) Activity of the major staphylococcal autolysin Atl. FEMS Microbiol Lett 259: 260–268.
- Hobot JA, Rogers HJ (1991) Intracellular location of the autolytic N-acetylmuramyl-L-alanine amidase in Bacillus subtilis 168 and in an autolysin-deficient mutant by immunoelectron microscopy. J Bacteriol 173: 961–967.
- Yamada S, Sugai M, Komatsuzawa H, Nakashima S, Oshida T, et al. (1996) An autolysin ring associated with cell separation of Staphylococcus aureus. J Bacteriol 178: 1565–1571.
- Sugai M, Komatsuzawa H, Akiyama T, Hong YM, Oshida T, et al. (1995) Identification of endo-beta-N-acetylglucosaminidase and N-acetylmuramyl-L-alanine amidase as cluster-dispersing enzymes in Staphylococcus aureus. J Bacteriol 177: 1491–1496.
- Oshida T, Sugai M, Komatsuzawa H, Hong YM, Suginaka H, et al. (1995) A Staphylococcus aureus autolysin that has an N-acetylmuramoyl-L-alanine amidase domain and an endo-beta-N-acetylglucosaminidase domain: cloning, sequence analysis, and characterization. Proc Natl Acad Sci U S A 92: 285–289.
- Lutzner N, Patzold B, Zoll S, Stehle T, Kalbacher H (2009) Development of a novel fluorescent substrate for Autolysin E, a bacterial type II amidase. Biochem Biophys Res Commun 380: 554–558.
- Swaminathan CP, Brown PH, Roychowdhury A, Wang Q, Guan R, et al. (2006) Dual strategies for peptidoglycan discrimination by peptidoglycan recognition proteins (PGRPs). Proc Natl Acad Sci U S A 103: 684–689.
- Wang ZM, Li X, Cocklin RR, Wang M, Fukase K, et al. (2003) Human peptidoglycan recognition protein-L is an N-acetylmuramoyl-L-alanine amidase. J Biol Chem 278: 49044–49052.
- Holm L, KS, Rosenström P, Schenkel A (2008) Searching protein structure databases with DalLite v.3. Bioinformatics. pp 2780–2781.
- Low LY, Yang C, Perego M, Osterman A, Liddington RC (2005) Structure and lytic activity of a Bacillus anthracis prophage endolysin. J Biol Chem 280: 35433–35439.
- Cho S, Wang Q, Swaminathan CP, Hesk D, Lee M, et al. (2007) Structural insights into the bactericidal mechanism of human peptidoglycan recognition proteins. Proc Natl Acad Sci U S A 104: 8761–8766.

18. Guan R, Wang Q, Sundberg EJ, Mariuzza RA (2005) Crystal structure of human peptidoglycan recognition protein S (PGRP-S) at 1.70 Å resolution. *J Mol Biol* 347: 683–691.
19. Bierbaum G, Sahl HG (1985) Induction of autolysis of staphylococci by the basic peptide antibiotics Pep 5 and nisin and their influence on the activity of autolytic enzymes. *Arch Microbiol* 141: 249–254.
20. Heilmann C, Schweitzer O, Gerke C, Vanittanakom N, Mack D, et al. (1996) Molecular basis of intercellular adhesion in the biofilm-forming *Staphylococcus epidermidis*. *Mol Microbiol* 20: 1083–1091.
21. Kabsch W (1993) Automatic processing of rotation diffraction data from crystals of initially unknown symmetry and cell constants. *J Appl Cryst* 26: 795–800.
22. Otwinowski Z, Minor W (1997) Processing of X-ray Diffraction Data Collected in Oscillation Mode; Carter CW, Sweet J, Sweet RM, editors. New York: Academic Press. pp 307–326.
23. Collaborative Computational Project, Number 4 (1994) The CCP4 Suite: Programs for Protein Crystallography. *Acta Cryst D* 50: 760–763.
24. Jones TA, Zou JY, Cowan SW, Kjeldgaard M (1991) Improved methods for building protein models in electron density maps and the location of errors in these models. *Acta Crystallogr A* 47(Pt 2): 110–119.
25. Emsley P, Cowtan K (2004) *Acta Cryst D* 60: 2126–2132.
26. Brunger AT, Adams PD, Clore GM, DeLano WL, Gros P, et al. (1998) Crystallography & NMR system: A new software suite for macromolecular structure determination. *Acta Crystallogr D Biol Crystallogr* 54: 905–921.
27. Brunger AT (2007) Version 1.2 of the Crystallography and NMR system. *Nat Protoc* 2: 2728–2733.
28. Friesner RA, Banks JL, Murphy RB, Halgren TA, Klicic JJ, et al. (2004) Glide: a new approach for rapid, accurate docking and scoring. 1. Method and assessment of docking accuracy. *J Med Chem* 47: 1739–1749.
29. Halgren TA, Murphy RB, Friesner RA, Beard HS, Frye LL, et al. (2004) Glide: a new approach for rapid, accurate docking and scoring. 2. Enrichment factors in database screening. *J Med Chem* 47: 1750–1759.
30. Friesner RA, Murphy RB, Repasky MP, Frye LL, Greenwood JR, et al. (2006) Extra precision glide: docking and scoring incorporating a model of hydrophobic enclosure for protein-ligand complexes. *J Med Chem* 49: 6177–6196.
31. Pettersen EF, Goddard TD, Huang CC, Couch GS, Greenblatt DM, et al. (2004) UCSF Chimera—a visualization system for exploratory research and analysis. *J Comput Chem* 25: 1605–1612.
32. Schrödinger L (2008) Schrödinger Suite 2008 QM-Polarized Ligand Docking protocol. New York.
33. de Jonge BL, Chang YS, Gage D, Tomasz A (1992) Peptidoglycan composition of a highly methicillin-resistant *Staphylococcus aureus* strain. The role of penicillin binding protein 2A. *J Biol Chem* 267: 11248–11254.
34. Thompson JD, Higgins DG, Gibson TJ (1994) CLUSTAL W: improving the sensitivity of progressive multiple sequence alignment through sequence weighting, position-specific gap penalties and weight matrix choice. *Nucleic Acids Res* 22: 4673–4680.
35. Edgar RC (2004) MUSCLE: multiple sequence alignment with high accuracy and high throughput. *Nucleic Acids Res* 32: 1792–1797.
36. Katoh K, Misawa K, Kuma K, Miyata T (2002) MAFFT: a novel method for rapid multiple sequence alignment based on fast Fourier transform. *Nucleic Acids Res* 30: 3059–3066.
37. Notredame C, Higgins DG, Heringa J (2000) T-Coffee: A novel method for fast and accurate multiple sequence alignment. *J Mol Biol* 302: 205–217.
38. Poirot O, O’Toole E, Notredame C (2003) Tcoffee@igs: A web server for computing, evaluating and combining multiple sequence alignments. *Nucleic Acids Res* 31: 3503–3506.
39. Krissinel E, Henrick K (2007) Inference of macromolecular assemblies from crystalline state. *J Mol Biol* 372: 774–797.

The structural basis of staphylococcal cell wall recognition by SH3b domains

Sebastian Zoll¹, Martin Schlag², Friedrich Götz², Thilo Stehle^{1,3}

¹Interfaculty Institute of Biochemistry, University of Tuebingen, Tuebingen, Germany, ²Department of Microbial Genetics, Faculty of Biology, University of Tuebingen, Tuebingen, Germany, ³Department of Pediatrics, Vanderbilt University School of Medicine, Nashville, TN 37232, USA

Introduction

The major autolysin AtlE from *S. epidermidis* plays a key role in the degradation of the cell wall during cell division and is therefore an appealing drug target. AtlE is secreted as a bifunctional precursor and cleaved extracellularly, yielding the mature N-Acetylmuramyl-L-alanine amidase and the glucosaminidase. The amidase is made up of the catalytic domain AmiE and a C-terminal cell wall binding region (CBR). The latter comprises four repeat domains, which are necessary for directing the amidase to the septum region that forms between dividing daughter cells [1].

Cell wall binding domains are widespread modules of surface-associated peptidoglycan hydrolases that connect either N- or C-terminally to the catalytic domain. Several different classes such as the LysM domain, the choline binding domain, the FtsN-peptidoglycan-binding domain and the SH3b domain are known and have been structurally characterized [2,3,4,5]. Cell wall binding domains are similar in that they are rather small and organized as repeating segments. The repeat domains of the AtlE amidase belong to the family of SH3b (bacterial SH3) domains that exhibit structural homology to the well-studied eukaryotic SH3 (Src Homology 3) domains. These 50-80 amino acid long domains are mainly involved in signal transduction pathways where

they mediate protein-protein interactions by recognition of proline-rich consensus sequences [6]. However, also DNA- and RNA-binding can be associated with the SH3-fold [7,8]. Although SH3b domains are larger than their eukaryotic counterparts, they share common structural features such as the RT-loop, the distal loop and the n-src loop. Similar to SH3 domains, SH3b domains show large variations in their loop regions, which might indicate similar substrate promiscuity.

It is widely accepted that SH3b domains bind cell wall components [9,10]. To date, such an interaction could only be demonstrated for the repeat domains of InlB from *Listeria monocytogenes*, which bind to lipoteichoic acids (LTA) [11]. In order to investigate substrate preferences of the amidase repeat domains, we determined the structure of the R_{3,4} tandem-repeat of the CBR and designed binding-impaired mutants to be tested for their ability to attach to staphylococcal cell walls.

Materials and Methods

Protein expression and purification

A DNA-fragment encoding AtlE residues 516 to 845 was PCR amplified from *S. epidermidis* O-47 genomic DNA and cloned into the pGEX 4T-3 expression plasmid using *Bam*H1 and *Xho*I restriction sites. These residues were predicted to encode the R₁₋₄ segment [12]. Overexpressing of R₁₋₄ fused to a thrombin cleavable, N-terminal GST-tag was done in *Escherichia coli* BL21 (DE3). After induction of protein expression, bacteria were grown for 12 h at 22°C. Soluble fusion protein was purified by GST affinity chromatography on GSTrap FF. After cleavage of the tag by incubation with thrombin, the protein was subjected to size exclusion chromatography to remove GST and thrombin. Subsequently, lysine residues of the purified protein were reductively methylated to improve its crystallization properties [13]. For the methylation reaction 1 ml of the protein solution (< 0.5 mg ml⁻¹) was mixed with 40 µl of 1 M formaldehyde and 20 µl of 1 M DMAB (Dimethylamine

borane complex) as a reducing agent. The reaction was kept at 4°C and repeated twice every two hours. In the last step only 10 µl of DMAB was added. The reaction was incubated for additional 12 hours. A size exclusion chromatography on Superdex 75 was conducted to remove aggregates. Successful methylation was judged by a shift in molecular weight relative to the unmethylated protein in SDS-PAGE.

Crystallization and structure determination

Purified and methylated R₁₋₄ was concentrated to 12 mg/ml and mixed with crystallization buffer (1.2 M NaH₂PO₄, 0.8 M K₂HPO₄, 0.2 M LiSO₄ and 0.1 M CAPS pH 10.5) in a 1:1 ratio. Crystals grew at 20°C within 4 days using the hanging-drop method. Prior to data collection, the crystals were soaked in crystallization buffer supplemented with 20% (v/v) glycerol and flash frozen in liquid nitrogen. Native data collection was carried out at beamline ID14-1 at the ESRF (Grenoble, France) using an ADSC Quantum Q210 detector. To prepare two derivatives for phase determination, crystals were soaked in crystallization solution supplemented with either 10 mM HgCl₂ or 5 mM K₂PtCl₄. After 5 minutes, the crystals were cryoprotected and frozen. Derivative data sets were collected on a Rigaku Micromax 007 HF rotating anode X-ray generator equipped with a Mar345 detector. X-ray data were indexed, integrated and scaled using the XDS package [14]. Experimental phases were determined by multiple isomorphous replacement. The programs HYSS, SOLVE and RESOLVE implemented in the AutoSol routine of the PHENIX software suite [15] were used for heavy-atom site identification, initial phases calculation and density modification. A preliminary model of R₃ and R₄ was then manually built into the experimental map using Coot [16]. Crystallographic refinement at 2.9 Å resolution was carried out using PHENIX (simulated annealing and rigid body refinement) and Refmac5 (individual coordinate and B-factor refinement) [17] (Table1).

The expressed protein comprised all four repeats (R₁₋₄) of the amidase CBR. The final electron density map for repeats R₃ and R₄ is of excellent quality and confirms the placement of all main chain and most side chain atoms, including

many methylated lysine residues. These two repeats also form a well-defined three-dimensional crystal lattice in space-group P6₁22. By contrast, the electron density for repeats R₁ and R₂ was not visible. R_{1,2} most likely projects into a large, solvent-filled cavity close to the N-terminus of R₃.

Construction of repeat domain mutants

The QuikChange II XL Kit (Agilent Technologies) was used to introduce point mutations into the CBR encoding pGEX 4T-3 expression vector. Two mutants were constructed, carrying point mutations at two (R1_A63L/R3_A227L) and four positions (R2_Y114R/R2_S162E/R4_H278R/R4_S326E), respectively. The purification of both mutants was conducted similar to the wildtype protein.

For *in vivo* studies, the same mutations were introduced into the CBR encoding region of the *E. coli/ Staphylococcus sp.* pRC20 shuttle plasmid. These mutants were tested on their ability to complement the *S. aureus* SA113 Δ *atlA* phenotype *in vivo*. Plasmids carrying the correct mutations were isolated from *E. coli* XL10-Gold, transformed into *S. aureus* RN4220 and subsequently into *S. aureus* SA113 Δ *atlA*. Transformants in *S. aureus* were selected with chloramphenicol.

The following primer pairs were used to introduce mutations in both, expression and shuttle plasmid: R1_K61A_FOR (5'-CTCTATCCGTTACT-GCAACTGCAACATTAGG-3'), R1_K61A_REV (5'-CCTAATGTTGCAGTTG-CAGTAACGGATAGAG-3'), R3_A227L_FOR (5'-CAGTGACGAAAGCTCTC-ACACTTGGTGAT-3'), R3_A227L_REV (5'-ATCACCAAGTGTGAGAGCTTT-CGTC ACTG-3'), R4_H278R_FOR (5'-CCTGGTGTTAAATTACGCACAGTA-CCTTGGGGC-3'), R4_H178R_REV (5'-GCCCCAAGGTACTGTGCGTAA-TTTAACACCAGG-3'), R4_S326E_FOR (5'-GTAAATCTGGTTGGATTGAGA-AATACTATTTAACTGC-3'), R4_S326E_REV (5'-GCAGTTAAATAGTATTT-CTCAATCCAACCAGATTTAC-3'), R2_Y114R_FOR (5'-CAGGGTCAACACT-TCGCACAGTTCCTTGGGG-3'), R2_Y114R_REV (5'-CCCCAAGGAACT-GTGCGAAGTGTTGACCCTG-3'), R2_S162E_FOR (5'-GTAAATCTGGTTG-GATTGAGAAATATACTTAACTAC-3'), R2_S162E_REV (5'-GTAGTTAAG-TAATATTTCTCAATCCAACCAGATTTAC-3').

Results and Discussion

Overall structure

Repeats three and four of the AtlE amidase CBR belong to the family of prokaryotic SH3 related domains (SH3b). Contrary to previous assumptions, which were solely based on sequence alignments, the structure of R_{3,4} revealed that the CBR comprises four shorter instead of two longer repeating units (Figure 1B). R_{1,2} and R_{3,4} form tandem-domains and are connected to each other and the catalytic domain via spacers that are approx. 15 amino acid long. Unfortunately, only the domains R₃ and R₄ of the second amidase tandem-repeat are visible in the electron density map while R_{1,2} protrudes into a solvent channel and is disordered in the crystals. However, the high sequence identity between R₁ and R₃ and between R₂ and R₄ allows us to predict the structure of the R_{1,2} segment with good accuracy.

All four repeats of the *S. epidermidis* CBR share common sequence and structural features such as the GW-motifs that are located in the centers of the central β -sheets. However, the conservation between every second repeat in the CBR is higher than between adjacent repeats, which are connected via an extensive network of hydrogen bonds. A similar arrangement is seen in *L. monocytogenes* SH3b domains [5]. R₃ and R₄ have an r.m.s deviation of 2.3 Å (over all C α). A superposition of both repeats shows that structural differences are most evident in the loop regions (Figure 1C). For simplification, these were named after corresponding regions in eukaryotic SH3 domains, which share the same fold. In addition, the loop region that lies C-terminal to the RT-loop has been named SU-loop by the authors.

R3 and R4 adopt a similarly shaped, half open beta-barrel conformation (Figure 1A). The structurally conserved β -sheets formed by strands β 1-4 in R₃, and β 6,9-11 in R₄ represent central platforms of the fold in both domains. They are capped by the projecting RT-loops, which bend inward around β 5 and β 12, respectively.

The almost parallel orientation of the R₃ RT-loop relative to the central sheet creates a shallow, hydrophobic groove, whose base formed by the side

chains of A227 of $\beta 2$ and V206 of the RT-loop. The walls of the groove are generated by residues of strands $\beta 1$, $\beta 3$ and the tip of the covering RT-loop.

The R_4 RT-loop is distinct from its counterpart in R_3 . It is wedged between the two half open β -barrels and stabilized by an extensive hydrogen bonding network with residues of the neighboring SU-loop/strand $\beta 2$ and the R_3 distal loop which is significantly longer than in R_4 . This results in the R_4 RT-loop having the lowest B-factors in the entire crystal structure. The tip of the R_4 RT-loop is bent 90° downwards and packs against the outside of the barrel-like β -sheet, formed by strands $\beta 9-11$. The barrel-like β -sheet in R_4 is even more twisted than the one in R_3 . This conformation creates a deep cavity on the opposite side of the protein. The bottom of the cavity is formed by W324 and walled by the tip of the RT-loop, $\beta 10,11$ and the short 3^{10} helix.

Unlike all other loop regions of R_3 and R_4 , which vary in length and orientation, the n-src loops are rather short in both domains and not engaged in any contacts.

Structural basis for construction of binding impaired mutants

Binding regions of the eukaryotic SH3-fold have been defined quite well [6]. Although domains possessing this fold interact with a variety of substrates, a proline-rich region with a PXXP consensus motif could be identified as a common feature [6]. Bacterial SH3b domains resemble the eukaryotic fold, but are less well characterized, as fewer structures are available [5,18,19]. It is widely accepted that SH3b domains interact with cell wall components while they anchor enzymes on the cell surface. However, the structural determinants of this process are currently not understood, as complexes with ligands are not available for any of these domains.

In order to localize putative substrate binding areas, conserved residues, which were derived from a multiple sequence alignment between AtIE repeats and repeat domains from seven other staphylococcal amidases, were mapped onto the surface of $R_{3,4}$. Most of the strictly conserved residues of both repeat domains cluster in recessed areas with strong electropositive

potential. Interestingly, these areas lie on opposite sites of the protein and show quite different topologies. While the R₃ groove is rather wide and shallow, the conserved residues line a deep cavity in R₄ (Figure 3).

The conserved R₃ patch covers a total solvent accessible area of approx. 230 Å², which is mainly made up of hydrophobic residues. The side chains of V206 and A227 form the bottom of a groove, which is confined by a wall-like elevation. This wall is made up by T205 in the upper part, L184 and V186 in the lower part and the bulky side chains of Y207 and W248 at the sides.

Another continuous patch of conserved residues can also be found at the interface between R₃ and R₄ where Y240, N241 and Q287 participate in a hydrogen-bonding network that promotes pairing of the tandem-repeat.

The side chain of W324 provides the base of the deep hydrophobic pocket on the downside of R₄ that is walled by the large side chains of H278, W282 and Y313. The histidine residue present at position 278 in R₄ is replaced with a tyrosine in R₂ and all other repeats in the sequence alignment.

Both conserved regions lie at the contact points between the tip of the RT loop and W248 and W324, respectively. Both tryptophan residues are located at equivalent positions in R₃ and R₄ in the innermost strand of the barrel-like β-sheet and are likely to take over pivotal roles as integral parts of the putative binding areas. The GW-dipeptide represents the consensus motif of all staphylococcal autolysin repeat domains in the alignment and is also present in the InIB targeting domain of *L. monozytogenes* (PDB: 1m9s) [5], the closest structural homologue of R_{3,4} that was identified by a DALI search (Z-score=10.3) [18].

In staphylococci, LTAs have long been discussed as substrates of the AtlE amidase repeat domains [19,20]. However, no experimental proof has been obtained yet. To gain further insights on this topic, we generated binding impaired mutants in which putative substrate bindings pockets are inaccessible and studied their ability to attach to staphylococcal cell walls. Due to the different topology and position of the putative binding grooves in R₃ and R₄, two different mutants with inaccessible binding grooves were

generated. These carry the same mutations in each of the sequence and structurally related domains R_1/R_3 and R_2/R_4 , respectively. In the first mutant, two conserved alanine residues that form the bottom of the putative binding groove in R_1 and R_3 were mutated to leucines. These mutations aim to create a shallower groove with a conformation that is unfavorable for accommodation of the substrate. The second mutant carries four point mutations, two in R_2 and two in R_4 . Each of the mutated residues pairs H228R/S316E and Y114R/S162E is predicted to form a salt-bridge that closes the binding pocket in the respective domain and thereby constrict its accessibility.

The different topologies and orientations of the putative binding grooves render it likely that each tandem repeat might recognize two different substrates or two different motifs on the same substrate. A putative substrate would most likely show repetitive elements since the segments of the AtIE amidase CBR are also repetitive. This supports the hypothesis that glycopolymers such as LTAs, rather than cell wall associated proteins, might display interaction partners of the repeat domains. However, for the CBR of ALE-1, a glycyglycine endopeptidase, a specific interaction with residues of the PGN interpeptide bridge was postulated [21]. The putative binding region of the ALE-1 SH3b domain exhibits a topology that is significantly different from the putative binding regions of the amidase repeats. The projecting RT-loop and a loop connecting N-terminally to the first β -strand of the central, barrel-like β -sheet create a narrow channel that might be suitable to accommodate a pentaglycine-peptide. Variation of the length of the RT-loop and its position relative of the central β -sheet might therefore display an important mechanism to modulate substrate-specificity.

The number of repeat domains within a CBR varies among cell wall associated enzymes. While the AtIE amidase contains four repeat domains, only two are present at the N-terminus of the AtIE glucosaminidase, which is part of the bifunctional AtIE precursor [22]. Other examples are the *L. monocytogenes* invasion protein InIB (three SH3b domains) [5] and NpPCP/AvPCP endopeptidases from *Anabaena variabilis* and *Nostoc punctiforme* (one SH3b domain) [9]. In *S. aureus*, Baba and Schneewind demonstrated that GST-fusionproteins with four amidase repeats exhibit a

higher binding affinity towards the cell surface than fusionproteins with only two repeats [1]. The attachment of additional SH3b domains to extracellular enzymes might therefore display a mechanism to enforce binding to a potential cell wall associated substrate.

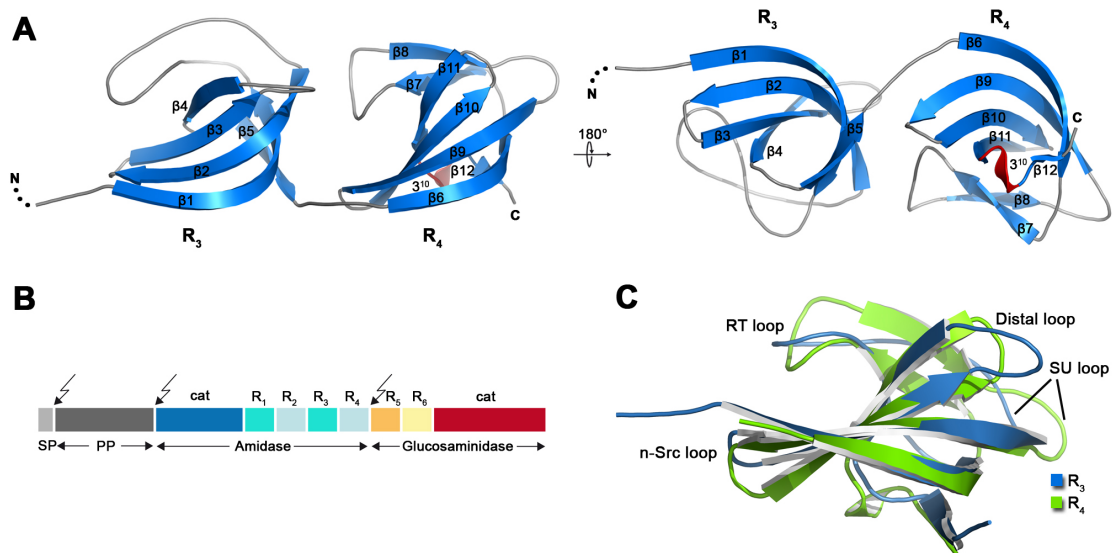


Figure 1: Crystal structure of R_{3,4} of the cell wall binding domain of the AtIE amidase. (A) Cartoon representation of the crystal structure of R_{3,4} in two orientations. (B) Domain arrangement of the bifunctional AtIE precursor protein. Arrows indicate the post-translational cleavage sites. **SP** signalpeptide, **PP** pro-peptide, **cat** catalytic domains, **R** repeat domains. (C) Structural comparison of R₃ and R₄, which have an r.m.s deviation of 2.3 Å (over all C α).

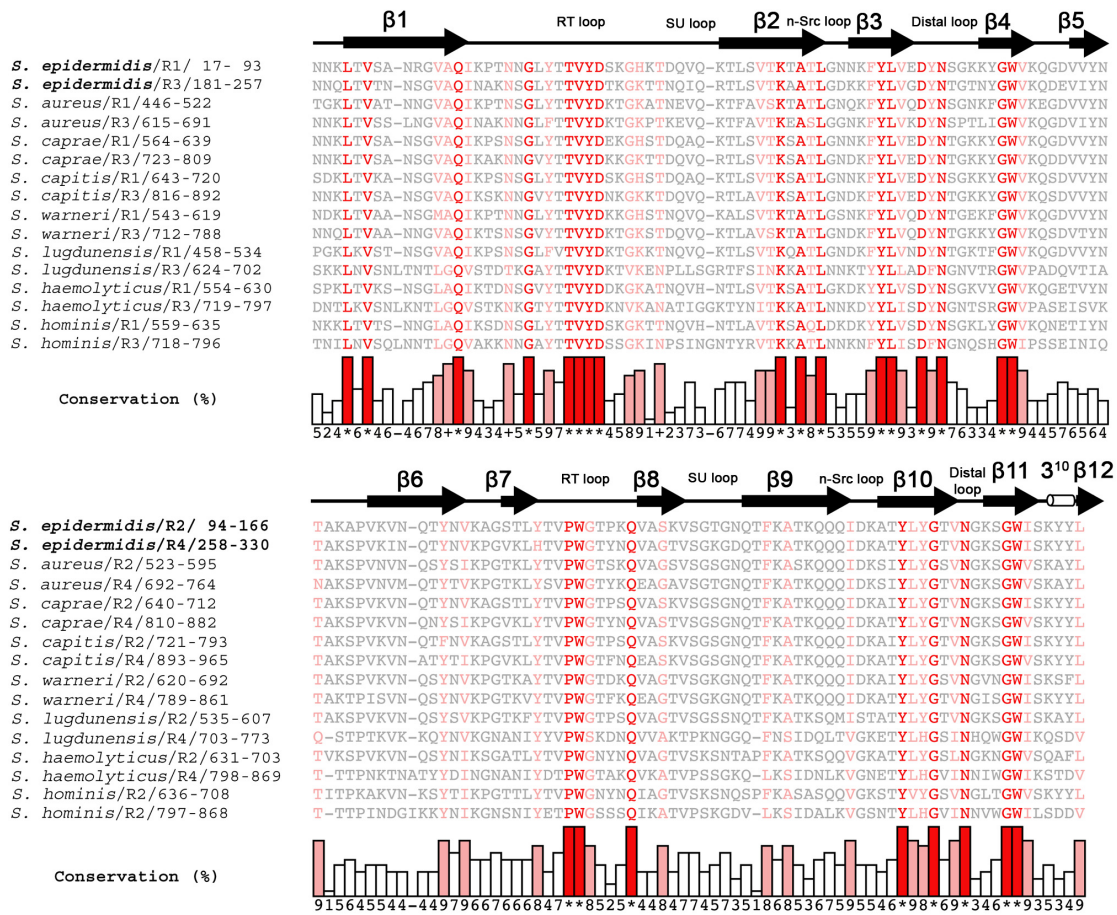


Figure 2: Sequence alignments of R₁/R₃ and R₂/R₄ with repeat domains of seven different staphylococcal amidases. Alignments were calculated with the programs ClustalW2 [23], MUSCLE [24] and MAFFT [25] and combined into a single output using COMBINE [26]. Conserved amino acids are color-coded according to their degree of conservation: Grey (<80%), pink (80-90%), red (100%).

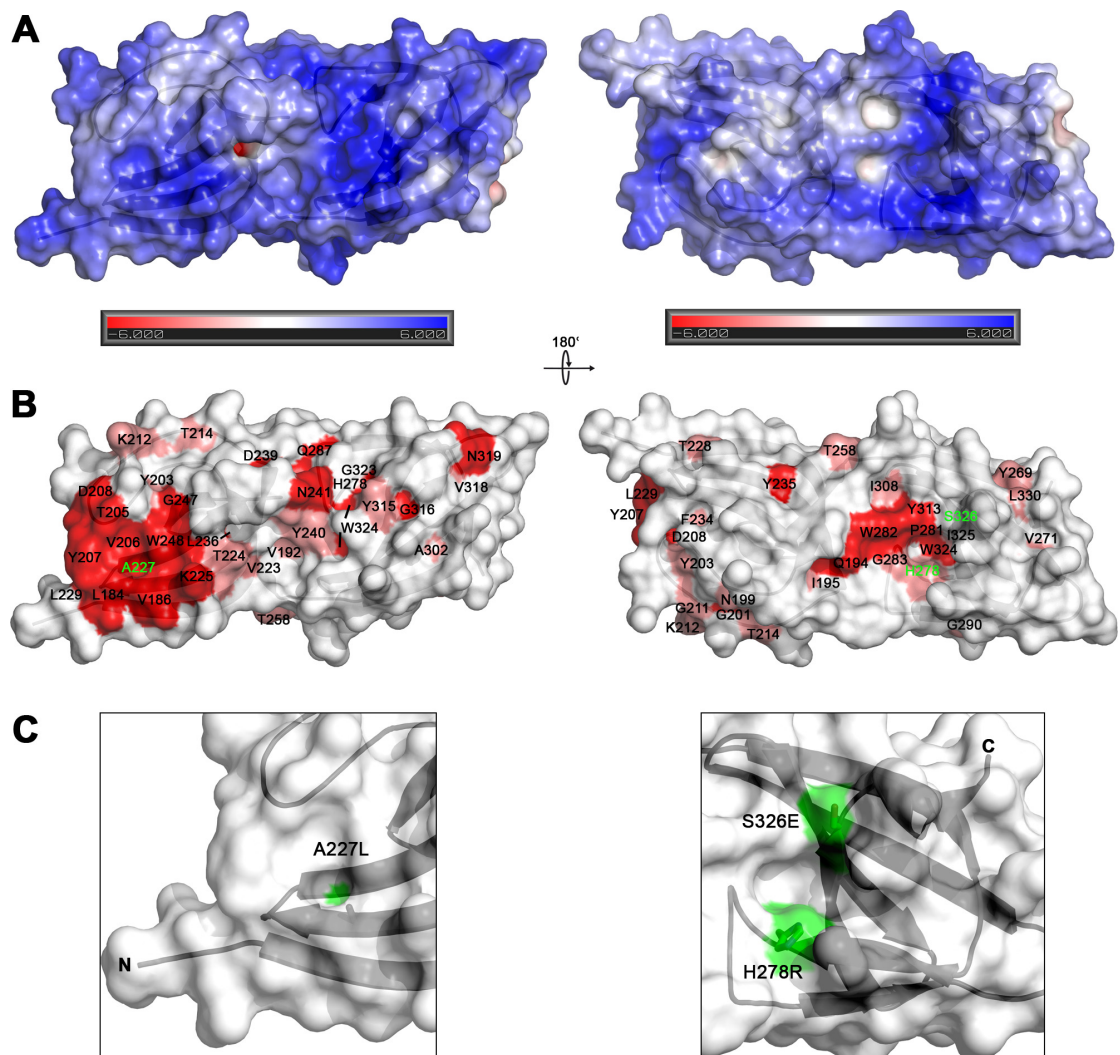


Figure 3: Conserved residues cluster in distinct regions of high electrostatic potential. (A) Electrostatic potential on the surface of R_{3,4} shown in two different views. **(B)** Conservation pattern on the surface of R_{3,4} shown in two different views. Amino acids are colored according to their degree of conservation using the color scheme of Figure 2. A distinct patch of conserved residues is present on the surface of each repeat in the tandem-domain. Amino acids with green labels were mutated. **(C)** Close-up views of the putative substrate binding sites with mutated amino acids labeled and colored in green.

	Native	HgCl ₂	K ₂ PtCl ₄
Data collection			
Space group	P6 ₁ 22	P6 ₁ 22	P6 ₁ 22
Cell dimensions (Å)	95.36, 95.36, 233.67	94.07, 94.07, 233.21	95.01, 95.01, 231.87
Wavelength (Å)	0.934	1.5418	1.5418
Resolution (Å)	30.0-2.90 (2.98-2.90)	30.0-3.70 (3.79-3.70)	30.0-4.1 (4.21-4.10)
R _{sym} * (%)	6.5 (38.8)	15.9 (49.3)	25.2 (45.1)
I/σ	15.3 (2.6)	15.3 (5.6)	12.7 (6.3)
Completeness (%)	98.9 (99.8)	98.9 (98.8)	99.1 (100.0)
Redundancy	3.6 (3.7)	13.1 (12.8)	11.2 (10.2)
Total reflections	51923	160036	102264
Unique reflections	14514	12231	9113
Refinement			
Resolution (Å)	25.7-2.9		
R _{work} /R _{free} [#] (%)	26.3/29.8		
Number of atoms			
Protein	1217		
Water	18		
B-factors (Å ²)			
Protein	55.6		
Water	43.9		
r.m.s deviations			
Bond lengths(Å)	0.01		
Bond angles (°)	1.23		
Ramachandran plot (%)			
Most favored region	98.6		
Additionally allowed region	1.4		

Table 1: Data collection and structure refinements statistics. r.m.s, root-mean-square. Values in parentheses correspond to highest resolution bin.

$$\#R_{\text{sym}} = \sum | |F_{\text{obs}}(\text{hkl})| - |F_{\text{calc}}(\text{hkl})| | / \sum |F_{\text{obs}}(\text{hkl})|,$$

$$*R\text{-factor} = \sum | | - \langle | \rangle | / \sum |$$

References

1. Baba T, Schneewind O (1998) Targeting of muralytic enzymes to the cell division site of Gram-positive bacteria: repeat domains direct autolysin to the equatorial surface ring of *Staphylococcus aureus*. *EMBO J*. pp. 4639-4646.
2. Bateman A, Bycroft M (2000) The structure of a LysM domain from *E. coli* membrane-bound lytic murein transglycosylase D (MltD). *J Mol Biol* 299: 1113-1119.
3. Fernandez-Tornero C, Garcia E, Lopez R, Gimenez-Gallego G, Romero A (2002) Two new crystal forms of the choline-binding domain of the major pneumococcal autolysin: insights into the dynamics of the active homodimer. *J Mol Biol* 321: 163-173.
4. Ursinus A, van den Ent F, Brechtel S, de Pedro M, Holtje JV, et al. (2004) Murein (peptidoglycan) binding property of the essential cell division protein FtsN from *Escherichia coli*. *J Bacteriol* 186: 6728-6737.
5. Marino M, Banerjee M, Jonquières R, Cossart P, Ghosh P (2002) GW domains of the *Listeria monocytogenes* invasion protein InlB are SH3-like and mediate binding to host ligands. *EMBO J*. pp. 5623-5634.
6. Kishan KVR, Agrawal V (2005) SH3-like fold proteins are structurally conserved and functionally divergent. *Curr Protein Pept Sci*. pp. 143-150.
7. Nakagawa A, Nakashima T, Taniguchi M, Hosaka H, Kimura M, et al. (1999) The three-dimensional structure of the RNA-binding domain of ribosomal protein L2; a protein at the peptidyl transferase center of the ribosome. *EMBO J* 18: 1459-1467.
8. Gao YG, Su SY, Robinson H, Padmanabhan S, Lim L, et al. (1998) The crystal structure of the hyperthermophile chromosomal protein Sso7d bound to DNA. *Nat Struct Biol* 5: 782-786.
9. Yamada S, Sugai M, Komatsuzawa H, Nakashima S, Oshida T, et al. (1996) An autolysin ring associated with cell separation of *Staphylococcus aureus*. *J Bacteriol* 178: 1565-1571.
10. Vollmer W, Joris B, Charlier P, Foster S (2008) Bacterial peptidoglycan (murein) hydrolases. *FEMS Microbiology Reviews*. pp. 259-286.
11. Jonquières R, Bierne H, Fiedler F, Gounon P, Cossart P (1999) Interaction between the protein InlB of *Listeria monocytogenes* and lipoteichoic acid: a novel mechanism of protein association at the surface of Gram-positive bacteria. *Molecular Microbiology*. pp. 902-914.
12. Heilmann C, Hussain M, Peters G, Götz F (1997) Evidence for autolysin-mediated primary attachment of *Staphylococcus epidermidis* to a polystyrene surface. *Molecular Microbiology*. pp. 1013-1024.
13. Walter TS, Meier C, Assenberg R, Au KF, Ren J, et al. (2006) Lysine methylation as a routine rescue strategy for protein crystallization. *Structure* 14: 1617-1622.
14. Kabsch W (2010) XDS. *Acta Crystallogr D Biol Crystallogr* 66: 125-132.
15. Adams PD, Afonine PV, Bunkoczi G, Chen VB, Davis IW, et al. (2010) PHENIX: a comprehensive Python-based system for macromolecular structure solution. *Acta Crystallogr D Biol Crystallogr* 66: 213-221.
16. Emsley P, Lohkamp B, Scott WG, Cowtan K (2010) Features and development of Coot. *Acta Crystallogr D Biol Crystallogr* 66: 486-501.

17. Collaborative Computational Project, Number 4 (1994) The CCP4 Suite: Programs for Protein Crystallography. *Acta Cryst D* 50: 760-763.
18. Holm L, KS, Rosenström P, Schenkel A. (2008) Searching protein structure databases with DaliLite v.3. *Bioinformatics*: 2780-2781.
19. Bierbaum G, Sahl HG (1985) Induction of autolysis of staphylococci by the basic peptide antibiotics Pep 5 and nisin and their influence on the activity of autolytic enzymes. *Arch Microbiol.* pp. 249-254.
20. Fischer W, Rosel P, Koch HU (1981) Effect of alanine ester substitution and other structural features of lipoteichoic acids on their inhibitory activity against autolysins of *Staphylococcus aureus*. *J Bacteriol* 146: 467-475.
21. Lu JZ, Fujiwara T, Komatsuzawa H, Sugai M, Sakon J (2006) Cell wall-targeting domain of glycylglycine endopeptidase distinguishes among peptidoglycan cross-bridges. *J Biol Chem.* pp. 549-558.
22. Heilmann C, Hussain M, Peters G, Gotz F (1997) Evidence for autolysin-mediated primary attachment of *Staphylococcus epidermidis* to a polystyrene surface. *Mol Microbiol* 24: 1013-1024.
23. Thompson JD, Higgins DG, Gibson TJ (1994) CLUSTAL W: improving the sensitivity of progressive multiple sequence alignment through sequence weighting, position-specific gap penalties and weight matrix choice. *Nucleic Acids Res* 22: 4673-4680.
24. Edgar RC (2004) MUSCLE: multiple sequence alignment with high accuracy and high throughput. *Nucleic Acids Res* 32: 1792-1797.
25. Katoh K, Misawa K, Kuma K, Miyata T (2002) MAFFT: a novel method for rapid multiple sequence alignment based on fast Fourier transform. *Nucleic Acids Res* 30: 3059-3066.
26. Poirot O, O'Toole E, Notredame C (2003) Tcoffee@igs: A web server for computing, evaluating and combining multiple sequence alignments. *Nucleic Acids Res* 31: 3503-3506.